SAND79-8188
Unlimited Release

Methanol-Based Heat Pumps for Storage of Solar Thermal Energy. Phase I

P. O'D. Offenhartz, M. J. Turner, F. C. Brown,
R. B. Warren, J. P. Pemsler, S. B. Brummer

Sandia Laboratories
energy report

SAND79-8188
Unlimited Release
Printed September 1979

METHANOL-BASED HEAT PUMPS FOR STORAGE
OF SOLAR THERMAL ENERGY.   PHASE I

FINAL REPORT

For Period April 25, 1977 – June 30, 1978

P. O'D. Offenhartz
M. J. Turner
F. C. Brown
R. B. Warren
J. P. Pemsler
S. B. Brummer

EIC Corporation
55 Chapel Street
Newton, Massachusetts   02158

January, 1979

ABSTRACT

The reaction of CH_3OH vapor with a solid-state inorganic salt substrate to produce a solid methanolated salt can be used as the basis of a combined solar heat pump/thermal energy storage system. Such a system should be capable of storing heat indefinitely at ambient temperature, and can be used both for heating and air conditioning. In solar heating, the coefficient of performance should be in the range 1.5-1.8, thus reducing the size of the solar collector required. In solar air conditioning, the coefficient of performance should be in the range 0.5-0.8, comparable with other solar air conditioners; however, the built-in long term storage feature should eliminate the need for resistive electrical backup, thus sharply reducing operating costs.

Experiments carried out in Phase I of this program indicate that the reaction of $CaCl_2$ with CH_3OH vapor to produce $CaCl_2 \cdot 2CH_3OH$ is well suited to both the heating and cooling applications. The heat of reaction is about 20 kcal per mole of CH_3OH, and the kinetics and thermodynamics of the reaction appear adequate down to a CH_3OH pool temperature around -10°C. The required solar collector temperature should be about 150°C. Analytical and experimental work on the design of the heat exchanger for the reacting salt bed indicate that high rates of heat transfer can be accomplished in a reasonably compact system; the indicated energy density for the solid-phase reactant is in excess of 13,000 BTU/ft^3, assuming that the void fraction for anhydrous $CaCl_2$ is 85% or less. Vapor pressure losses through the bed can be minimized by the use of pelletized $CaCl_2$. Furthermore, this material appears to react without apparent degradation of the rate of methanolation or demethanolation through 300 complete cycles, and does not appear to corrode aluminum. No major technical obstacles to the development of a CH_3OH-based solar heat pump/ storage system are apparent, and Phase II work is now proceeding on the development of a prototype system.

i

TABLE OF CONTENTS

LIST OF FIGURES

I. INTRODUCTION: CHEMICALLY DRIVEN HEAT PUMPS

Heat can flow spontaneously from a high to a low temperature, but the reverse process requires an input of work. This work can be provided by any form of energy: electrical or mechanical, as in the case of an air conditioner/heat pump; or thermal and chemical, as in the systems we describe next.

In a chemically driven heat pump, as we define it here, high temperature (100-150°C) thermal energy is used to drive a chemical decomposition:

$$AB \rightarrow A + B(g) \tag{1}$$

At a lower temperature, say 40°C, the gaseous product B reacts with a second substrate C or condenses:

$$B(g) + C \rightarrow BC \tag{2}$$

or

$$B(g) \rightarrow B(\ell) \tag{2'}$$
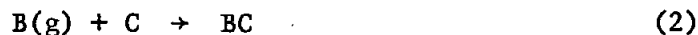
Heat is absorbed in reaction (1) and is given off in reaction (2) or (2'). These two processes describe one-half of the heat pump system. In essence, a gas has been "evaporated" in process (1) and has condensed in process (2) or (2'). No heat pumping has occurred, however. Heat has been transferred from a high temperature source to a lower temperature sink. According to the first and second laws of thermodynamics, if the transfer is carried out reversibly, energy will be stored in the chemicals.

To complete the heat pump cycle, the product BC (or liquid B) is heat exchanged with the ambient air, and substrate A is likewise heat exchanged. In air conditioning applications, BC (or B) is heat exchanged with the indoor air and A with the outdoor air. In heat pumping, BC (or B) is heat exchanged with the (cold) outdoor air, and A with the indoor air. In either case, the product BC spontaneously decomposes (or B evaporates) and AB is formed. Heat is pumped from a low temperature source to a high temperature sink, and the cycle is completed.

The driving force for the heat pump comes from the difference in thermodynamic affinity of the gas for the two substrates. In this sense, the heat pump is "chemically driven." But the ultimate source of the pumping energy is the decrease in the temperature of the heat from the collector (100-150°C) to the point of delivery (20-40°C).

1

In many ways, a chemically driven heat pump is similar to an ammonia-water refrigerator fueled by propane or natural gas: high-temperature heat is used to pump heat from inside the refrigerator to the outside. But a chemically driven heat pump separates the two parts of the cycle, heat absorption at high temperature, and heat pumping. It is therefore both a heat pump and an energy storage system. Furthermore, in a chemically driven heat pump, heat can be stored indefinitely without thermal loss.

We next consider examples of two types of units, with one and two substrates, respectively. The advantages and disadvantages of each are discussed. The examples noted use NH_3 rather than CH_3OH. This is because of the relative abundance of thermodynamic data for salt-NH_3 reactions. As we note in 3 below, the use of CH_3OH appears preferable to NH_3.

1. A Chemically Driven Heat Pump with One Substrate

Anhydrous $CaCl_2$ binds NH_3 vapor in a series of stepwise reactions (references 1,2):

$$CaCl_2(s) + NH_3(g) \rightleftarrows CaCl_2 \cdot NH_3(s) \tag{3}$$

$$CaCl_2 \cdot NH_3(s) + NH_3(g) \rightleftarrows CaCl_2 \cdot 2NH_3(s) \tag{4}$$

$$CaCl_2 \cdot 2NH_3(s) + 2NH_3(g) \rightleftarrows CaCl_2 \cdot 4NH_3(s) \tag{5}$$

$$CaCl_2 \cdot 4NH_3(s) + 4NH_3(g) \rightleftarrows CaCl_2 \cdot 8NH_3(s) \tag{6}$$
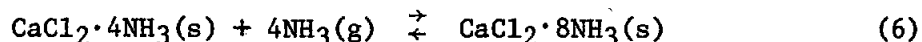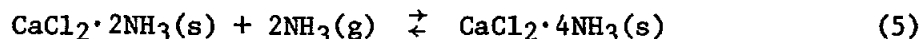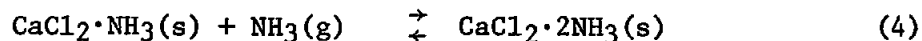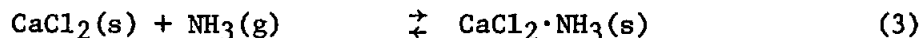
The last reaction is of particular interest for heat pumping. The standard enthalpy of the reaction as written is -9.8 kcal/mole-NH_3, while the standard entropy is -32.1 cal/mole-°C. Ignoring heat capacity changes, the equation of state for the equilibrium pressure of NH_3 (P_{NH_3}, in atmospheres) above a mixture of $CaCl_2 \cdot 8NH_3$ and $CaCl_2 \cdot 4NH_3$ is (ref. 2)

$$1.987 \, \ell n P_{NH_3}^{(1)} = 32.1 - 9800/T_1 \tag{7}$$

The equation of state for NH_3 gas condensing to liquid is

$$1.987 \, \ell n P_{NH_3}^{(2)} = 21.6 - 5100/T_2 \tag{8}$$

Here, T_1 and T_2 are the equilibrium temperatures in degrees Kelvin.

To operate the two processes

$$CaCl_2 \cdot 8NH_3(s) \rightleftarrows CaCl_2 \cdot 4NH_3(s) + 4NH_3(g) \tag{9}$$

2

$$4NH_3(g) \; \rightleftharpoons \; 4NH_3(l) \tag{10}$$

as a heat pump, the following elements are needed:

(a) A pressurized heat exchange unit to contain the solid mixture. The heat given off or absorbed in reaction (9) must be exchanged with air.

(b) A pressurized heat exchange unit to condense or evaporate the NH_3, as well as a pressurized storage vessel to contain the excess NH_3 liquid.

(c) Ducts to bring indoor or outdoor air to either heat exchanger, and to bring heated air from the (solar) collector to the solids heat exchanger.

In the first half of the cycle ("storage mode"), hot air from the heat collector is exchanged with the solids and NH_3 gas is given off. As shown by Equations (7) and (8), this process will occur spontaneously if T_1 (the temperature of the solids) is greater than 95°C and T_2 (the temperature of the liquid NH_3) is 40°C. The heat given off when the gas condenses is either used to heat the indoors (indoor air flows across the NH_3 condenser) or is discarded (outdoor air flow), depending on the need for space heating at the time. Ignoring the heat capacities of the solids, liquids, and gases, which are relatively small, the heat absorbed by the solids is 9.8 kcal (39 BTU) per mole of NH_3 released, while the heat given off in condensation is 5.1 kcal (20 BTU). Roughly 19 BTU per mole of NH_3 have been stored.

In the second half of the cycle ("heat pump mode"), air from either the outdoors (air conditioning) or the indoors (heating) is used for heat exchange with the solids, so that the temperature in this unit is about 40°C. A separate supply of air from indoors (air conditioning) or outdoors (heating) is used for heat exchange with liquid NH_3. As can be shown by substitution in Equations (7) and (8), heat pumping will occur spontaneously provided that T_2 is 40°C and T_1 is greater than -27°C. In the heat pump operation, 20 BTU per mole of NH_3 is absorbed from outdoors and an additional 19 BTU is recovered from storage, so that 39 BTU of heating is provided. In air conditioning, 20 BTU is absorbed from outdoors.

2. A Chemically Driven Heat Pump with Two Substrates

The reaction of anhydrous $CaCl_2$ with NH_3 can be coupled with the reaction of anhydrous $FeCl_2$ with NH_3 to form a two-substrate heat pump, in which the reactions are:

$$FeCl_2 \cdot 6NH_3(s) \; \rightleftharpoons \; FeCl_2 \cdot 2NH_3(s) + 4NH_3(g) \tag{11}$$

AIR FLOW →

PRESSURIZED HEAT
EXCHANGER CONTAINING
THE SOLIDS

HEAT EXCHANGER FOR
CONDENSING AND
EVAPORATING GAS

AIR FLOW →

PRESSURIZED VESSEL
TO CONTAIN LIQUID
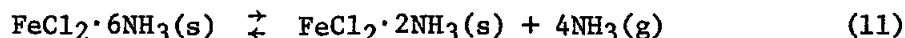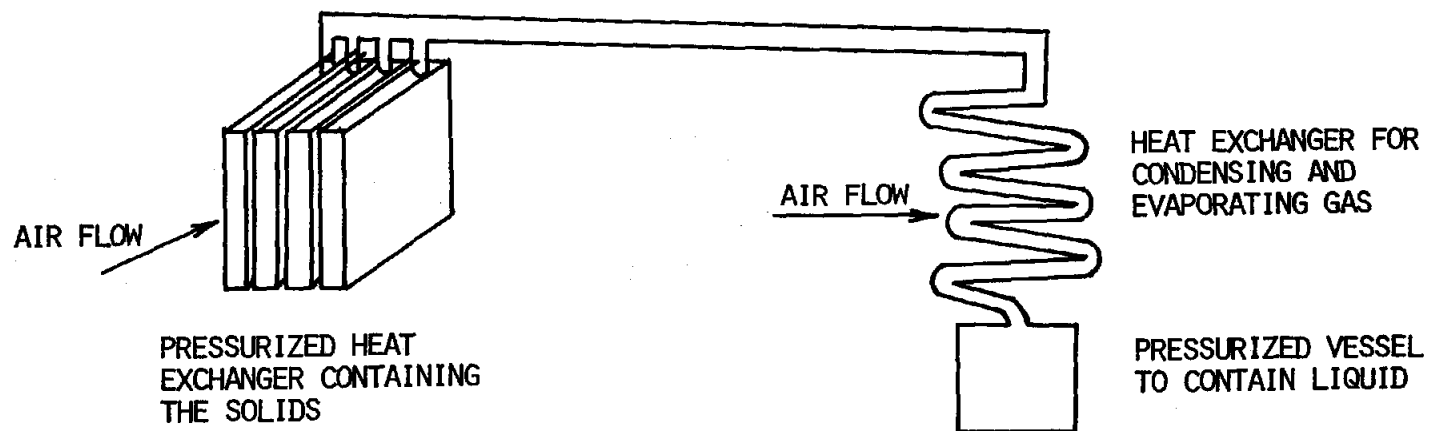
Fig. 1a: Schematic diagram of the one-substrate heat pump.

AIR FLOW →

$FeCl_2$ CONTAINER AND
HEAT EXCHANGER

AIR FLOW →

$CaCl_2$ CONTAINER AND
HEAT EXCHANGER
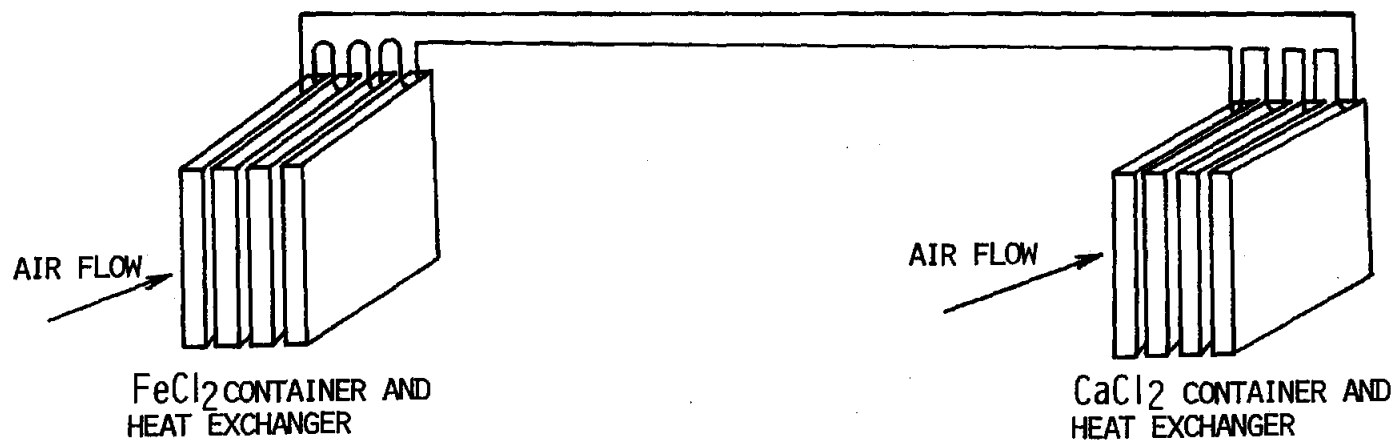
Fig. 1b: Schematic diagram of the two-substrate heat pump.

$$CaCl_2 \cdot 4NH_3(s) + 4NH_3(g) \rightleftharpoons CaCl_2 \cdot 8NH_3(s) \qquad (12)$$
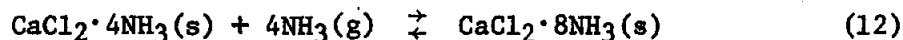
The corresponding equations of state are (2)

$$1.987 \, \ell nP_{NH_3}^{(1)} = 31.6 - 12550/T_1 \qquad (13)$$

$$1.987 \, \ell nP_{NH_3}^{(2)} = 32.1 - 9800/T_2 \qquad (14)$$

In this case, two solid-to-air heat exchangers are used, with the $FeCl_2$ salts placed in the exchanger that is tied to the heat collector (Figure 1b).

If the $CaCl_2$ salt is kept at 40°C during the storage mode, NH_3 gas will flow from the $FeCl_2$ exchanger to the $CaCl_2$ exchanger provided that the temperature of the $FeCl_2$ salts is kept above 125°C. The heat absorbed by the $FeCl_2$ systems is about 12.25 kcal (49 BTU) per mole of NH_3 released, while the heat given off in the reaction with $CaCl_2$ is 39 BTU.

In the heat pump mode, the $FeCl_2$ system is heat exchanged at about 40°C. Ammonia flows spontaneously from the $CaCl_2$ side to the $FeCl_2$ side if the temperature of the $CaCl_2$ salts is above -24°C. In air conditioning, 39 BTU is absorbed from indoors per mole of NH_3. In heat pump operation, 39 BTU is absorbed from outdoors and an additional 10 BTU is recovered from storage, so that 49 BTU is delivered indoors.

3. Comparative Merits of One- and Two-Substrate Heat Pumps

The one-substrate system is obviously less costly: it uses less salt, and has only one solid-to-air heat exchanger.

The two-substrate system has better coefficients of performance for both heating and cooling. For heating, the overall COP (heat delivered indoors divided by solar heat absorbed) is approximately

$$COP(heating) = \frac{\Delta H_1 + \Delta H_2}{\Delta H_1} \qquad (15)$$

For cooling,

$$COP(cooling) = \frac{\Delta H_2}{\Delta H_1} \qquad (16)$$

In the one- and two-substrate systems described above,

5

$$COP(\text{heating, one substrate}) = 1.52 \qquad COP(\text{heating, two substrates}) = 1.78$$
$$COP(\text{cooling, one substrate}) = 0.52 \qquad COP(\text{cooling, two substrates}) = 0.78 \tag{17}$$

The reason for the inherent disadvantage of the one-substrate system is that the heat of evaporation of NH_3 (ΔH_2) is smaller than the heat of reaction of NH_3 gas with a salt (ΔH_1). In the two-substrate systems, the two heats are more nearly equal.

A second disadvantage of the one-substrate system is that gas pressures are substantially higher. In a one-substrate system using liquid NH_3, the maximum pressure in the heat exchangers is nearly 20 atm (300 psi). In the two-substrate system, the maximum overpressure never exceeds 1 atm (15 psi). The heat exchangers can be designed from lighter gauge materials in a two-substrate system, and will be correspondingly less costly per unit. Of course, a one-substrate system has but one solid-to-air heat exchanger.

The question, therefore, is whether a low-cost, one-substrate system can be designed with (a) coefficients of performance higher than for the $CaCl_2/NH_3$ system; (b) lower pressures; and (c) comparable total costs. We believe this can be done by using methanol in place of ammonia. Methanol has two major advantages over ammonia: its boiling point is greater (65°C vs. -33°C), so that its vapor pressure is lower; and its heat of vaporization is larger (9.2 kcal vs. 5.1 kcal), in part because of association in the liquid state. (Water could be useful in a one-substrate air conditioning system, but freezes at too high a temperature to be used in a heat pump.)

Unfortunately, thermodynamic data for the reactions of gases with solid substances such as metal salts have been reported for only a limited number of reactions. Data on the reactions of methanol vapor with inorganic salts are particularly scarce. For this reason, the first step in our research program, as described in Section II, has been to search for salts that react with methanol vapor in a thermodynamically useful fashion.

4. Liquid-Based Systems

The examples of one- and two-substrate heat pumps discussed above have involved solid substrates. In principle, liquid substrates could also be used, as in the H_2SO_4/H_2O system under development by Rocket Research Corporation (3). However, in a liquid-based system, the vapor pressure is an explicit function of the extent of reaction as well as the temperature. In a solid substrate system, as seen in Equations (7), (11), and (12), the vapor pressure is independent of the extent of reaction. Thus, maintaining a constant vapor pressure in a solid-substrate system involves constant temperatures, while in a liquid-based system, the collection temperature to drive reaction (1) must rise as B(g) is driven

6

off. Whether this is a serious disadvantage in practice depends on the extent of the temperature change in a liquid-based system, and on other system trade-offs. Heat exchange is unquestionably simplified in a liquid-based system, but at the cost of higher maximum temperatures and a sharply restricted choice of chemicals. For these reasons, our work has been limited to solid-substrate chemical reactions.

5. Thermodynamic Principles

The general thermodynamic principles governing the operation of a heat pump may be stated simply. Heat (q_1) is absorbed from a low temperature source (T_1) and is discharged at a higher temperature (T_2). Since this process is not spontaneous, work $(\underline{W})$ must be done to accomplish it. From the first law of thermodynamics, the heat discharged at the upper temperature (q_2) is the sum of W and q_1. From the second law, assuming reversibility, the sum of the entropy changes is zero. Thus,

$$\frac{q_1}{T_1} = \frac{q_2}{T_2} \qquad (18)$$

$$q_2 = q_1 + W = \frac{T_1}{T_2} q_2 + W \qquad (19)$$

$$W = \left(1 - \frac{T_1}{T_2}\right) q_2 = \left(\frac{T_2}{T_1} - 1\right) q_1 \qquad (20)$$

We see that the minimum work $\underline{W}$ necessary to pump heat is determined by the ratio of the two absolute temperatures T_2 and T_1.

The coefficient of performance of a heat pump is defined as

$$COP = \frac{q_2}{W} \qquad (21)$$

Under reversible conditions,

$$COP = \frac{T_2}{T_2 - T_1} \qquad (22)$$

For example, if heat is extracted from the environment on a cold day, such that $T_1 = -10°C$ (263°K), and delivered indoors at $T_2 = 20°C$ (293°K), the maximum coefficient of performance is 9.8. In practice, efficient heat exchange requires that the heat be transferred at temperatures 15-25°C different from the equilibrium values. Thus, realistic coefficients will be in the range

$$COP = \frac{T_2 + 15}{T_2 - T_1 + 30} \text{ to } \frac{T_2 + 25}{T_2 - T_1 + 50} \tag{23}$$

that is, 4.0 to 5.1 for the indoor and outdoor temperatures just mentioned. Such values are not far above the actual coefficients of performance (2.6-3.0) achieved by commercial heat pumps (4) operating at the same temperatures; the reduction is caused by inefficiencies in converting electrical energy to mechanical energy, and by the electric power needed to run the heat-exchange fans.

The equations for a heat engine are the same as those for a heat pump. However, in a heat engine, heat q_2 is absorbed at the higher temperature T_2 and heat $q_1 = q_2 - W$ is discharged at the lower temperature T_1. The maximum work that can be done by the system is given in Equation (20).

A heat engine may be coupled with a heat pump to form a thermally powered heat pump. Suppose heat q_3 is collected at a temperature T_3 in the range 100-150°C. If heat q_2 is discharged at T_2 (40°C), the heat delivered at T_2 is

$$q_2 = \frac{T_2}{T_3} q_3 \tag{24}$$

and the maximum work done is

$$W = \left(1 - \frac{T_2}{T_3}\right) q_3 \tag{25}$$

If this work is used to pump heat from the ambient temperature T_1 to T_2, the heat absorbed from the environment is

$$q_1 = \frac{T_1}{T_2 - T_1} W - \frac{T_1}{T_3}\left(\frac{T_3 - T_2}{T_2 - T_1}\right) q_3 \tag{26}$$

and the additional heat delivered at T_2 is

$$q_2' = q_1 + W = \frac{T_2}{T_2 - T_1} W = \frac{T_2}{T_3}\left(\frac{T_3 - T_2}{T_2 - T_1}\right) q_3 \tag{27}$$

The coefficient of performance of the system is the ratio of the total heat delivered at T_2 ($q_2 + q_2'$) to the heat absorbed at T_3:

$$COP = \frac{q_2 + q_2'}{q_3} = \frac{T_2}{T_3} \frac{T_3 - T_1}{T_2 - T_1} \qquad (28)$$

For $T_3 = 125°$, $T_2 = 40°$, and $T_1 = -20°$, the maximum coefficient of performance of a thermally powered heat pump is 1.9. In other words, for each unit of heat absorbed at 125°, 0.9 units of heat can be pumped from the ambient temperature T_1 up to T_2.

A thermally powered heat pump can also be used as an air conditioner. The coefficient of performance is the ratio of the heat removed at T_1 to the heat absorbed at T_3:

$$COP = \frac{q_1}{q_3} = \frac{T_1}{T_3} \left(\frac{T_3 - T_2}{T_2 - T_1} \right) \qquad (29)$$

For $T_3 = 125°$, $T_2 = 50°$, $T_1 = 10°$, the maximum coefficient of performance is 1.3.

6. Development of a Methanol-Based Heat Pump

Work on the development of a methanol-based system for heat pumping and solar thermal storage has followed two main lines of effort: (1) laboratory work designed to screen and test candidate salts; to determine their thermodynamic, kinetic, and heat transfer properties; to determine their ability to withstand long-term cycling; to examine their propensity to corrode likely materials of construction; (2) analytical engineering work, aimed primarily at heat exchanger design for the salt bed, as well as overall system design. These two lines of effort are not totally independent. For example, to strictly define the desired range of thermodynamic properties of the salt-vapor reaction, information is needed on the temperature drops required for heat exchange, and on the trade-off between the cost of high temperature solar collection and the cost of high efficiency heat exchange. Since such data were not initially available -- and are still fragmentary -- we planned our experimental work along fairly broad lines, such that the screening process for salts would not reject any candidates too readily.

The criteria initially developed for candidate salts included low cost per mole; high prospective volumetric energy densities; rapid rates of reaction; absence of obvious side reactions; and appropriate thermodynamics. By "appropriate" we mean that the salt-methanol reaction should be capable of pumping heat from temperatures below 0°C to temperatures above 40°C. This preliminary choice of temperatures is somewhat arbitrary. Nevertheless, 40°C appears to be a reasonable minimum if indoor air at 20°C is to be heated. Likewise, 0°C appears to be a reasonable maximum if heat is to be extracted from outdoor air, from underground heat exchange,

or from a body of water. If anything, the temperature span should be greater so that the screening process is more selective.

Initial engineering design work has proceeded on the assumption that daytime solar energy collection ordinarily proceeds at a rate sufficiently rapid that heat obtained in condensing methanol vapor (see Figure 1) is sufficient to meet the heating load. For example, if the system COP is 1.5, the solar collection rate is 40,000 BTU/hr, and the daytime building load is 20,000 BTU/hr, then the load will just be met by methanol condensation. Further assuming eight hours of active solar collection, 320,000 BTU will be stored during this period. Thus, during the 16 "nighttime" hours, heat can be supplied from storage at the same 20,000 BTU/hr rate. This rough calculation illustrates an important feature of the system: because the heat pump COP is greater than unity, collection of 320,000 BTU (40,000 x 8 hours) is sufficient to meet a 480,000 BTU load (20,000 x 24 hours). Furthermore, considerations of this type help to define the desired storage capacity and charge/discharge rates, and have been used to define rates of reaction that are "reasonable" and acceptable -- that is, faster than the 8 hour charge time or 16 hour discharge time.

The results of the first 14 months of our effort to develop a methanol-based heat pump are presented in the following two sections. Section II is largely concerned with experimental aspects of the work, although some attention is also paid to analytical modeling of the methanolation/demethanolation process. Section III is devoted to engineering design and analysis, particularly to the heat exchange process. Future plans are discussed in Section IV, and listings of the computer programs used in the analytical work are given in the appendices.

1. Candidate Salt Screening

A Cahn RG electrobalance was used for salt screening. The complete experimental setup consisted of the balance, a vacuum pump, a mercury manometer, a thermostatted methanol pool, and a thermostatted oil bath used to control the temperature of the salt sample. A small sample of a powdered salt, typically 30 mg, was placed on a Teflon pan, suspended inside a glass hangdown tube, which was in turn immersed in the oil bath. The system was sealed and evacuated, and the temperature of the oil bath was increased to drive off water. (The salt samples as purchased were usually hydrated.) Dehydration was generally continued until completion, as indicated by the absolute weight change, or by the failure of the sample to lose additional water overnight at a temperature indicated by the literature to be sufficient for complete dehydration.

Following initial dehydration, the salt sample was cooled to ca. 60°C, and CH_3OH vapor was introduced into the balance. For screening purposes this was accomplished by thermostatting a CH_3OH pool at 15°C, where the vapor pressure is 71 torr (ca. 0.1 atm), and connecting the pool to the balance. The temperature of the salt was gradually decreased to ca. 30°C over a period of several hours, and the weight monitored. In this way, we were able to observe formation of salt-methanol complexes. The temperature was then increased over a period of several hours until demethanolation of the salt was complete.

A literature search of Chemical Abstracts was performed to obtain information on previously reported methanolates of inorganic compounds. Fifty such compounds were identified from 27 pertinent references and are listed below:

$AlCl_3 \cdot 6MeOH$	(16)	$CoBr_2 \cdot 6MeOH$	(29)
$AlCl_3 \cdot 4MeOH$	(16)	$CoBr_2 \cdot 4MeOH$	(13)
$Ba(ClO_4)_2 \cdot 8MeOH$	(26)	$CoBr_2 \cdot 3MeOH$	(29)
$CaBr_2 \cdot 4MeOH$	(11)	$CoBr_2 \cdot 2MeOH$	(13,29)
$CaBr_2 \cdot 3MeOH$	(11)	$CoBr_2 \cdot MeOH$	(17,29)
$CaBr_2 \cdot MeOH$	(11)	$CoCl_2 \cdot 4MeOH$	(5,13)
$CaCl_2 \cdot 4MeOH$	(11)	$CoCl_2 \cdot 3MeOH$	(13)
$CaCl_2 \cdot 3MeOH$	(11)	$CoCl_2 \cdot 2MeOH$	(5)
$CaCl_2 \cdot 2MeOH$	(23)	$CoCl_2 \cdot MeOH$	(17)
$CaCl_2 \cdot MeOH$	(11)	$Co(NO_3)_2 \cdot 6MeOH$	(20)
$Ca(ClO_4)_2 \cdot 8MeOH$	(26)	$Co(NO_3)_2 \cdot 4MeOH$	(20,31)
$Ca(ClO_4)_2 \cdot 2MeOH$	(26)	$Co(NO_3)_2 \cdot 2MeOH$	(20)

$CoI_2 \cdot 6MeOH$	(13)	$MgSO_4 \cdot 3.5MeOH$	(15)
$CoI_2 \cdot 5MeOH$	(13)	$MgSO_4 \cdot 2MeOH$	(22,24)
$CuCl_2 \cdot 2MeOH$	(19)	$MnBr_2 \cdot MeOH$	(8)
$CuCl_2 \cdot MeOH$	(19)	$MnCl_2 \cdot 2MeOH$	(8,21)
$CsCO_3 \cdot 6MeOH$	(7)	$MnCl_2 \cdot MeOH$	(8)
$FeCl_2 \cdot 4MeOH$	(12)	$SbCl_5 \cdot MeOH$	(10)
$FeCl_2 \cdot 2MeOH$	(12)	$ScCl_3 \cdot nMeOH^*$	(6)
$LiBr \cdot 4MeOH$	(25)	$ScBr_3 \cdot nMeOH^*$	(6)
$K_2CS_4 \cdot MeOH$	(28,30)	$SnCl_4 \cdot 2MeOH$	(18)
$MgCl_2 \cdot 6MeOH$	(9,14,27)	$Sr(ClO_4)_2 \cdot 8MeOH$	(26)
$MgCl_2 \cdot 4MeOH$	(14)	$Sr(ClO_4)_2 \cdot 6MeOH$	(26)
$MgCl_2 \cdot MeOH$	(14)	$ZnSO_4 \cdot 2.5MeOH$	(15)
$Mg(ClO_4)_2 \cdot 6MeOH$	(26)	$ZnSO_4 \cdot MeOH$	(15)

---

*n not given

Information on these compounds was, in general, quite sketchy. Some references gave only evidence for formation; others gave approximate decomposition temperatures in air or crystallographic data. Some thermodynamic data are available for the methanolates of $CoCl_2$, $CoBr_2$, $CuCl_2$ and $MnCl_2$.

Based on the literature data, and on data for corresponding hydrate reactions, 20 salts were selected for screening. The results of these experiments are summarized in Table 1. Based on the thermodynamic criteria established in Section I.6, four salts were selected for further study: $CaCl_2$, $CoBr_2$, $FeBr_2$, and $MgCl_2$. Judging by the maximum temperature of formation, these salts all take up two moles of CH_3OH at or above 65°C from a pool at 15°C.

To narrow down the choice of salts, and to gain additional information on the temperatures of complex formation and decomposition, additional measurements on these four salts were carried out at a CH_3OH pool temperature of -10°C, corresponding to a vapor pressure of 15 torr. Results for $CoBr_2$, $FeBr_2$, $MgCl_2$ and $CaCl_2$ are as follows:

(a) CoBr_2

A 40.88 mg pulverized sample of $CoBr_2 \cdot 6H_2O$ was placed in the vacuum balance and heated to 170°C. The weight loss, 12.22 mg, corresponds to 5.41 moles of H_2O; in a previous experiment, the weight loss corresponded to 5.03 moles of H_2O. The salt was then exposed to CH_3OH vapor and allowed to cool to 40°C; 1.19 moles of CH_3OH reacted. Subsequent heating to 115°C removed all CH_3OH. After cooling to 25°C, 1.77 moles of CH_3OH reacted.

During the initial cooling cycle, the first sign of weight gain began at 55°C. Cooling to 46°C over a 30 minute period resulted in a gain of 0.78 moles CH_3OH; subsequent maintenance of the temperature at

TABLE 1

RESULTS OF SALT SCREENING EXPERIMENTS

1. Salts that do not methanolate

     $Na_2B_4O_7$
     Na_2CO_3
     Na_2SO_4
     CH_3COONa
     $MgSO_4$

2. Salts that hydrolyze or decompose

     $FeCl_3$
     $Co(NO_3)_2$
     Na_2S

3. Salts that methanolate with CH_3OH at 15°C

	Methanol, moles	Δmoles	Temperature Range, °C Formation		Decomposition
$AlNH_4(SO_4)_2$	0.3		55		
$CaBr_2$	2.0		110–75	2–1	130–145
$CaCl_2$	1.96		65–47		109–132
$Ca(NO_3)_2$	1.80		32		55
$CoBr_2$	3	0–1	82–73		113–132
		1–2	65–47		87–108
		2–3	45–38		65–80
$CoCl_2$	∼0.5				
$FeBr_2$	1.95	0–1	98–75		132–140
		1–2	72–55		101–115
$FeCl_2$	1.93	0–1	95–52		135–145
		1–2	32–26		80–95
$MgCl_2$	3.92	0–2	90–50	0–4	95–120
		2–4	50–30		
$MnCl_2$	1.91	0–1	82–55		140–178
		1–2	30–26.5		75–94
$MnBr_2$	1.87	0–1	80–55		130–159
		1–2	53–43		85–96
$NiCl_2$	>2		130–30		40–140
$NiBr_2$	>5		60–27		50–115

45°C for 3 hours resulted in the formation of a complex with the stoichiometry $CoBr_2 \cdot 1.12CH_3OH$. Decreasing the temperature to 42°C for 16 hours resulted in the stoichiometry $CoBr_2 \cdot 1.19CH_3OH$. Upon reheating, the first sign of weight loss was seen at 60°C.

Based on the data obtained at 71 torr, we had expected $CoBr_2$ to gain approximately 2 moles of CH_3OH at a temperature above 40°C when reacted with CH_3OH vapor at 15 torr. Our experiments confirm that more than one mole of CH_3OH is gained under these conditions, but reaction of the second mole is very slow. Thus, the useful range of reactivity of $CoBr_2$ appears limited to one mole of CH_3OH when used in a forced-air heat pump cycle. With a source temperature above 0°C, it appears that 2 moles of CH_3OH can react.

(b) FeBr_2

A 37.60 mg pulverized sample of $FeBr_2 \cdot 6H_2O$ was placed in the vacuum balance and heated to 175°C. The weight loss corresponded to 5.02 moles of H_2O.

When the salt was exposed to CH_3OH vapor at 15 torr and cooled, the first sign of weight gain was noted at 85°C. Subsequent cooling to 63°C over a 60 minute period resulted in formation of a complex with stoichiometry corresponding to $FeBr_2 \cdot 0.76CH_3OH$. Further cooling to 45°C over a 90 minute period resulted in the complex $FeBr_2 \cdot 1.96CH_3OH$.

Upon subsequent heating, the first sign of weight loss was noted at 77°C, and heating to 98°C over a 30 minute period resulted in the loss of 0.97 moles of CH_3OH. The second mole of CH_3OH was lost over a 30 minute period of heating between 115° and 122°C.

Both the thermodynamics and kinetics of the reaction of CH_3OH with $FeBr_2$ indicate that this salt should be useful in a forced-air heat pump cycle.

(c) MgCl_2

A 44.00 finely pulverized sample of $MgCl_2 \cdot 6H_2O$ was placed in the vacuum balance, which was then pumped to remove the first 2 moles of H_2O. The sample was then gradually heated until the final 4 moles were removed.

The dehydrated salt was then exposed to CH_3OH vapor at 15 torr. The first sign of weight gain began at 110°C. During relatively rapid cooling to 54°C over a 75 minute period, 0.66 moles of CH_3OH reacted. Holding the salt temperature at 49°C over a 19 hour period resulted in formation of a complex with stoichiometry corresponding to $MgCl_2 \cdot 1.92CH_3OH$.

14

Upon heating the salt, initial weight loss was noted at 68°C. However, only one mole of CH_3OH was readily removed. The last traces of the second mole were not lost until the temperature reached 175°C.

The formation of $MgCl_2 \cdot 2CH_3OH$ appears thermodynamically favorable at 50°C at 15 torr, although the rate of reaction is relatively slow. There is some question as to whether both moles of CH_3OH can be removed at a reasonable rate below 150°C, and some indications of hydrolysis have been observed.

(d) $CaCl_2$

Preliminary experiments on the reaction of $CaCl_2$ with CH_3OH vapor at 15 torr indicated that two moles of CH_3OH vapor could be added at a salt temperature around 55°C. Furthermore, at this pressure, demethanolation was observed below 75°C. These experiments indicated that $CaCl_2$ might well be useful in a forced-air heat pump cycle. Furthermore, the low cost of $CaCl_2$ relative to $FeBr_2$ and $CoBr_2$ is attractive: it is doubtful whether a cost-effective storage system could be based on a salt bromide. Relative to $MgCl_2$, $CaCl_2$ appears attractive because both moles of CH_3OH can be removed at a relatively low solar collector temperature. For these reasons, $CaCl_2$ was selected as the first salt to be studied more intensively.

2. Gas-Salt Reaction Data: Thermodynamics and Kinetics

2.1 Temperature-Pressure Composition Experiments with $CaCl_2$

A 27.76 mg sample of $CaCl_2 \cdot 2H_2O$ was dehydrated in the vacuum balance and then heated to 138°C _in vacuo_. The final weight, 18.56 mg, corresponds to a loss of 2.71 mole H_2O per mole $CaCl_2$.

The sample was exposed to CH_3OH vapor at 70 torr and the temperature of the salt sample was decreased to 100°C. No weight gain was noted over a 12-hour period. The first increase in weight was noted at 87°C; when the temperature was increased to 90°C, a distinct decrease in weight was found. On subsequent temperature cycling, weight increase was again noted at 86°C, and weight decrease at 90°C. It appeared that equilibrium occurred at 88 ± 2°C.

The salt temperature was decreased to 75°C, and a rapid increase in weight occurred (90% reaction in less than 4 hours). With 1.9 moles of CH_3OH added, the sample was held at 82°C for 12 hours; the weight remained constant. When the temperature was increased, the first sign of weight loss occurred at ca. 85°C. These data are consistent with a single step reaction

$$CaCl_2 + 2CH_3OH \rightarrow CaCl_2 \cdot 2CH_3OH \qquad (30)$$
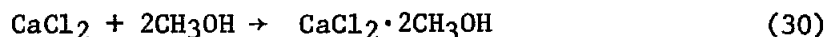
with equilibrium at 88°C at 70 torr. However, other data indicate the possibility of two (closely spaced) steps.

15

To remove the CH_3OH, the sample (still at 70 torr) was heated to ca. 120°C; over 85% of the CH_3OH was driven off within an hour. However, the reaction slowed down sharply near the end, and the final 0.03 moles were not removed.

The next set of experiments was carried out at 15 torr. The temperature of the salt was slowly decreased from 60°C to 45°C; at ca. 53°C, a rapid weight gain began and, within 4 hours, the reaction was over 90% complete. In order to bracket the equilibrium temperature, a number of separate experiments were carried out. At 13 torr, and at a composition corresponding to $CaCl_2 \cdot 0.7CH_3OH$, a weight gain was observed below 70°C, and a weight loss above 67°C. A very slow weight gain was found when the temperature was held constant at 68°C over the weekend.

A second experiment was carried out at 16 torr at a composition corresponding to $CaCl_2 \cdot 0.3CH_3OH$; weight loss was noted above 72°C, and weight gain below 69°C. Taken together, these data point toward equilibrium for the reaction

$$CaCl_2 + CH_3OH \rightleftharpoons CaCl_2 \cdot CH_3OH \qquad (31)$$
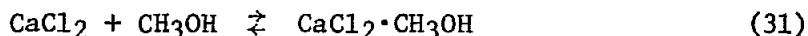
at 70 ± 2°C at 15 ± 2 torr.

A corresponding equilibrium temperature for the second reaction,

$$CaCl_2 \cdot CH_3OH + CH_3OH \rightleftharpoons CaCl_2 \cdot 2CH_3OH \qquad (32)$$
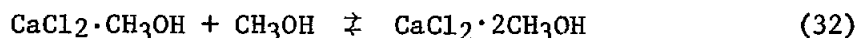
was determined by cycling the temperature of the salt at a composition corresponding to $CaCl_2 \cdot 1.7CH_3OH$; at 15 torr, a definite weight loss was observed above 64°C, and a definite weight gain below 66°C, corresponding to equilibrium at 65 ± 1°C at 15 ± 1 torr. The equilibrium temperatures for the two reactions are nearly equal within experimental error; it is, of course, possible that the overall reaction

$$CaCl_2 + 2CH_3OH \rightleftharpoons CaCl_2 \cdot 2CH_3OH \qquad (33)$$
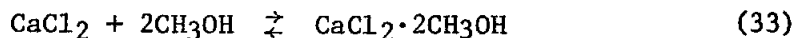
does not occur in a single step, but in two closely spaced steps.

A third set of experiments was carried out at ca. 40 torr. Starting at $CaCl_2 \cdot 0.1CH_3OH$, the first sign of rapid addition of CH_3OH occurred at 65°C; the maximum rate of reaction at this temperature was 0.5 moles CH_3OH per hour, although the reaction did not go to completion. After 14 hours at 62°C, the composition corresponded to $CaCl_2 \cdot 1.6CH_3OH$, and the weight was increasing very slowly. To determine the equilibrium

temperature, the sample temperature was increased; at 76°C, the first distinct sign of weight loss was noted. A distinct weight gain was noted at 80°C (38 torr). When the sample was kept overnight at 81°C at 38 torr, no change in weight was found. Our best estimate of the equilibrium temperature for the reaction

$$CaCl_2 \cdot CH_3OH + CH_3OH \rightleftharpoons CaCl_2 \cdot 2CH_3OH \qquad (34)$$
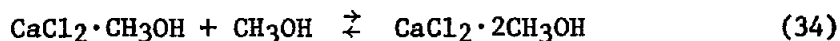
at 38 torr is 78 ± 3°C.

Following this experiment, the sample was partially demethanolated by reducing the CH_3OH vapor pressure, until the composition corresponded to $CaCl_2 \cdot 0.6CH_3OH$. At 40 torr, a distinct weight gain was first noted at 83°C; below 75°C, the gain was quite fast. The temperature for the corresponding initial weight loss was not determined carefully, but was approximately 80°C. Once again we see some evidence that the equilibrium temperature for the addition of the first CH_3OH to $CaCl_2$ may lie a few degrees above the equilibrium temperature for the second addition.

Accurate determination of the transition temperatures is complicated by a number of factors. First, it appears likely that the rate of reaction is exponentially dependent on the temperature difference from equilibrium; within a few degrees, rates are so slow that it becomes difficult to see measurable changes. Second, the salt sample in a TGA apparatus is not in good thermal contact with the oil bath, and since the enthalpy of reaction is large, a substantial temperature difference between sample and bath may exist. Third, nucleation phenomena in the reaction may abnormally reduce the reaction rate under near-equilibrium conditions. Finally, secondary phenomena, such as surface adsorption, may produce small weight changes that do not correspond to the chemical reaction under observation. Nevertheless, we believe we have obtained the equilibrium values within ± 3°C.

The equilibrium data obtained to date are graphed as log (pressure) versus 1/T in Figure 2. The data for the reaction

$$CaCl_2 + CH_3OH \rightleftharpoons CaCl_2 \cdot CH_3OH$$
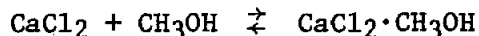
fit the equation

$$\ell nP = 27.05 - 10628/T \qquad (35)$$

well within the experimental error; the excellent fit is almost certainly fortuitous. The data for the second step,
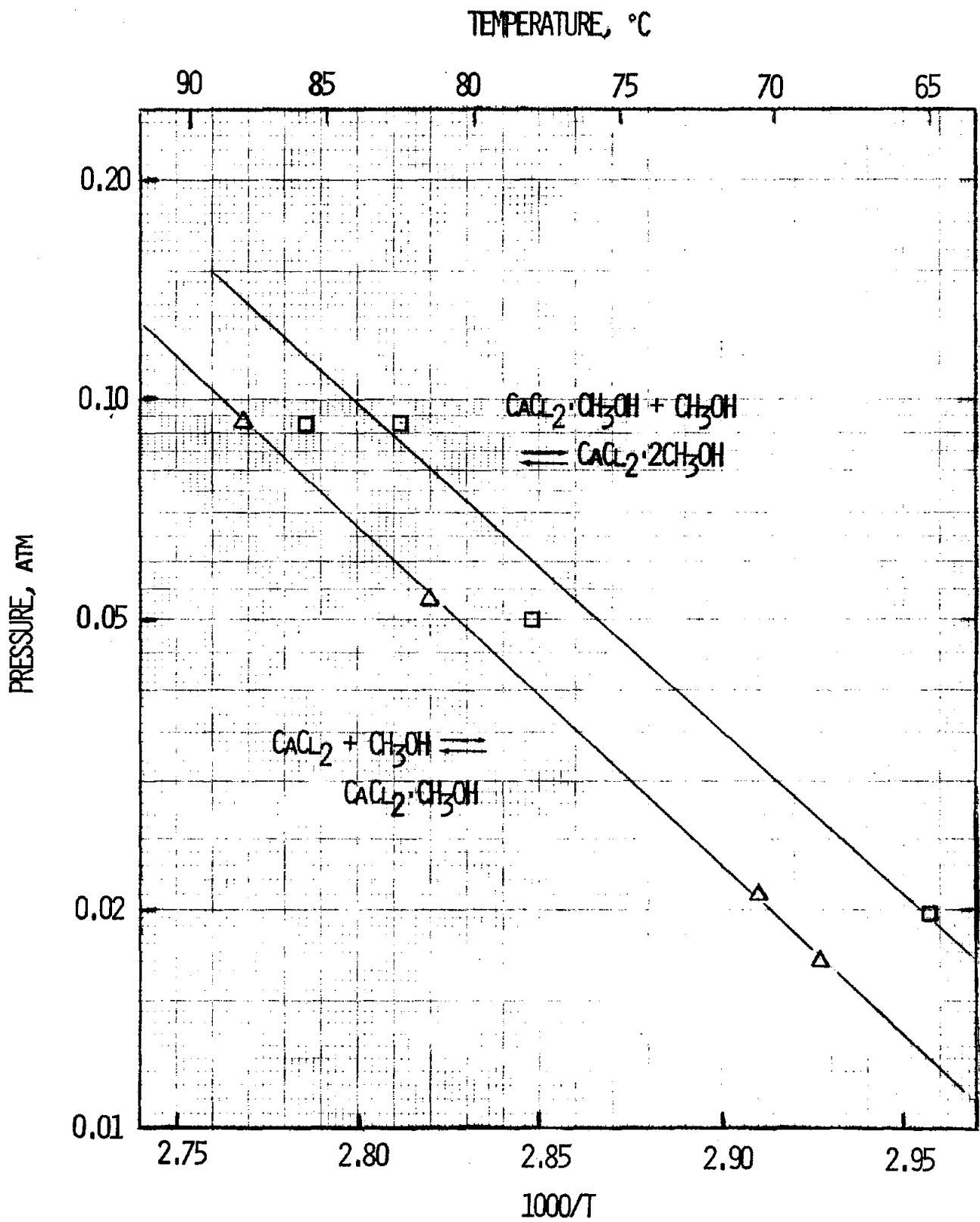
Fig. 2: Equilibrium-pressure-temperature-composition relations for the reaction of $CaCl_2$ and CH_3OH.

$$CaCl_2 \cdot CH_3OH \; \overset{\rightarrow}{\leftarrow} \; CaCl_2 \cdot 2CH_3OH$$
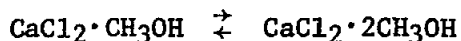
fit the equation

$$\ell nP = 24.16 - 9502/T \qquad\qquad (36)$$

within an average error of 1.5°C. For the first reaction, $\Delta H = 21$ kcal/mole and $\Delta S = 54$ cal/mole-°C; for the second reaction, $\Delta H = 19$ kcal/mole and $\Delta S = 48$ cal/mole-°C. In both cases, ΔS is considerably higher than we had expected. A survey we have made of salt hydrate reactions indicates that $\Delta S = 35.7 \pm 1.6$ cal/mole-°C; for the ammoniates, $\Delta S = 31.8 \pm 1.5$ cal/mole-°C. Since the data presented here are not of high accuracy, and since the temperature range investigated is rather small, the actual entropy changes for the reactions of $CaCl_2$ with CH_3OH may be considerably smaller than reported here. Assuming a possible error of ± 2°C in the estimation of the equilibrium temperature, the data are consistent with entropy values between 37 and 70 cal/mole-°C, and enthalpy values between 17 and 27 kcal/mole.

2.2 Kinetics of Methanolation of CaCl₂ Powder

Studies on the reaction of $CaCl_2$ with CH_3OH vapor were carried out in the Cahn RG microbalance. Initially, the $CaCl_2$ complex was partially demethanolated by heating the salt sample and removing the vapor under vacuum. The temperature of the oil bath was then reduced to the desired temperature, and the salt sample was maintained at this temperature for at least an hour while still under vacuum to allow the salt sample to come to thermal equilibrium with the bath. Methanol vapor was then introduced into the system by opening a valve connected to the CH_3OH pool, thermostatted at -10°C, +5°C, or +15°C. The rate of reaction was monitored by recording the sample mass.

Results of these experiments are given in Figures 3-9. Figures 3 and 4 illustrate the course of reaction at a vapor pressure of 14 torr, corresponding to the CH_3OH pool at -10°C. When the temperature of the oil bath surrounding the salt was 29°C, reaction was quite rapid, with reaction roughly 90% complete in 45 minutes. However, with the oil bath at 38°C, two distinct reactions can be seen, the first,

$$CaCl_2 + CH_3OH \;\rightarrow\; CaCl_2 \cdot CH_3OH \qquad\qquad (37)$$

reaching completion in 4 hours, and the second requiring an additional 11 hours to reach 80% completion. At 50°C, at least three separate steps can be seen: first, a nucleation-type reaction requiring ca. 1-2 hours; the second, reaction (37) above, requiring another 2 hours; and the third step, possibly consisting of both nucleation and reaction, requiring over 24 hours.

19
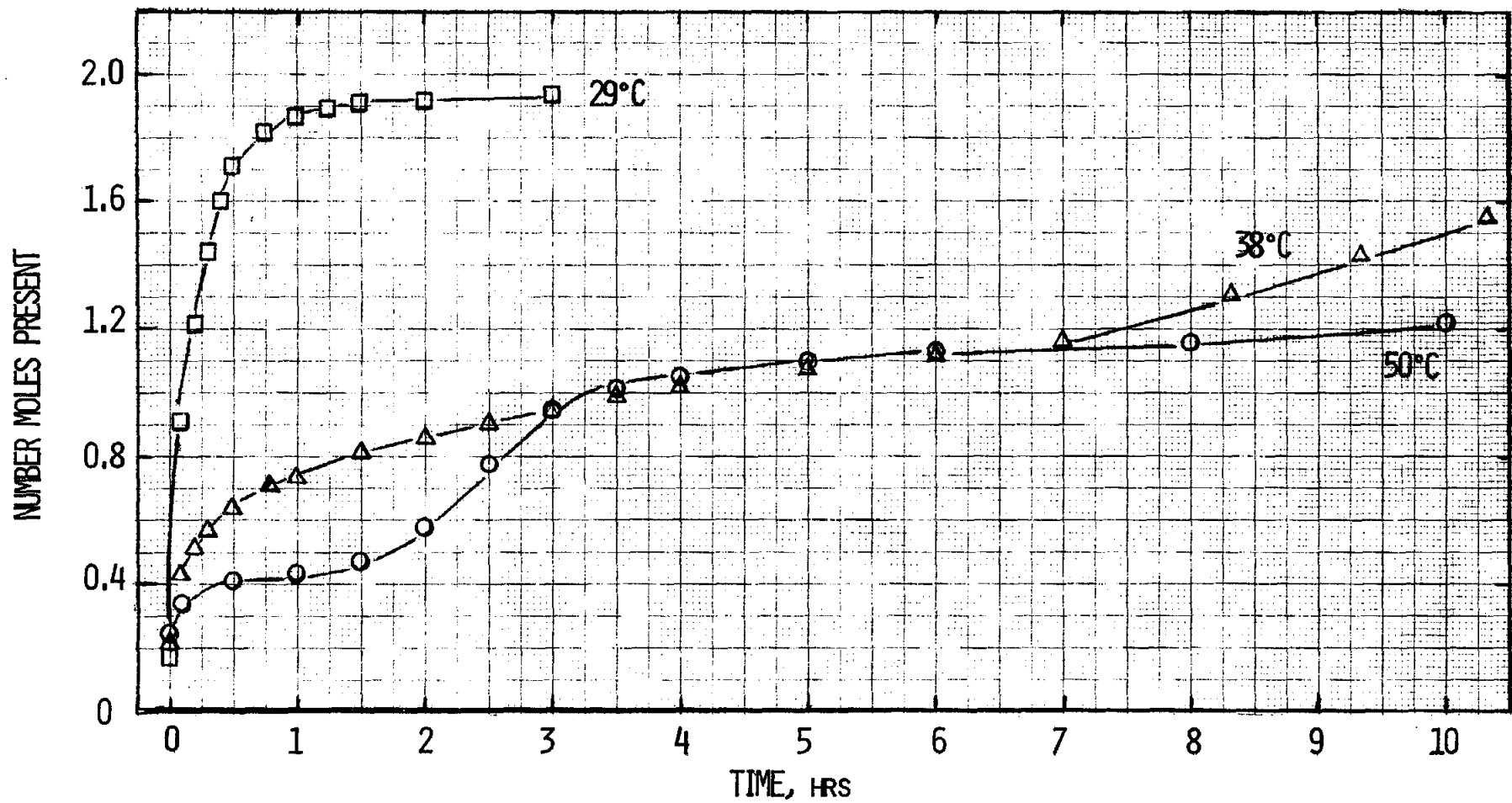
Fig. 3: Absorption kinetics of $CaCl_2$ with CH_3OH at 14 torr as a function of bed temperature.

20
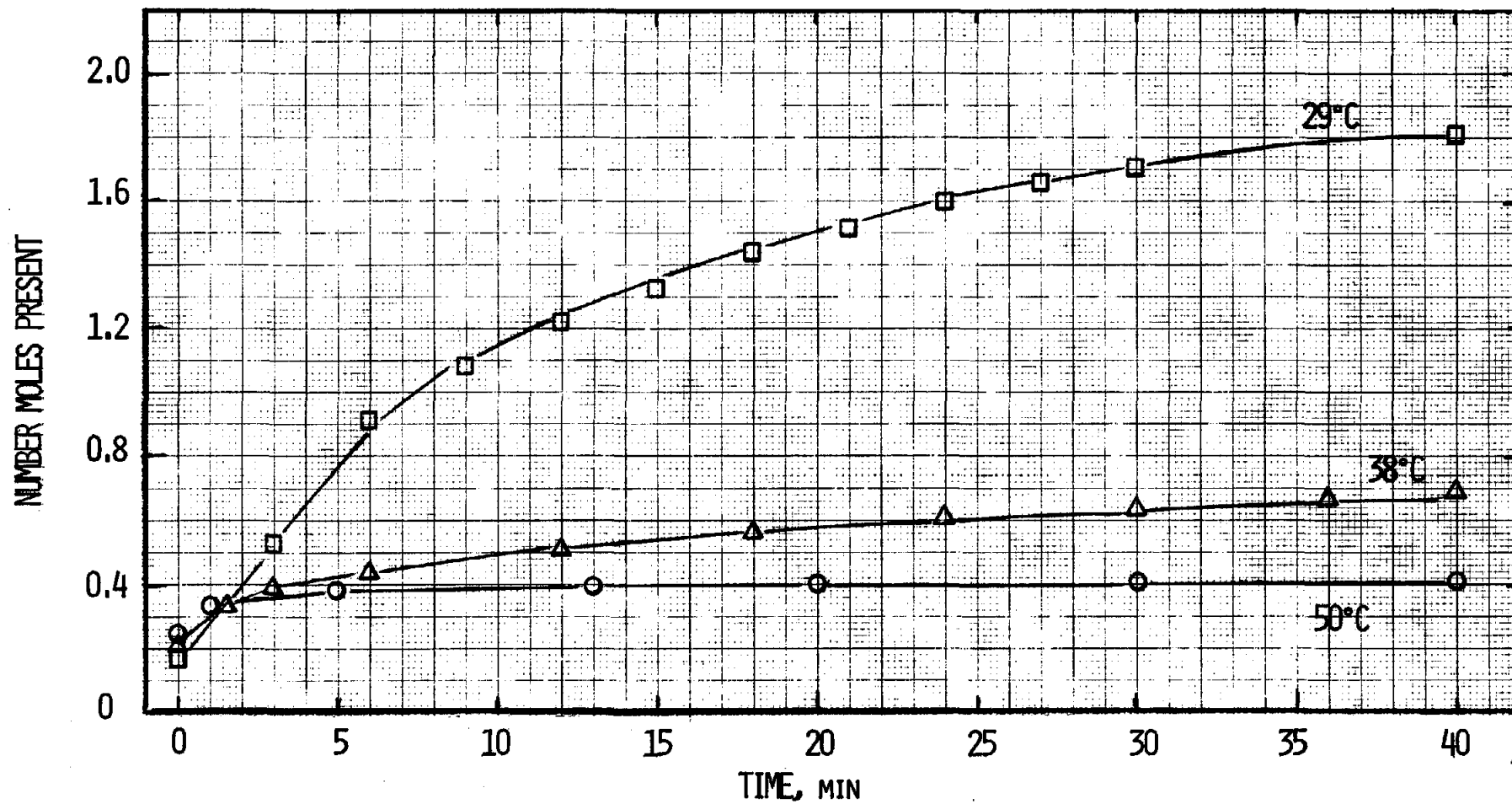
Fig. 4: Initial absorption of $CaCl_2$ at different temperatures while CH_3OH pool was maintained at -10°C.

Figures 5 and 6 illustrate the reaction course at 37 torr, corresponding to the CH_3OH pool at 5°C. The reaction is rapid at oil bath temperatures below 60°C; however, above 60°C, only reaction (37) was observed, and the deceleration in rate was dramatic. When the CH_3OH pool temperature was raised to 15°C (70 torr), reaction was 90% complete in 12 minutes at 50°C, in 50 minutes at 60°C, and in 20 hours at 70°C (Figures 7 and 8).

A comparison of reaction rates at a constant salt-bed temperature is shown in Figure 9. Here the oil bath is maintained at ca. 50°C, while the CH_3OH pool is at +15, +5, and -10°C, respectively. In all cases, the rate of reaction (37), addition of the first mole of CH_3OH, is more than adequate. However, between +5°C and -10°C, the rate of addition of the second mole is sharply reduced. According to the results presented in 2.1, the equilibrium pressure of CH_3OH vapor for addition of the first mole at 50°C is ca. 2 torr, and for the second mole ca. 3.6 torr. Thus, at the experimental pressures, 70, 37, and 14 torr respectively, there is a substantial driving force for reaction, and it is somewhat surprising that the reaction rate decreases so sharply with decreasing vapor pressure.

It should be noted that in the experimental arrangement used, the temperature of the salt cannot be monitored accurately, and thermal equilibrium between the salt and the oil bath may be slow. Since the reaction of $CaCl_2$ and CH_3OH is highly exothermic, the actual salt-bed temperatures may be higher than the oil bath temperatures reported here. However, this effect only causes our estimate of the reaction temperature to be on the conservative side. In any event, the heating effect should be small except at the higher reaction rates.

2.3 Interpretation of the Rates

It is quite difficult to derive a mechanism and obtain rate constants from a reaction as complex as we observe here. For a simple one-step reaction of the type

$$CaCl_2 + 2CH_3OH \rightleftarrows CaCl_2 \cdot 2CH_3OH \qquad (38)$$

i.e.,
$$A + 2G \rightleftarrows C \qquad (39)$$
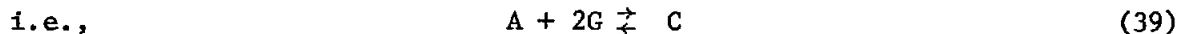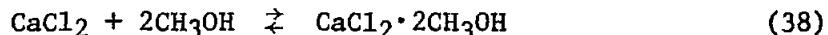
one might expect a first-order rate law when the reaction is carried out at constant pressure. In such a case, a rate law of the general type

$$\frac{dx}{dt} = k(2-x) \qquad (40)$$

22
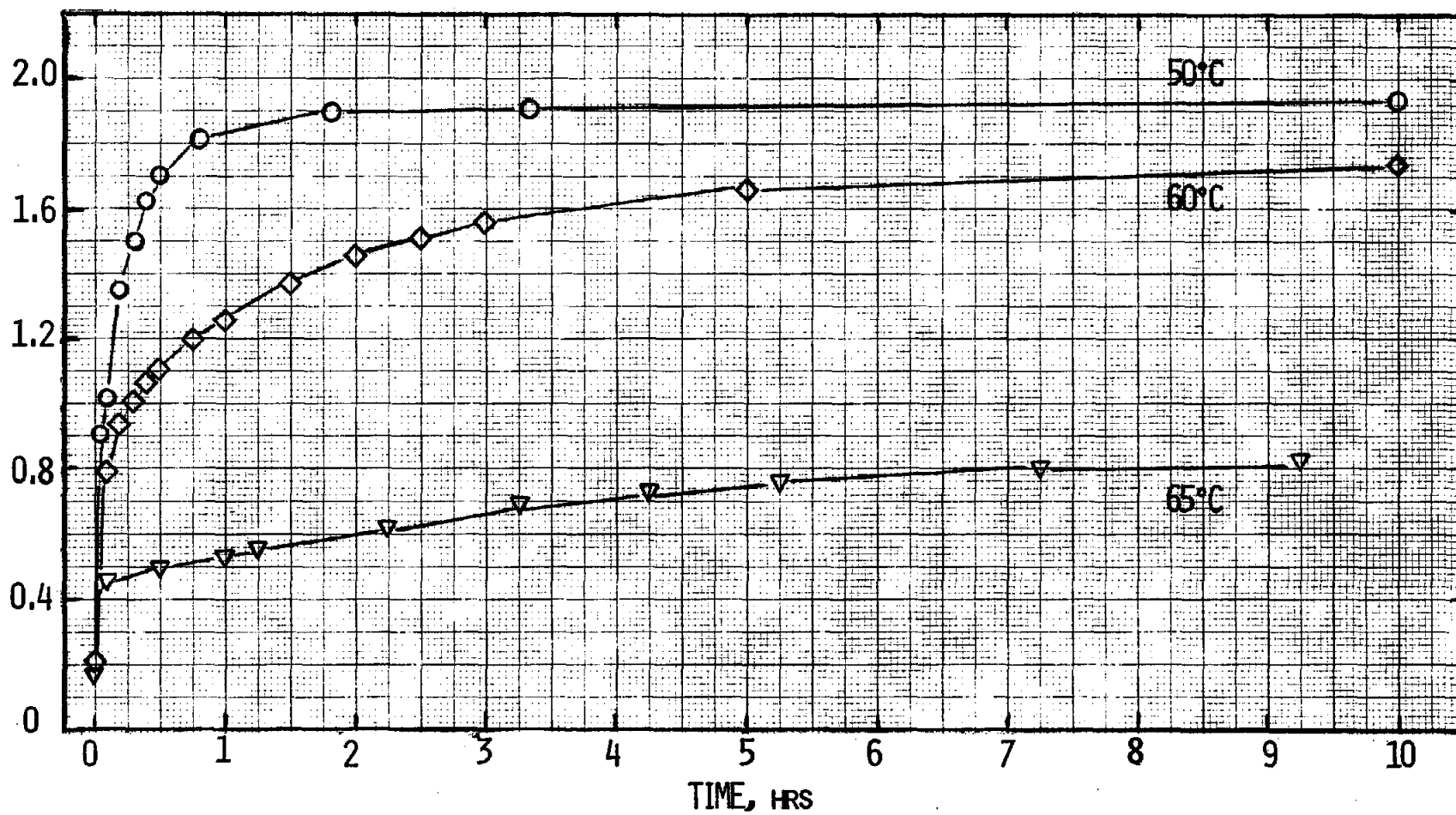
Fig. 5: Absorption kinetics of $CaCl_2$ with CH_3OH at 38 torr as a function of bed temperature.
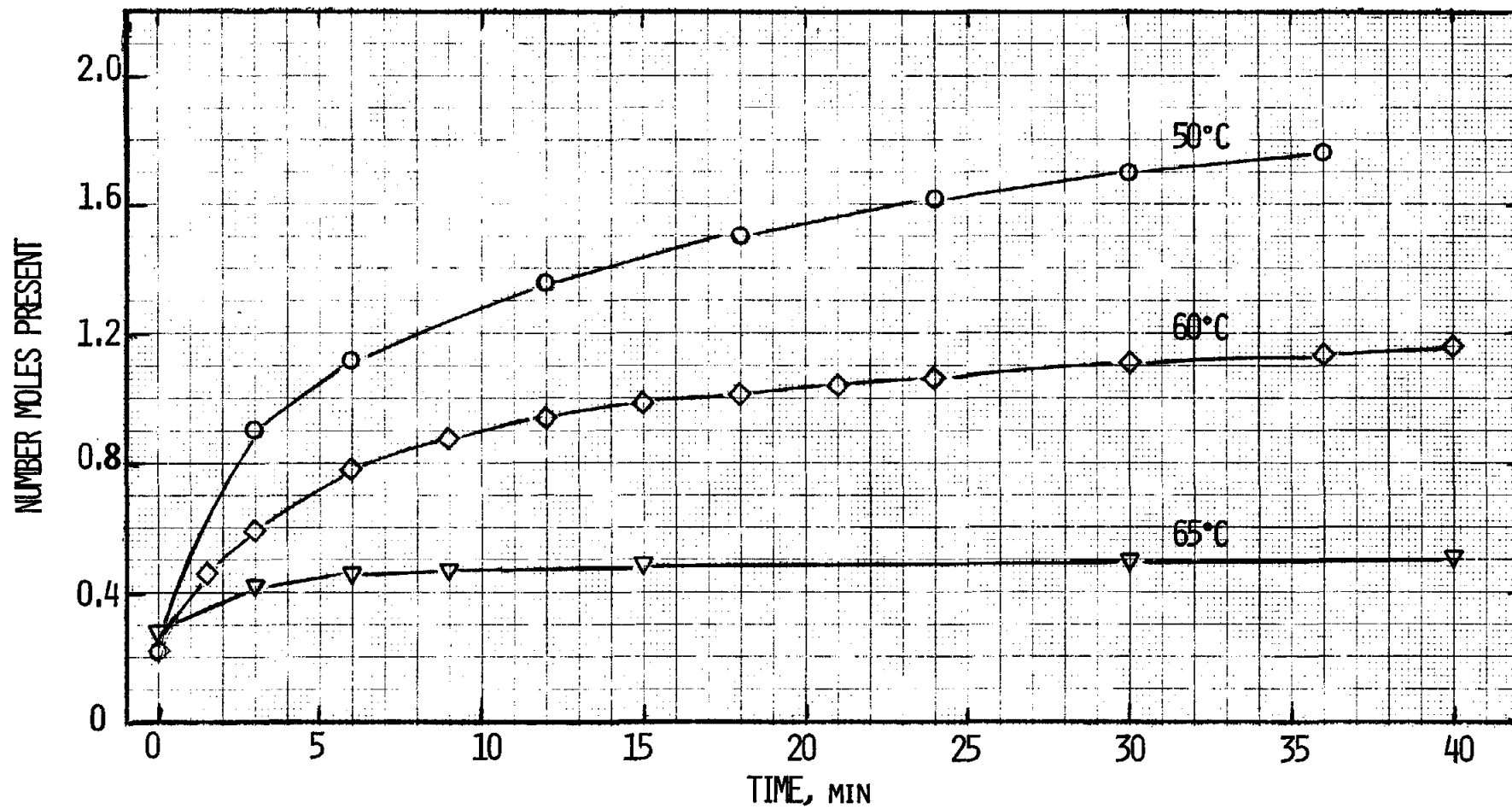
Fig. 6: Initial absorption of CaCl₂ at different temperatures while CH₃OH pool was maintained at +5°C, i.e., 38 torr.
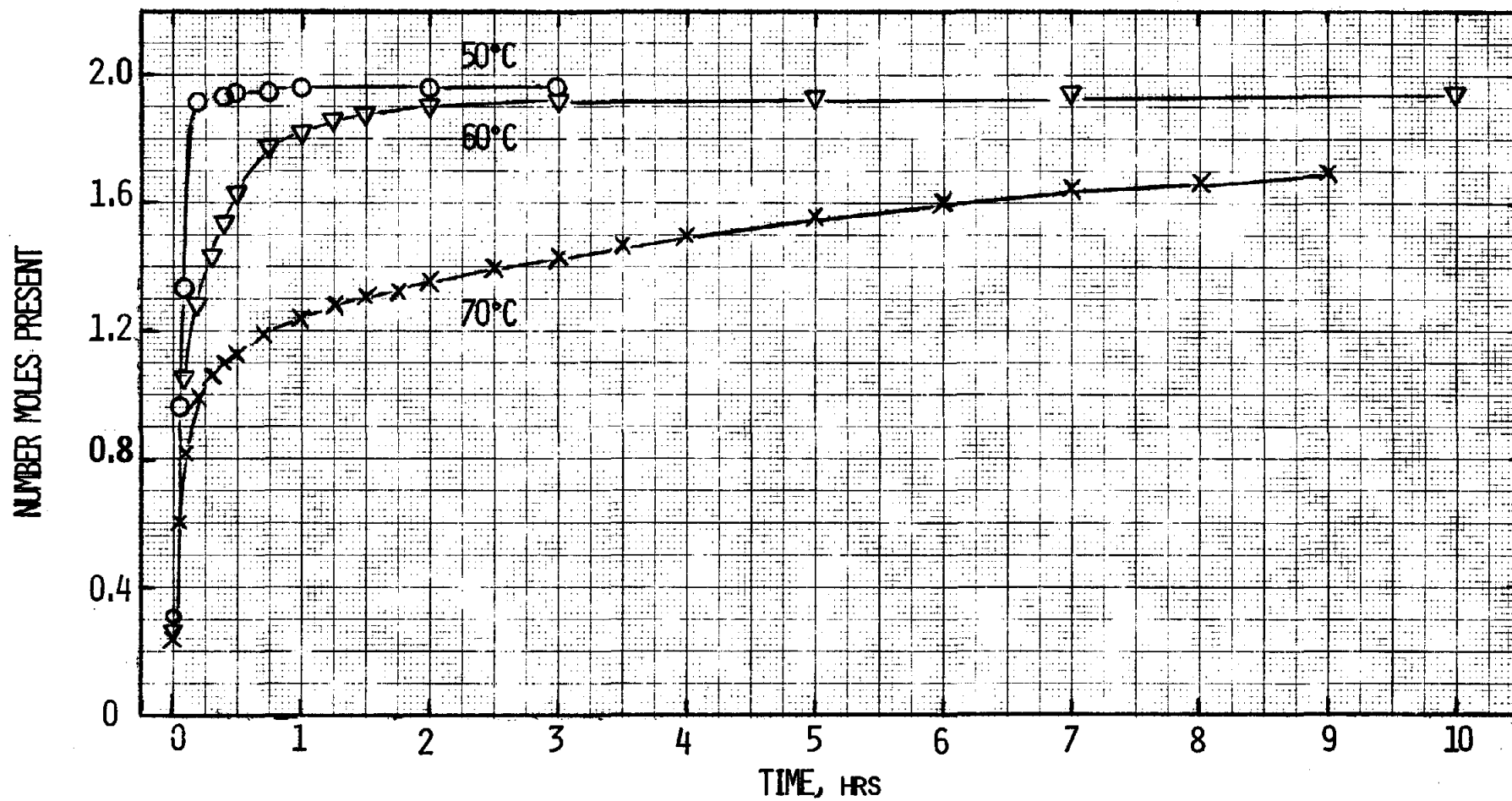
Fig. 7: Absorption kinetics of $CaCl_2$ with CH_3OH at 70 torr as a function of bed temperature.
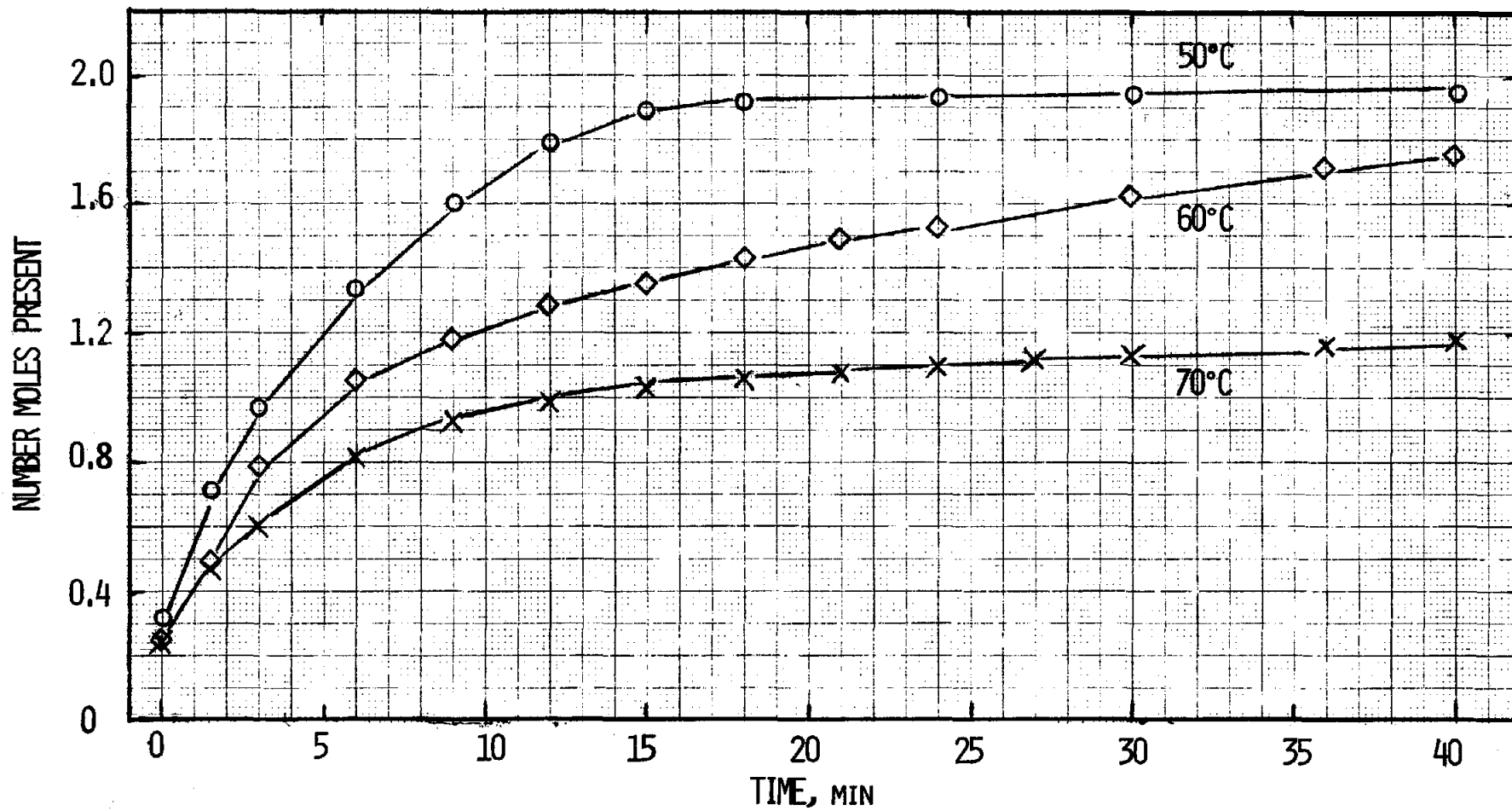
Fig. 8: Initial absorption of $CaCl_2$ at different temperatures while CH_3OH pool was maintained at +15°C, i.e., 70 torr.
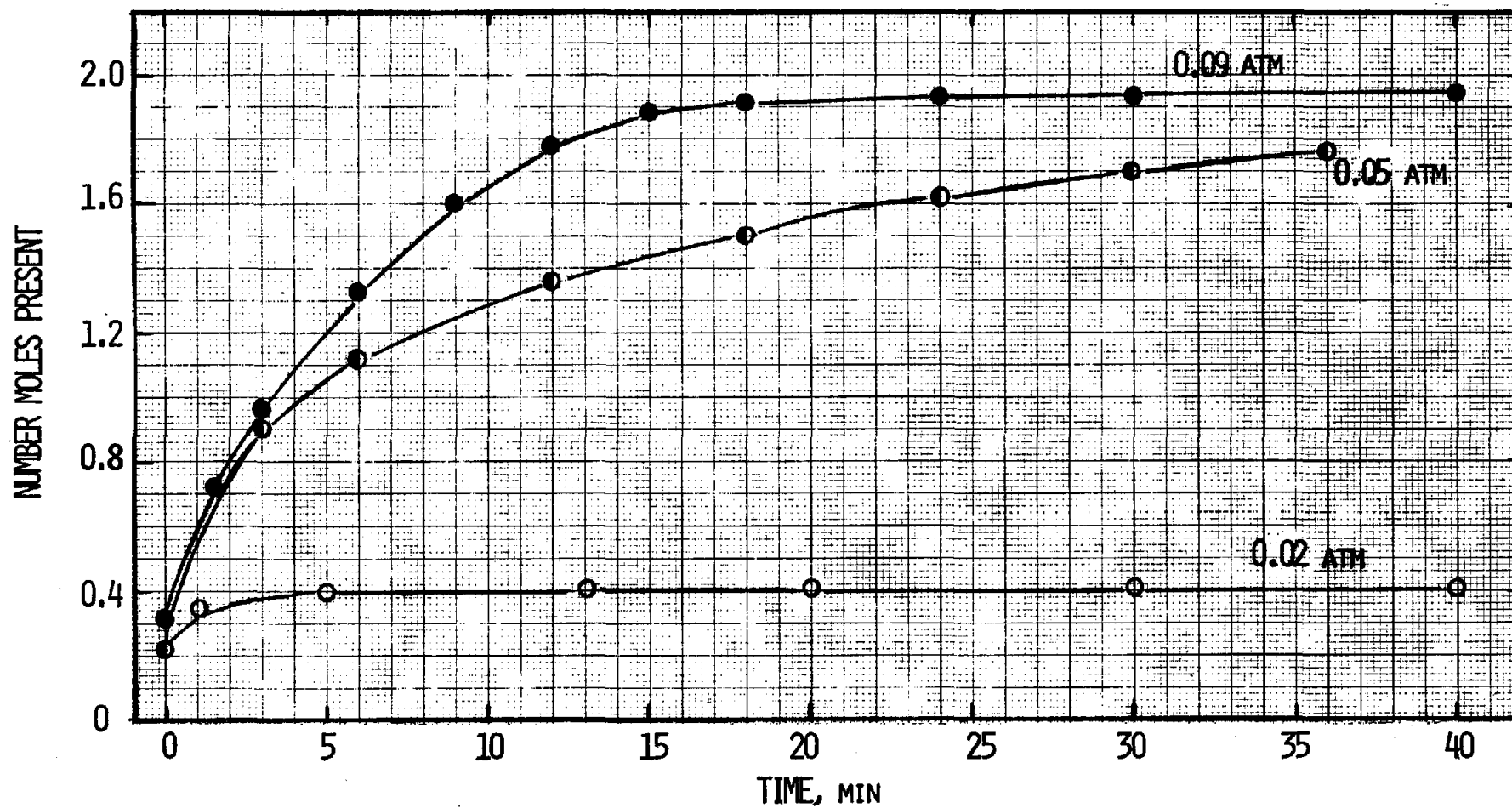
Fig. 9: Comparison of absorption kinetics of $CaCl_2$ at 50°C as a function of CH_3OH pressure.

should be found, where x is the number of moles of CH_3OH reacted per mole of $CaCl_2$. In integrated form, we obtain

$$\ln\left(1 - \frac{x}{2}\right) = -kt \qquad (41)$$

We have plotted this function in Figures 10 and 11 for data obtained at 70 torr and at 14 torr. A straight-line function versus time was found in only one case, for the data taken at 70 torr and 50°C, where the rate constant was approximately 11 hr^{-1}. This was the fastest rate observed. In two other cases -- 70 torr, 60°C, and 14 torr, 29°C -- the data fall in two straight-line segments, with the "knee" occurring close to the point at which x = 1. The rate constants for the second (slower) part of the reaction were approximately 2.3 hr^{-1} and 2.8 hr^{-1} respectively. However, in the slowest case for which we have reasonably complete data (14 torr, 38°C), three distinct reactions can be seen, with the slowest segment (k = 0.06 hr^{-1}) occurring in the region around x = 1, and a faster segment (k = 0.22 hr^{-1}) occurring after ca. x ≈ 1.25.

The existence of logarithmically straight segments is consistent with a series of first-order reactions of the type

$$A + G \rightleftarrows B$$
$$B + G \rightleftarrows C \qquad (42)$$

However, it can be shown that the data taken at 14 torr and 38°C are inconsistent with this scheme. The slow linear segment around x = 1 requires, at a minimum, a "nucleation" type event in which the intermediate B (i.e., $CaCl_2 \cdot CH_3OH$) rearranges to an "active" form B':

$$A + G \rightleftarrows B \rightleftarrows B'$$
$$B' + G \rightleftarrows C \qquad (43)$$
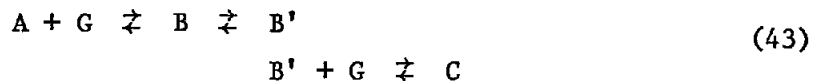
Furthermore, the "knee" seen in Figure 3 for the data taken at 14 torr and 50°C implies an additional nucleation type event involving A. Thus, the actual mechanism for the overall reaction appears quite complex, although it seems possible that the individual reactions that make up the sequence are first-order. Unfortunately, it appears that this complexity will prevent us from obtaining individual rate constants and activation energies, and accurate extrapolation of these data to other conditions of pressure and temperature does not appear possible. Nevertheless, the data are sufficiently complete that we will be able to estimate the useful range of operating pressures and temperatures for the heat pump.
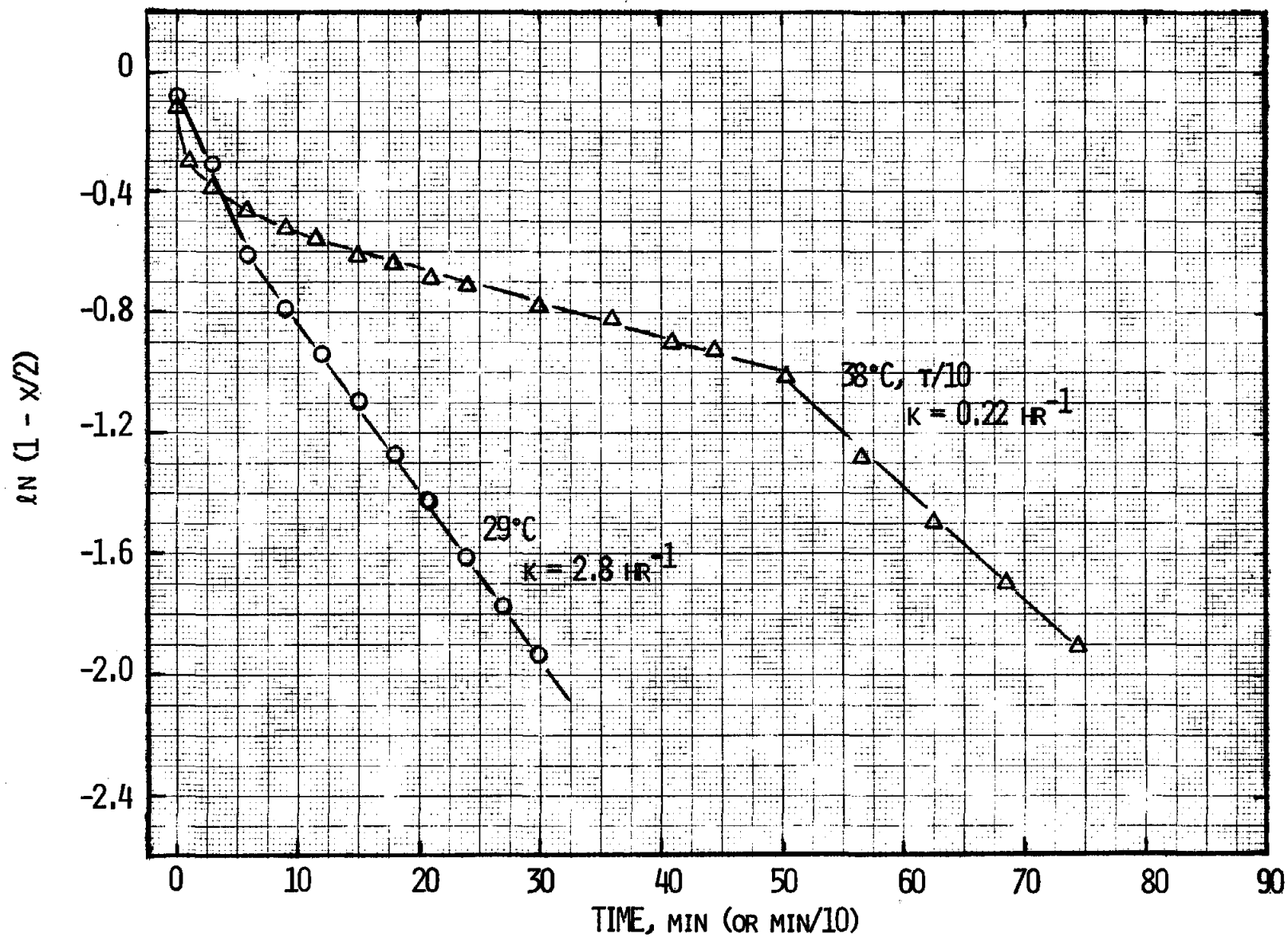
Fig. 10: Rates of CH$_3$OH absorption at 14 torr, -10°C, as a function of CaCl$_2$ bed temperature.
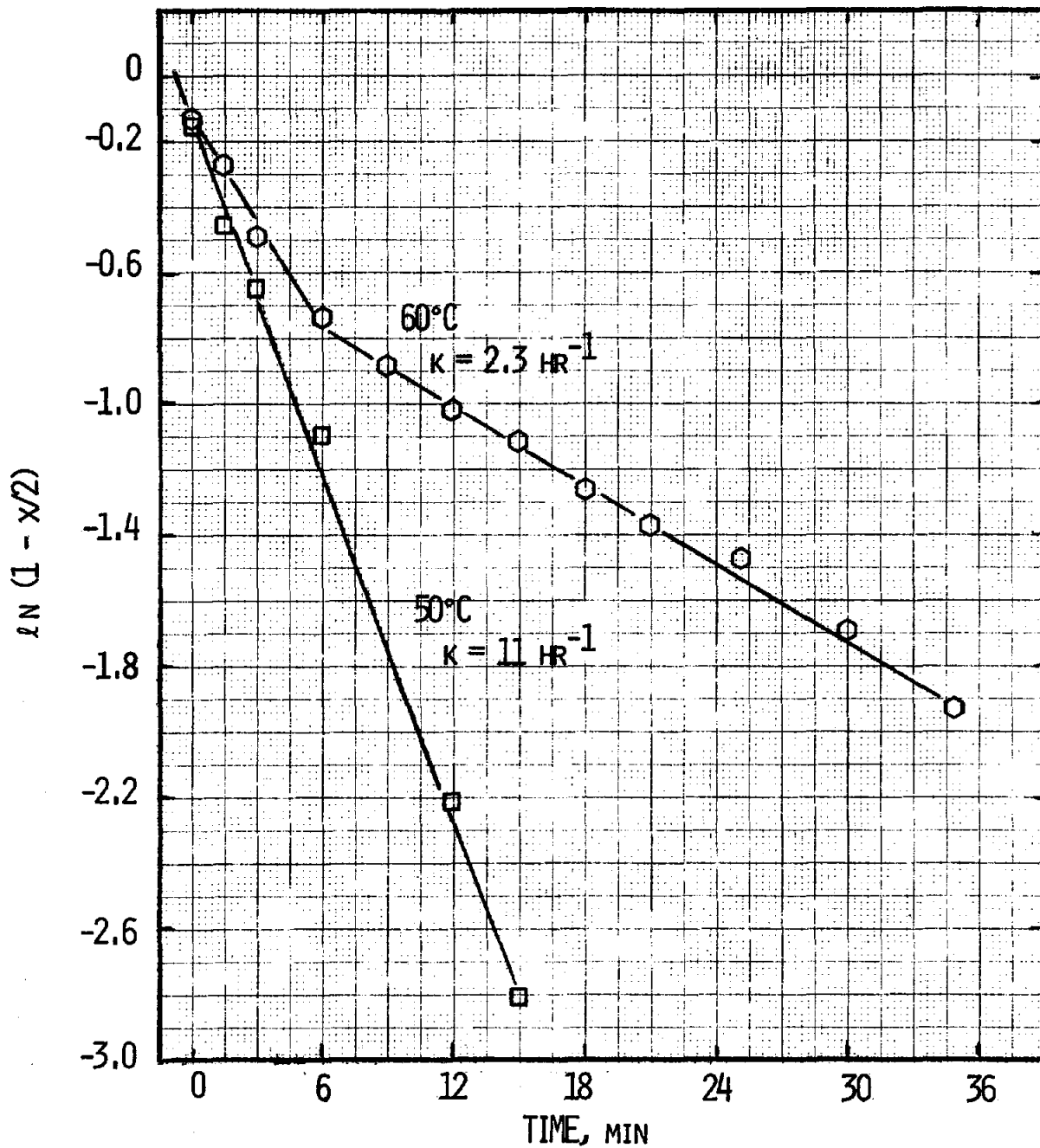
Fig. 11: Rate of CH_3OH absorption at 70 torr as a function of $CaCl_2$ bed temperature.

2.4 Kinetics of Methanolation of CaCl₂ Pellets

One of the potential obstacles to development of a heat pump storage system based on a solid-phase absorbent is a loss of thermodynamic driving force (i.e., CH_3OH pressure) caused by a pressure drop as the CH_3OH vapor passes through a bed of salt. Preliminary calculations indicate that this pressure drop could become serious when the average particle size in the bed falls below 20 μm, or when the bed depth exceeds an inch. Furthermore, it is likely that repeated methanolation/demethanolation cycling could cause the salt particles to fragment, thus gradually reducing the particle size. For this reason, some thought was given to the use of $CaCl_2$ pellets, held together with an appropriate binder, as is commonly done for $CaCl_2$ desiccants. Such pellets would provide a path for vapor flow, thus eliminating any pressure drop from the top to the bottom of the bed, and beds of substantial thickness could be used -- at least several inches. Furthermore, the use of a binder should help prevent particle fragmentation and dusting. The major question regarding the use of desiccant pellets is whether their intrinsic rate of reaction with CH_3OH vapor is sufficiently rapid.

Methanolation experiments on $CaCl_2$ pellets were carried out in the microbalance. In each case, the temperature of the salt was maintained at 50°C, while the CH_3OH pool was maintained at 5°C. Experiments were undertaken with 4, 12, and 100 mesh $CaCl_2$ from several different sources. The 4 mesh material (particle diameters ca. 5 mm) was Mallinckrodt anhydrous porous desiccant unanalyzed. The 12 mesh (particle diameters ca. 1.5 mm) was Baker analyzed reagent of 95.0% assay. The 100 mesh (particle diameters ca. 0.15 mm) was Mallinckrodt analytical reagent $CaCl_2 \cdot 2H_2O$ (assay 74-78% $CaCl_2$) which was sieved through a 100 mesh screen and then oven dried.

The results of these absorption experiments are shown in Figures 12-16. In each case, the rate of methanolation was substantially faster for the second and third absorption cycle than for the first cycle. In Figures 12 and 14, it can be seen that the rate of absorption in the second and third cycles is approximately the same. This is not the case for the 4 mesh material (Figure 15); however, the rate of reaction in the first cycle was so slow that it was necessary to force the reaction by subsequently reducing the salt bed temperature to 30°C. Thus, preconditioning was not complete after the first cycle in this case.

The results shown in Figure 13 for 100 mesh material seemed anomalously slow. It was subsequently determined that the salt had not been completely dehydrated prior to methanolation. As can be seen in Figure 12, methanolation of more carefully dehydrated material is much more rapid. However, the absorption rate comparison shown in Figure 16 still indicates an anomaly: while the reaction rate generally increases with decreasing particle size as expected (powder > 100 mesh > 12 mesh), the 4 mesh material reacted faster than the 12 mesh, which is unexpected. This result may be related to the source or type of the material: the
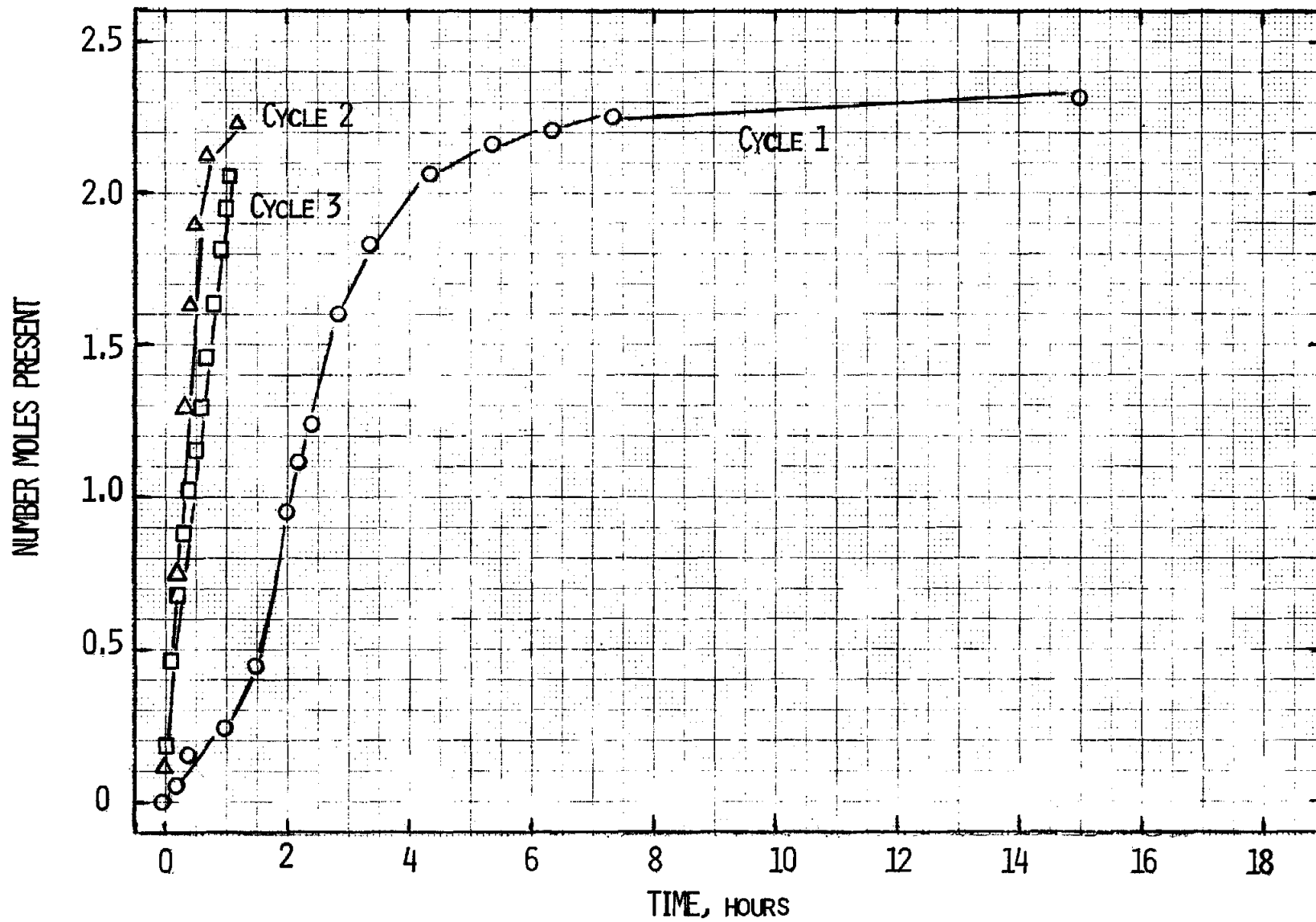
Fig. 12: Absorption of 100 mesh $CaCl_2$ at 50°C while CH_3OH pool was maintained at +5°C.

32
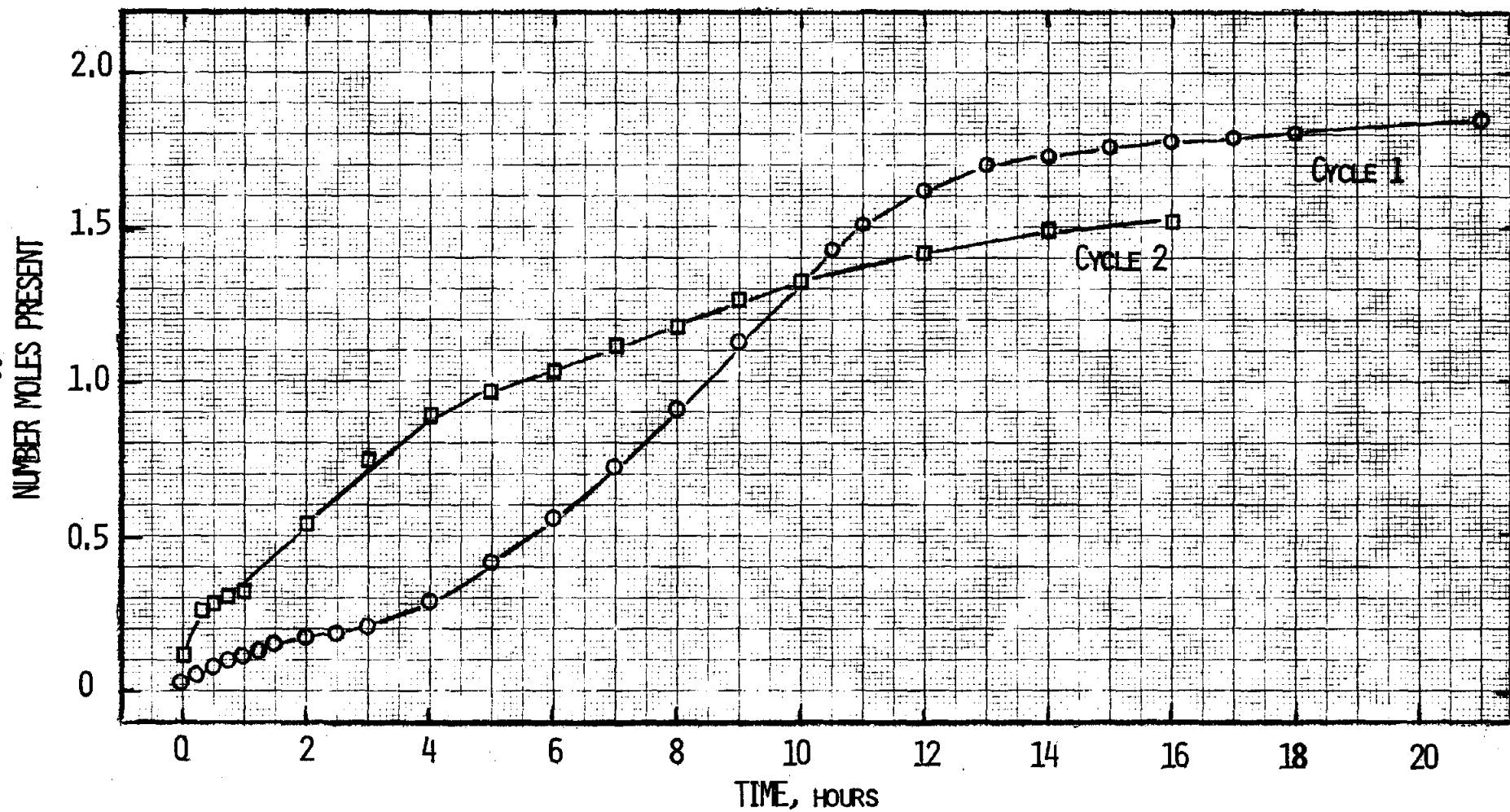
Fig. 13: Absorption of 100 mesh $CaCl_2$ sample not completely dehydrated at 50°C while CH_3OH pool maintained at +5°C.
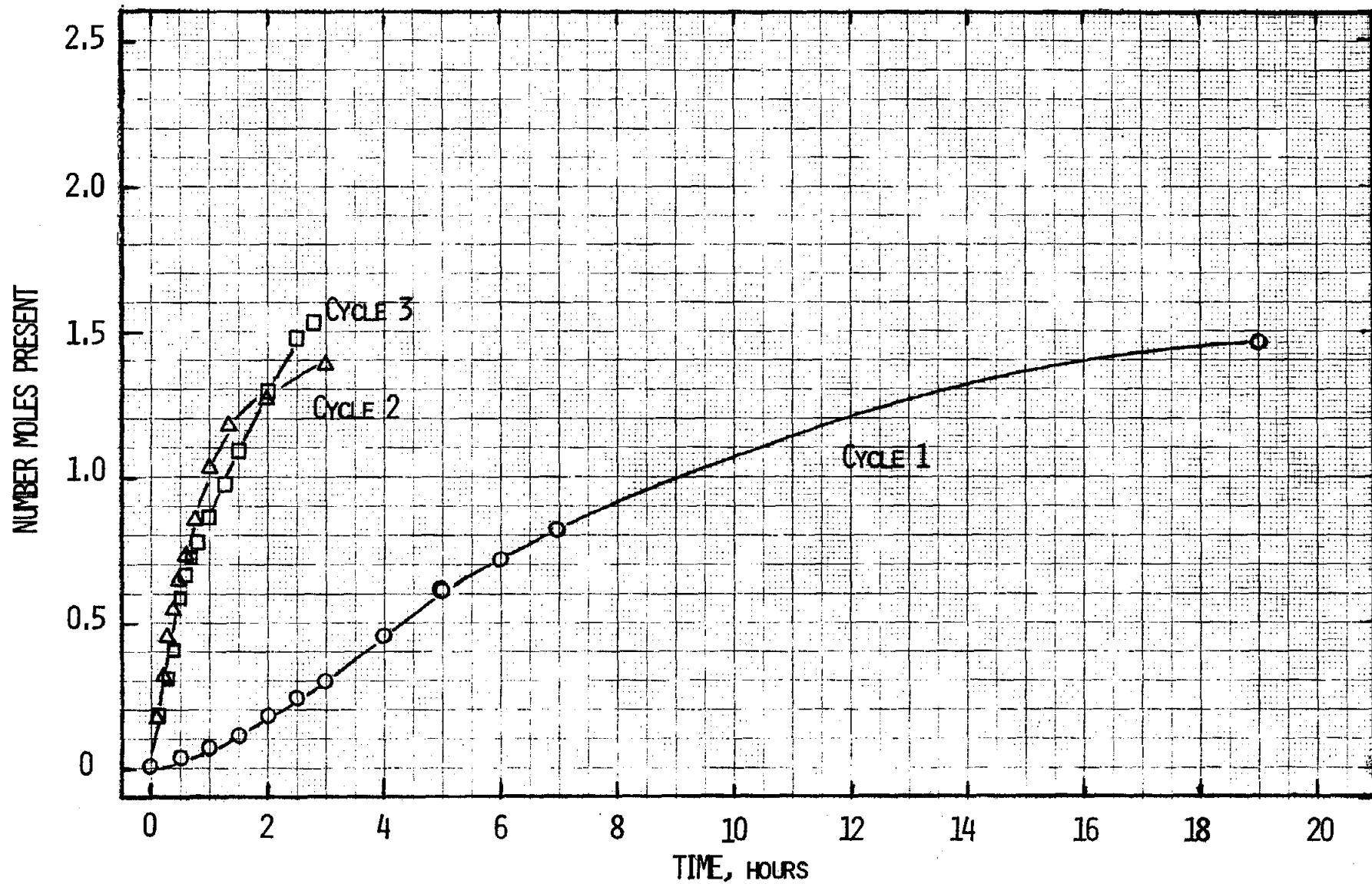
Fig. 14: Absorption of 12 mesh $CaCl_2$ at 50°C while CH_3OH pool was maintained at +5°C.
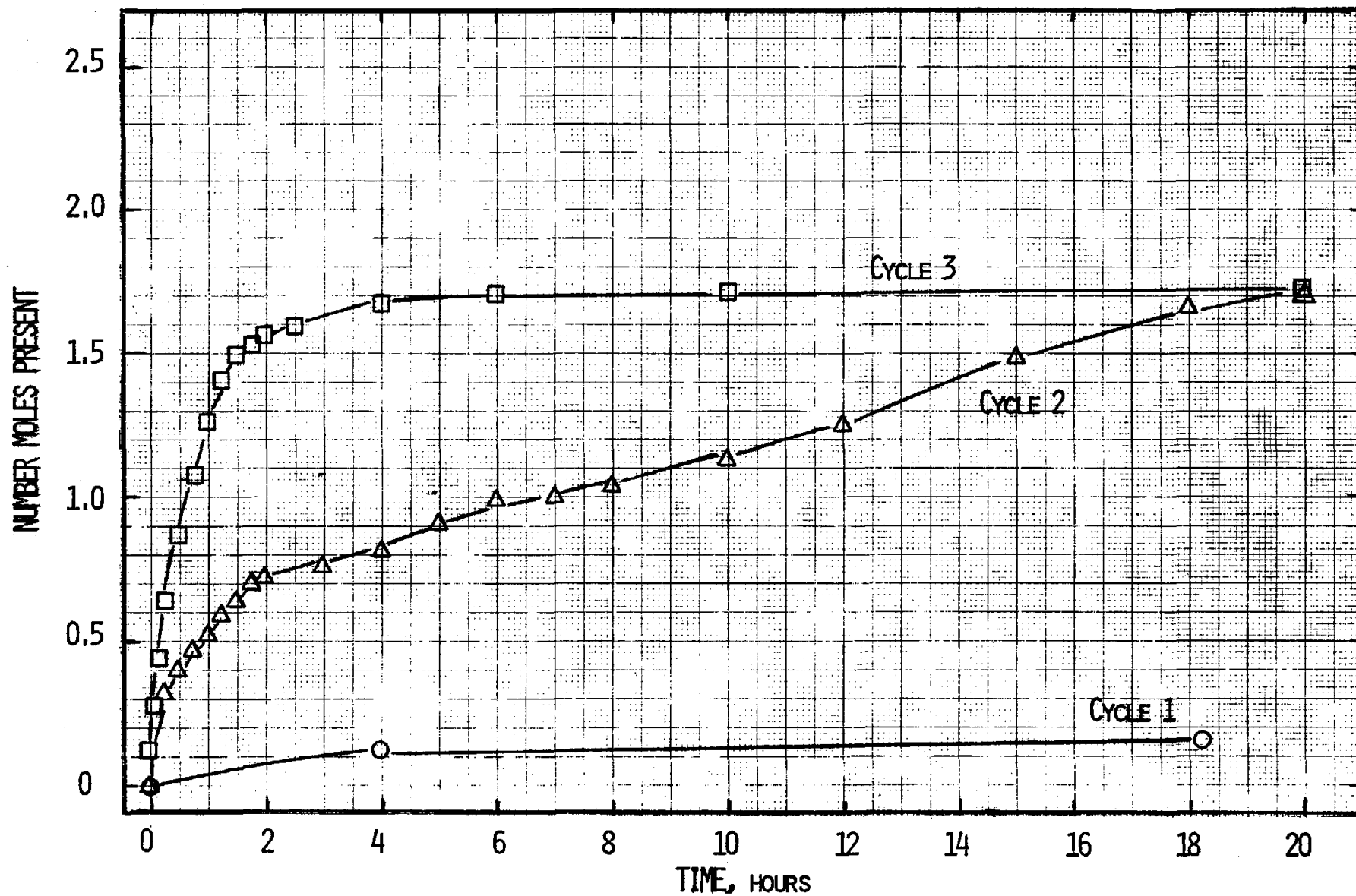
Fig. 15: Absorption of 4 mesh $CaCl_2$ at 50°C while CH_3OH pool was maintained at +5°C.
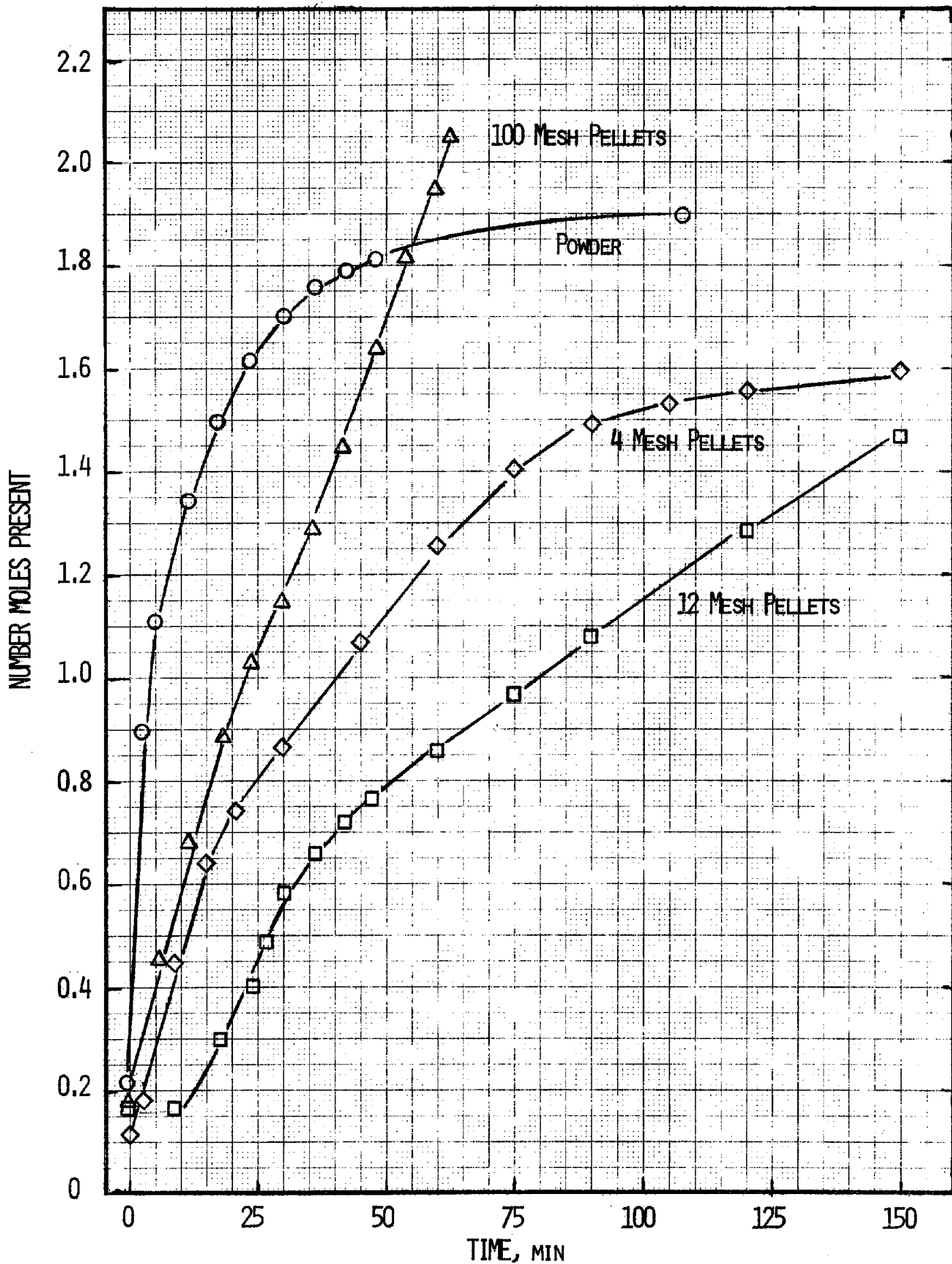
Fig. 16: Comparison of 3rd cycle absorptions of CaCl₂ at 50°C while CH₃OH pool at +5°C.

36

Baker 12 mesh assay of 95% was by silver titration. We do not have an accurate estimate of the amount of binder material which may be present in the different meshes.

Two other points are worth noting. First, the extent of absorption ranged from 2.3 moles of CH_3OH (100 mesh) down to 1.55 moles (12 mesh). This effect is probably associated with the purity of the absorbing material, although it is not understood why the extent of reaction sometimes exceeded 2 moles of CH_3OH per mole of $CaCl_2$. Second, it was observed that the $CaCl_2$ swelled substantially during the first cycle. This decrease in material density, and the associated increase in pore volume, is probably the origin of the increase in reaction rate after the first cycle.

The most important result of this study is that the absorption rates of all materials studied were considerably faster than would be required for operation of the heat pump/storage system. (This conclusion is, of course, limited to the operating temperatures employed.) Thus, it may be possible to use large-mesh $CaCl_2$ in the heat exchanger, and thereby increase the bed depth substantially.

2.5 Kinetics of Demethanolation of $CaCl_2$

Demethanolation experiments at fixed vapor pressure can be difficult to carry out when the pressure is above that necessary for condensation at room temperature: the entire experimental apparatus must be heated. Previous attempts to demethanolate at a vapor pressure corresponding to equilibrium with liquid at 40°C were unsuccessful in large part because it was difficult to maintain the entire TGA apparatus above 40°C.

In an effort to obtain a preliminary measure of the temperature required for desorption, an experiment was carried out at a vapor pressure (40 torr) corresponding to equilibrium with liquid at 5°C. As can be seen in Figure 17, the rate of desorption of a 4 mesh pellet at 95°C was relatively slow -- 14 hours for 80% reaction -- but only about a factor of 2 slower than the 8-hour rate necessary for the operation of a system with one day storage capacity.

Subsequent experiments were carried out at 184 torr, a vapor pressure corresponding to equilibrium with liquid at 33°C. When 4 mesh material was demethanolated at 110°C, the initial rate of reaction was reasonably fast (Figure 18), but only about one mole of CH_3OH was removed. To remove the second mole at a reasonable rate required an increase in temperature to 125°C.

A second demethanolation experiment, carried out at 130°C, showed no distinct break between removal of the two moles of CH_3OH. Furthermore, the reaction rate was considerably faster, with removal of the first mole requiring about half an hour (Figure 19). However, removal of the final ca. 0.3 moles of CH_3OH was very slow. (This effect is probably not
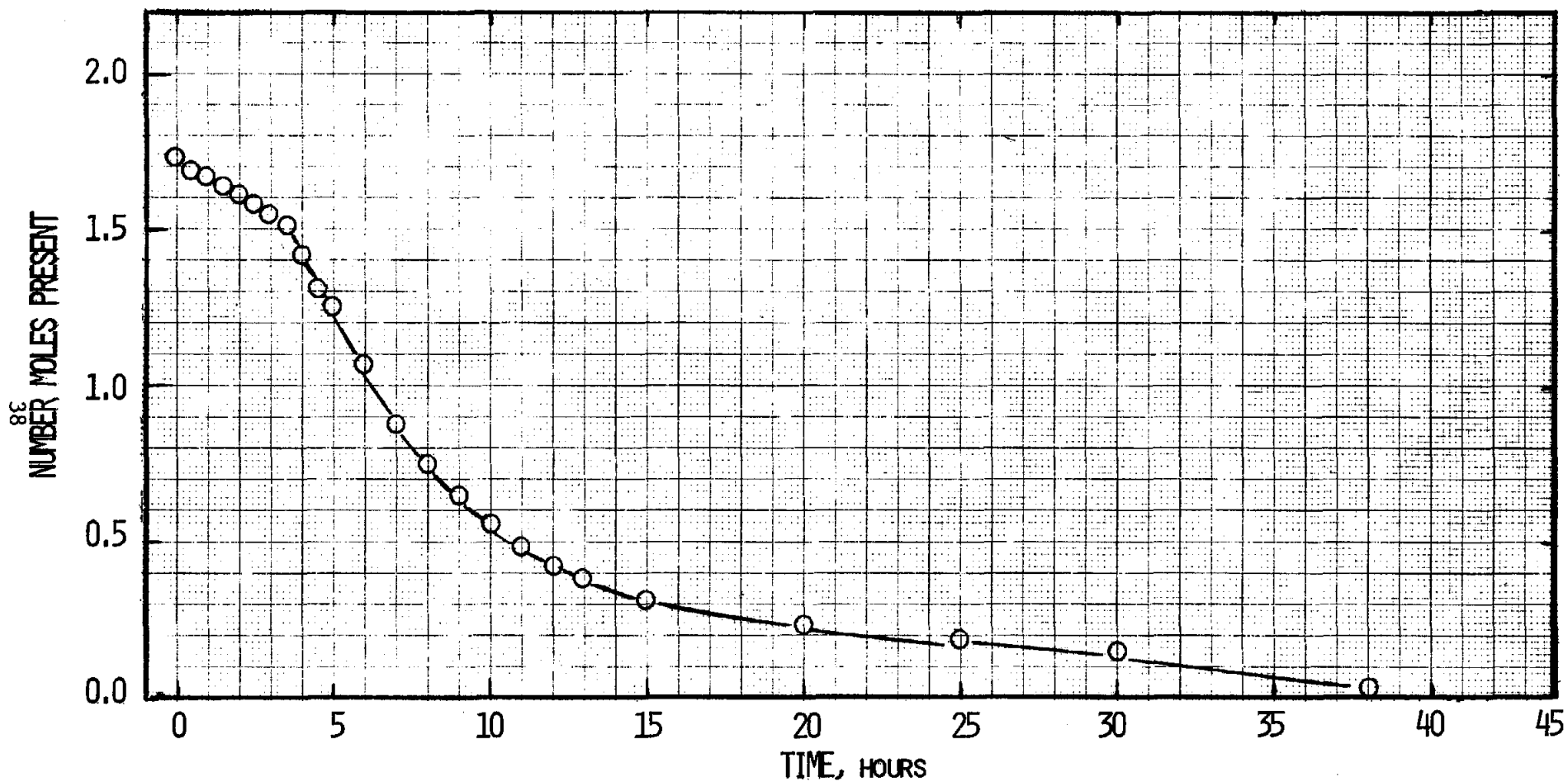
Fig. 17: Desorption of 4 mesh CaCl₂ pellet at 95°C while CH₃OH at +5°C.
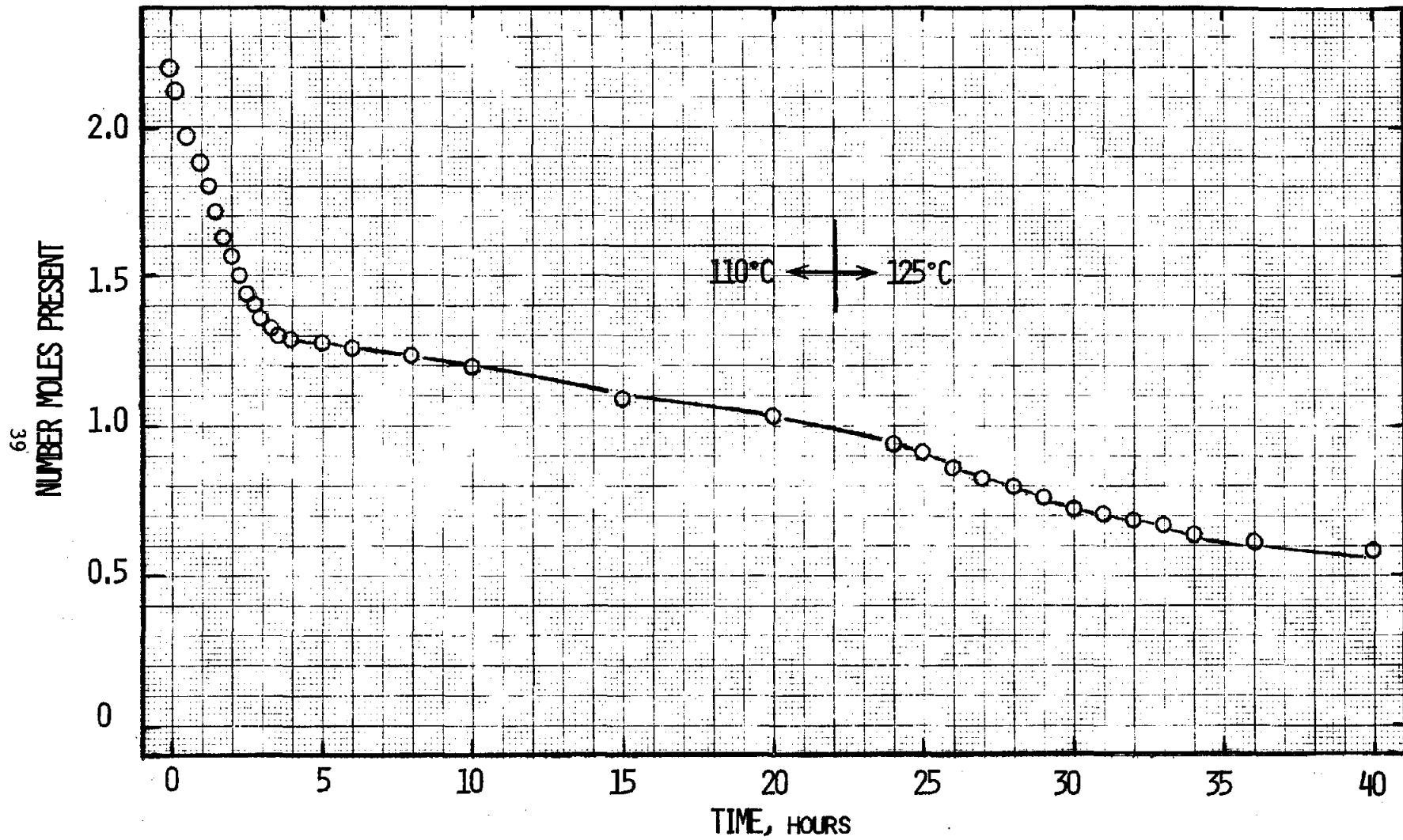
Fig. 18: Desorption of 4 mesh CaCl$_2$ at 110°C and then increased to 125°C while CH$_3$OH at +33°C.

39
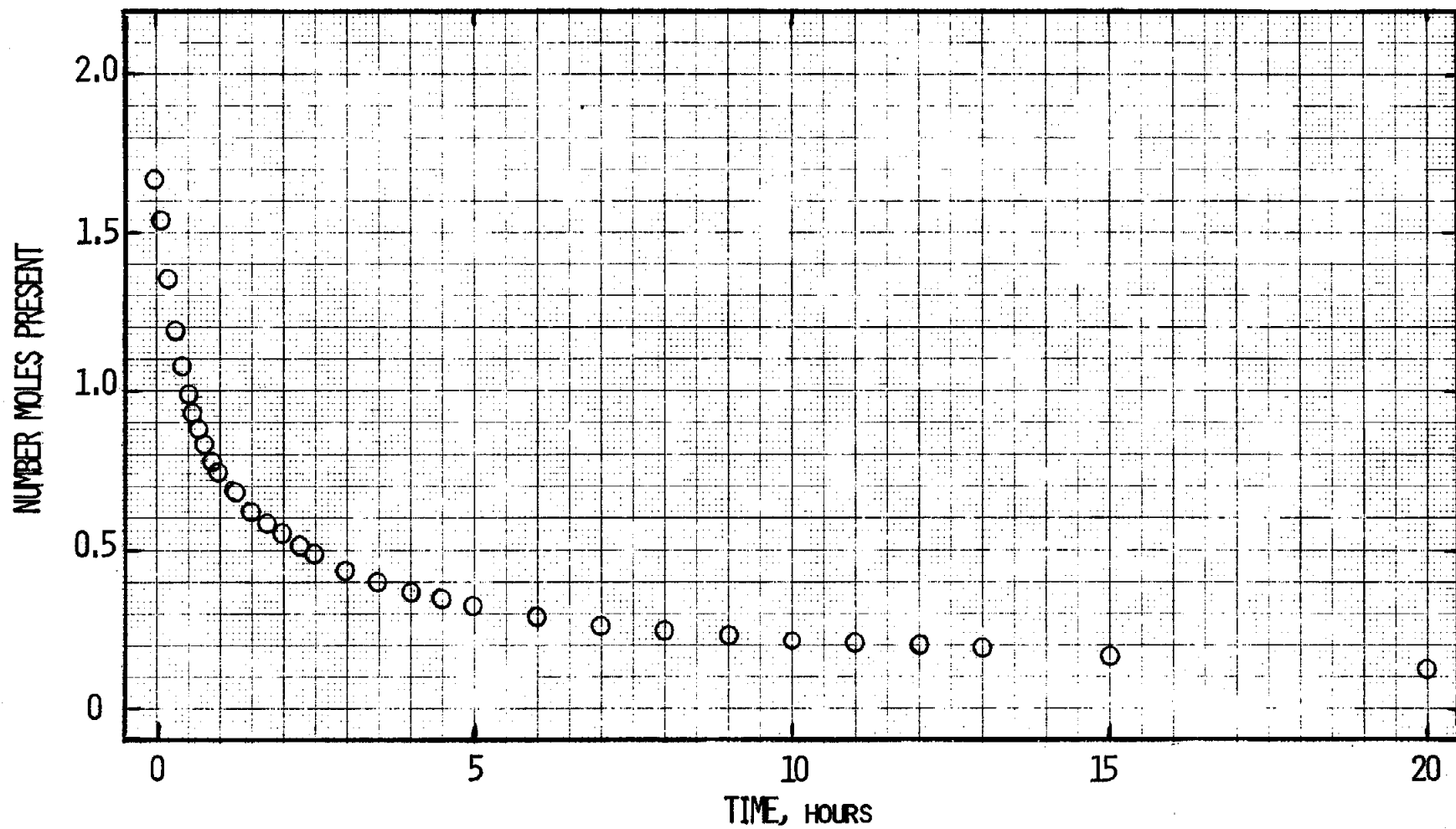
Fig. 19:   Desorption of 4 mesh $CaCl_2$ at 130°C while CH_3OH at 33°C.

important in practice, since the system could be operated between 0.3 and 1.7 moles of CH_3OH per mole of $CaCl_2$. Furthermore, reaction rates should be faster for finer-mesh material.)

A final demethanolation experiment was carried out at 140°C. As can be seen in Figure 20, all but the last 0.25 moles of CH_3OH were removed within two hours.

The initial rates of demethanolation of 4 mesh $CaCl_2$ at 184 torr are compared in Figure 21. These initial rates are consistent with the equations (rate in moles/hr per mole of $CaCl_2$)

$$\ln .(\text{rate}) = 30.095 - 11950/T \qquad (44)$$

$$\text{rate} = 1.18 \times 10^{13}\ e^{-11950/T}$$

Temp.	Obs. Rate	Calculated Rate
110°C	0.312	0.331
130°C	1.58	1.56
140°C	3.00	3.19

i.e., an activation energy of about 25 kcal/mole. This expression is of course only valid when the vapor pressure is 184 torr. Nevertheless, at higher vapor pressures, e.g., corresponding to equilibrium with liquid at 40°C or 50°C (temperatures suitable for heat rejection), the rates at temperatures 7-17°C higher should be the same or faster. Thus, it appears likely that a solar collector temperature well below 150°C will be adequate to demethanolate the salt bed while simultaneously condensing methanol vapor at a temperature between 40° and 50°C.

3. Methanolation and Demethanolation of $CaCl_2$ Beds

3.1 Design of the Heat Exchange Test Rig

The purpose of constructing a heat exchange test rig is to obtain design data on reaction rates and conditions, which will be used as a basis for design and construction of the heat pump storage system. It is expected that the rate of heat pumping will be limited either by the intrinsic rate of salt-CH_3OH reaction or by the rate of heat flow through the solid bed. The rate of heat flow will be influenced by the heat transfer coefficients of the various solid phases, by the effective bed density, by the bed thickness, by the particle size, and by the temperature difference between the salt bed and the heat exchange plate. The most straightforward way of measuring the influence of these parameters on heat flow is to construct a small test rig in which reaction rates and temperatures can be monitored. The rig must be constructed so that
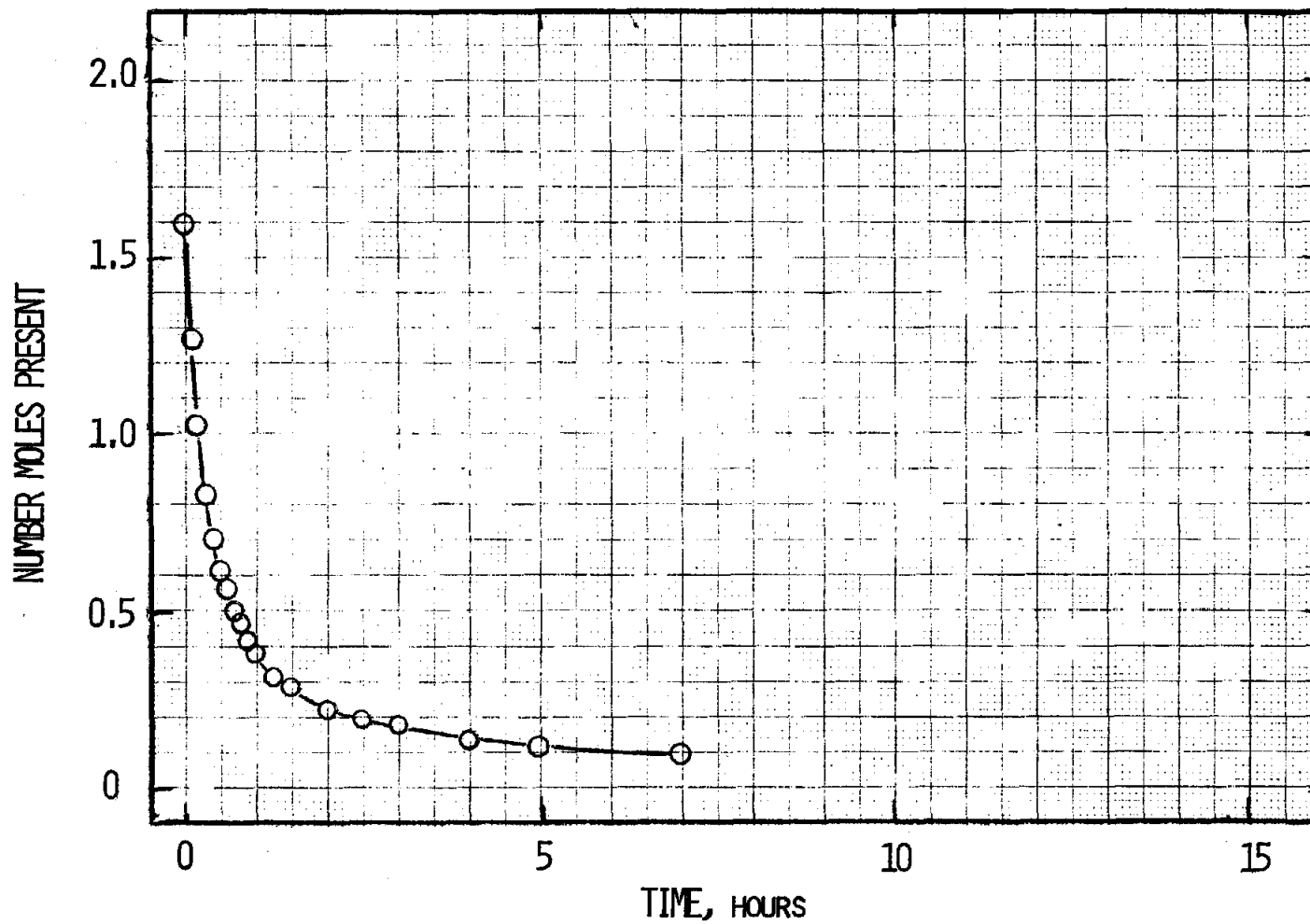
Fig. 20: Desorption of 4 mesh $CaCl_2$ at 140°C while CH_3OH at +33°C.

42
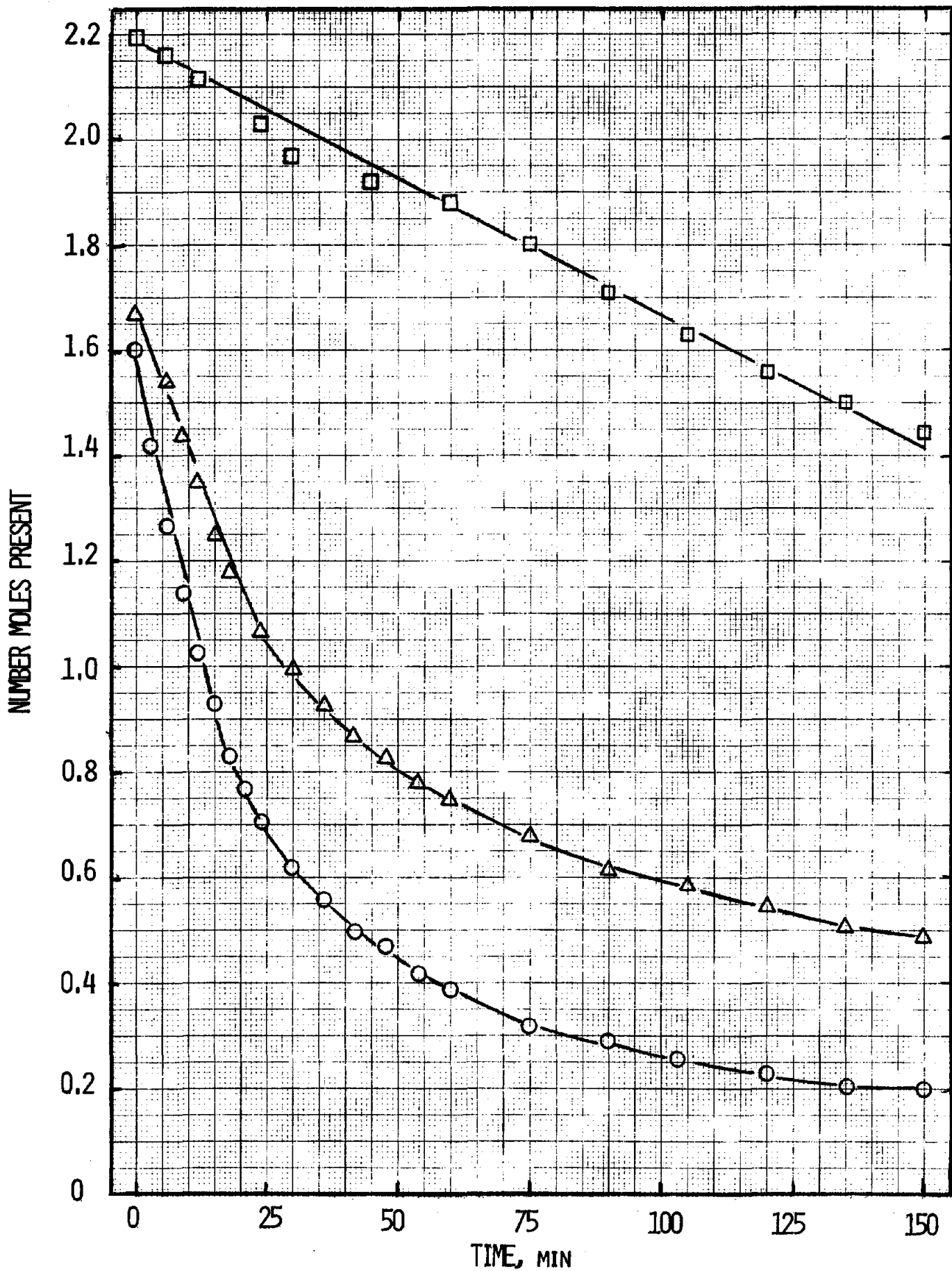
Fig. 21: Initial desorption of 4 mesh CaCl₂ while CH₃OH pool at 33°C.

43

the bed material and depth can be changed easily, and so that results can be readily extrapolated to final design conditions.

We decided to build a sufficiently large test system so that the reaction rate could be measured by monitoring the volume of liquid CH_3OH evaporated or condensed per unit time; this method should prove more accurate than monitoring the rate of vapor flow. Thermostatted 10 and 25 ml burettes were obtained, and were used to control the CH_3OH pool temperature (and vapor pressure), and to measure the volume of liquid. The accuracy is roughly $\pm$ 0.05 ml.

The salt bed was loaded on a copper plate approximately 0.25" thick. The bed was confined and insulated on the sides by a thick-walled Teflon pipe. The temperature of the copper plate was maintained by circulating oil to the underside of the plate. The pressure of the system was maintained by covering the salt bed and Teflon pipe with a bell jar gasketed to the copper plate. Schematic drawings of the apparatus are shown in Figure 22.

Two details of the design were given particular attention. First, we were concerned that the rate of evaporation (or condensation) in the methanol pool is adequate, so that an excessive pressure drop does not occur. Our calculations indicate that the net rate of condensation, in grams per cm^2 per second, is

$$0.331 \ \frac{P}{\sqrt{T}} - 1.56 \times 10^7 \ e^{-4668/T} \tag{45}$$

where P is the pressure (in torr) and T the temperature (°K). (This equation is readily derived by assuming that the activation energy for evaporation is the same as the heat of evaporation, i.e., that the activation energy for condensation is zero.) Even at -20°C (P_{eq} = 7.3 torr), the rate for a pressure drop of 1 torr is 0.021 grams/cm^2-sec, or 75 grams/cm^2-hr, which is more than adequate for the present experiments. Second, we were concerned that the pressure drop of the CH_3OH vapor in the vacuum tubing does not limit the rate of reaction. Calculations indicate a negligible pressure drop when tubing of 0.5" ID is used, although an important pressure drop could occur with 0.25" ID tubing at the lowest pressures (ca. 5 torr) and largest flow rates (ca. 100 grams/hr).

3.2 Kinetics of Methanolation of CaCl₂ Beds

Anhydrous 12 mesh $CaCl_2$, 137 grams, was placed in the test rig described above and heated to 150°C for 4 hours. The initial bed depth was 2 cm. (Since the inside diameter of the bed is 9 cm, the average density of this material is ca. 1.1 g/cm^3. The density of crystalline $CaCl_2$ is 2.15, so the average void fraction of this material is ca. 50%). The oil bath temperature was then set at 40°C, and the methanol pool at
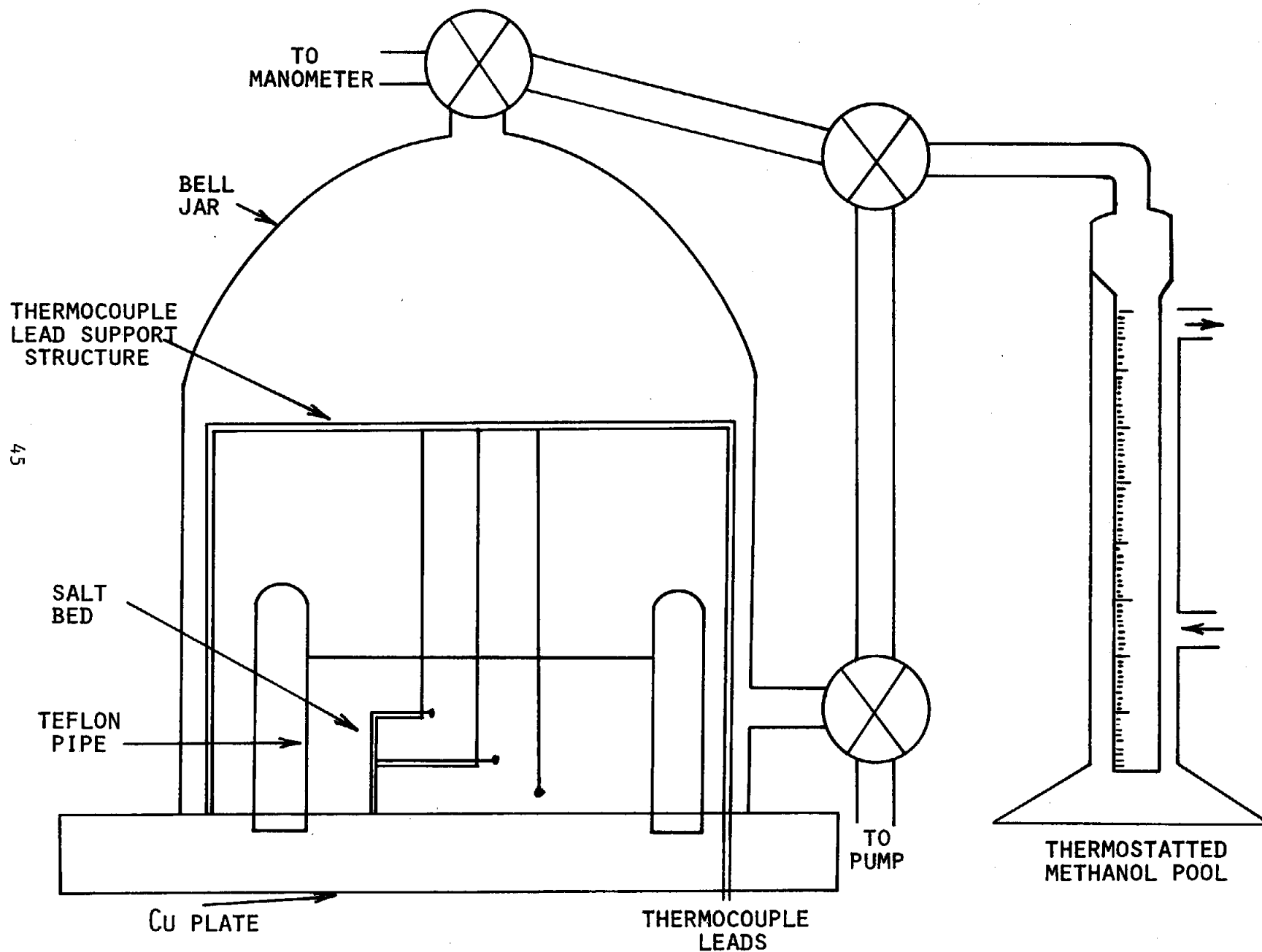
Fig. 22: Schematic diagram of laboratory apparatus for measuring heat and mass transfer properties
of salt beds. The thermocouples shown were not actually installed during Phase I.

5°C, so that the vapor pressure was 38 torr. As seen in Figure 23, it took 15 hours for one mole to react and at least that for the second. During methanolation the center of the bed expanded to a height of 6 cm. The edges of the bed also increased though to a lesser extent, e.g., 4 cm at the extreme edge. Subsequent to the absorption of 2.0 moles, 1.03 moles of methanol were removed and then the absorption process was repeated. As seen in Figure 23 the rate is almost the same as in the first methanolation, although the depth of the bed is almost a factor of 3 deeper. (Independent measurements of the density only show a doubling of the volume.)

It was felt that the reaction rate of the deeper bed might be more favorable if the mesh size of the $CaCl_2$ were varied. Figure 24 shows the methanolation of a 2.0 cm bed of 20 mesh $CaCl_2$ maintained at a plate temperature of 40°C under a vapor pressure of 39 torr. When this is compared with the 12 mesh material, the rates are not significantly different, although one mole of methanolated salt is formed after about 13 hours (cf. 14.5 hours).

We examined the rate of methanolation of this 20 mesh material as a function of bed depth, as shown in Figure 25. Using only 1.25 cm, one mole of salt is formed in 7.5 hours. Comparing (Figure 26) the data for this 20 mesh with the data observed on powder for a 1.25 cm bed depth shows only a slight decrease in rate for the coarser material. The important point is that from 12 mesh down to fine powder the most significant rate limiting parameter is not mesh size but bed depth, which was expected. The rate is limited by the thermal conductivity of the bed, not by the intrinsic rate of reaction.

Since the $CaCl_2$ bed expands during the first methanolation, but does not seem to change in volume thereafter, we examined the methanolation behavior on cycling. Figure 27 shows the results obtained both during methanolation of a bed initially 1.25 cm thick and during remethanolation after removal of 1.09 moles of CH_3OH. The rates during the first two hours are comparable but subsequently, during the second cycle, the reaction rate is faster.

Figure 28 shows the results obtained during three separate methanolation cycles. Initially, the 1.0 cm bed was allowed to react to ca. 0.85 moles of CH_3OH, following which 0.5 moles were removed. Methanolation was resumed, and terminated when ca. 1.25 moles had reacted. Once again, 0.5 moles were removed, and methanolation was resumed. As can be seen in Figure 28, the data points lie on a smooth curve, indicating no acceleration of the rate. This is somewhat puzzling, but may be related to the fact that relatively little CH_3OH was removed prior to the resumption of methanolation, or -- alternatively -- to the fact that the methanolation was never allowed to approach completion.

The bed depth was reduced to 0.5 cm for the next experiment. Methanolation was allowed to proceed to 1.0 moles CH_3OH, followed by
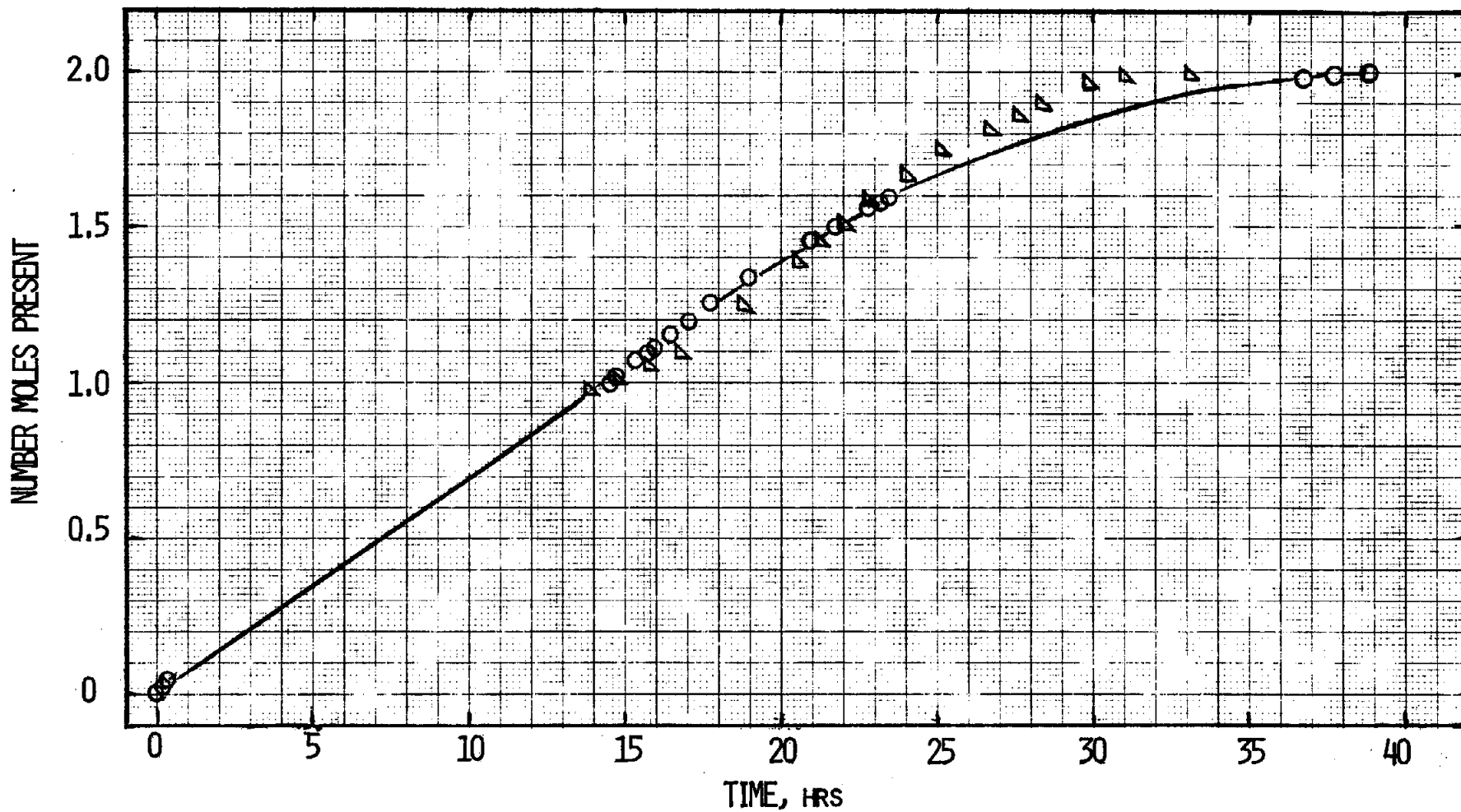
Fig. 23: Absorption kinetics of 12 mesh $CaCl_2$ from a 2 cm bed at 40°C and 38 torr (O, initial run, Δ, subsequent run after removal of 1.03 moles).
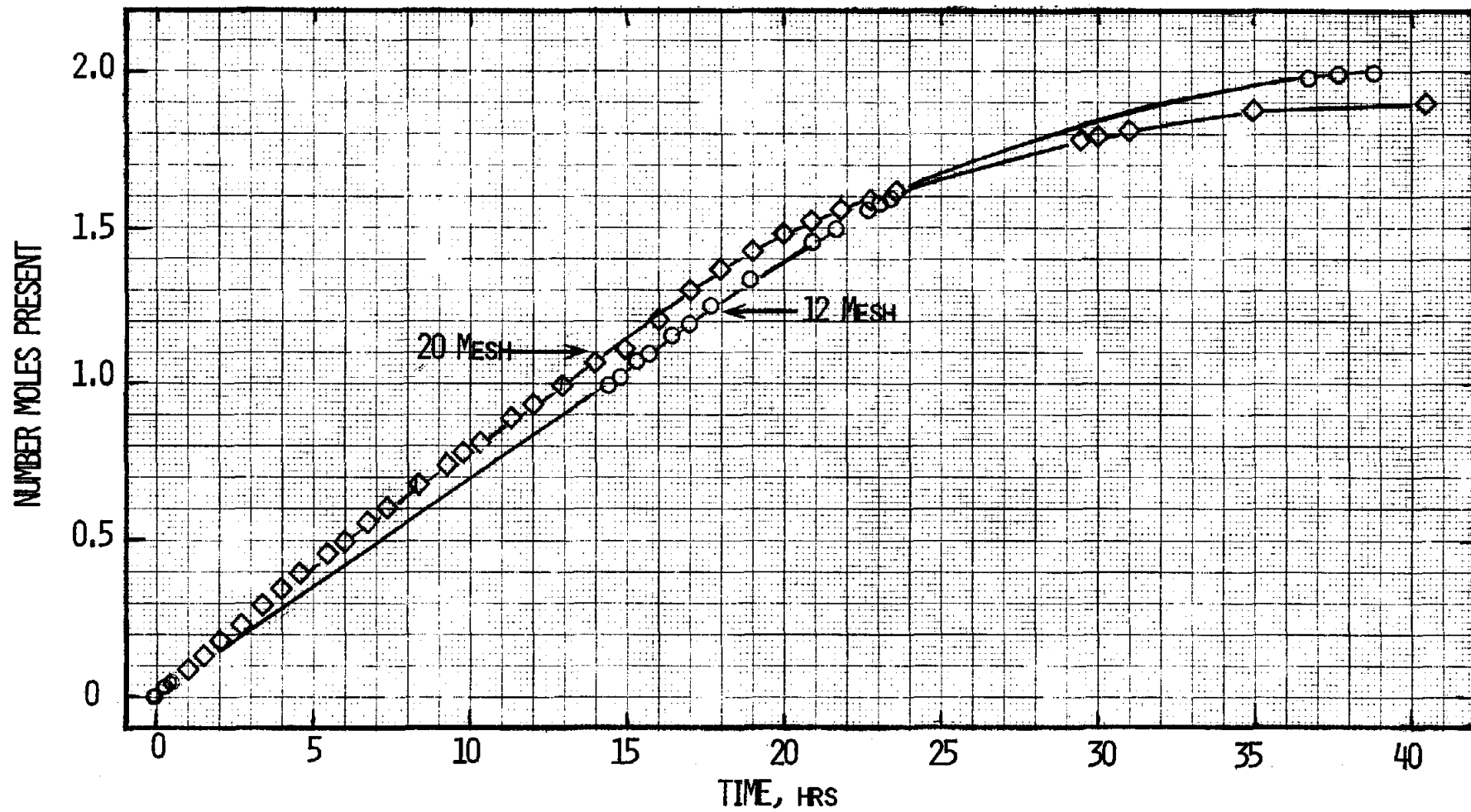
Fig. 24: Absorption kinetics from a 2 cm bed depth of $CaCl_2$ at 40°C and 38 torr.
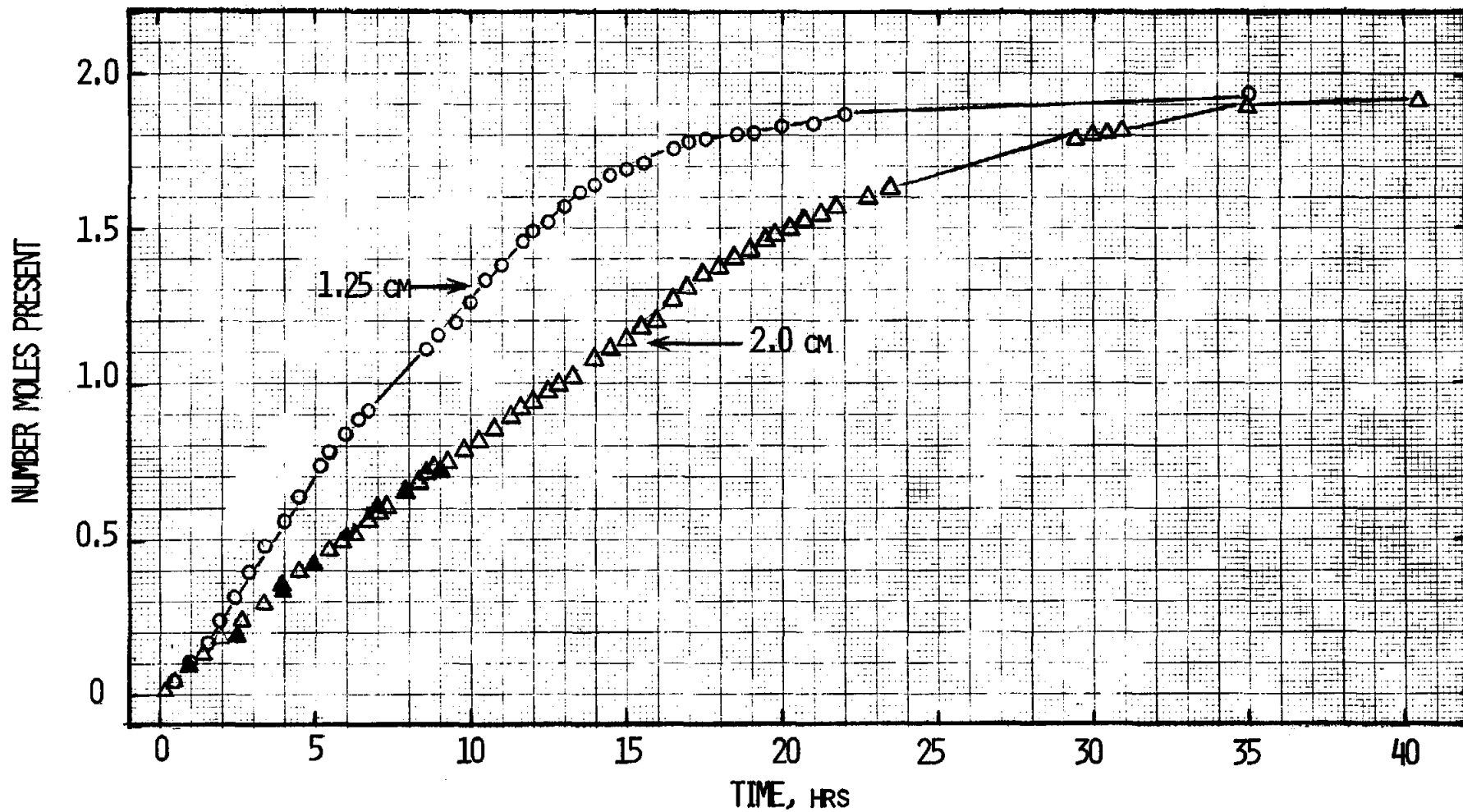
Fig. 25: CH$_3$OH absorption of 20 mesh CaCl$_2$ as a function of bed depth. Plate temperature 40°C and vapor pressure 38 torr. (▲,△ two different runs.)
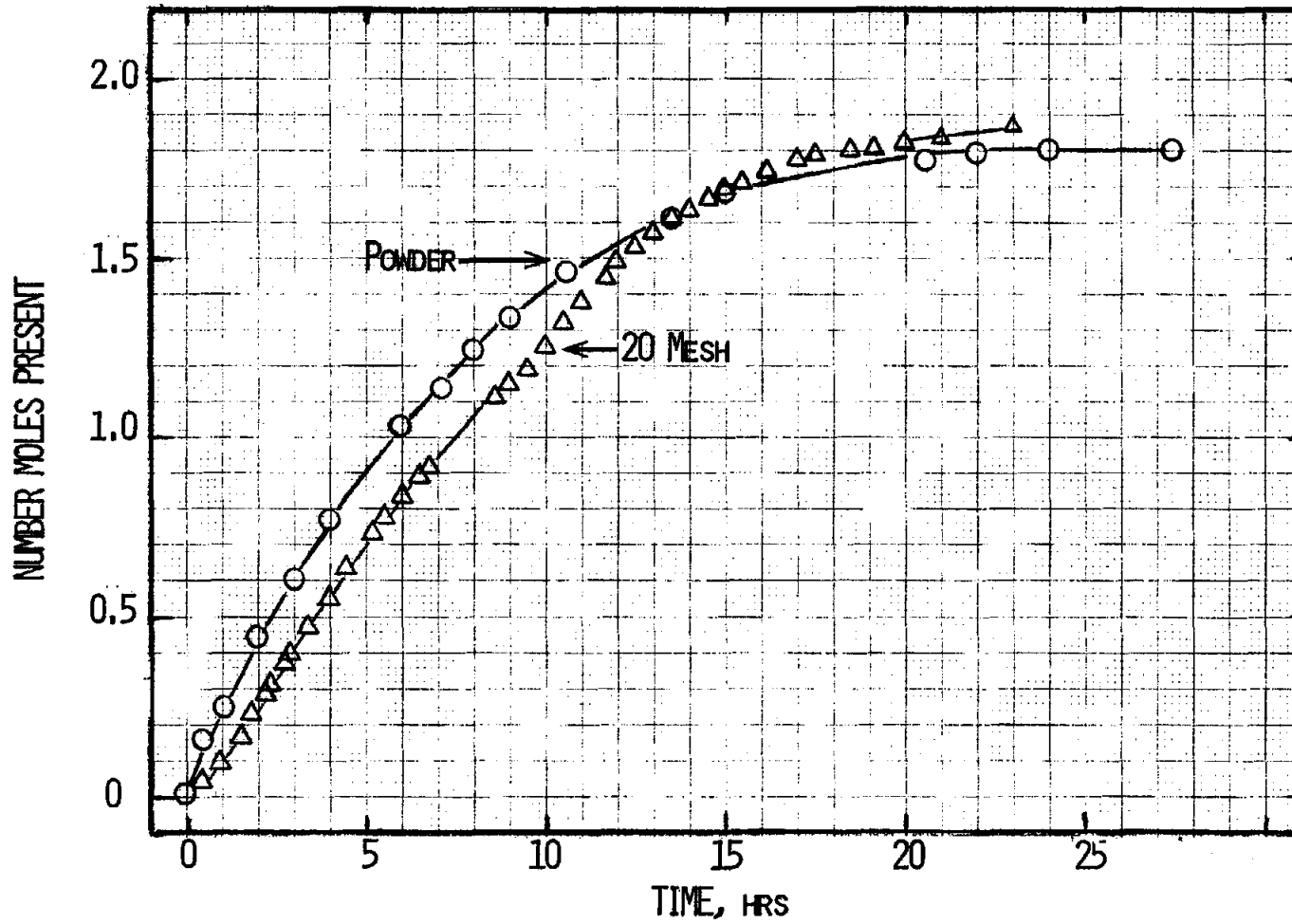
Fig. 26: Absorption kinetics from a 1.25 cm bed depth of CaCl$_2$ at 40°C and CH$_3$OH at 38 torr.
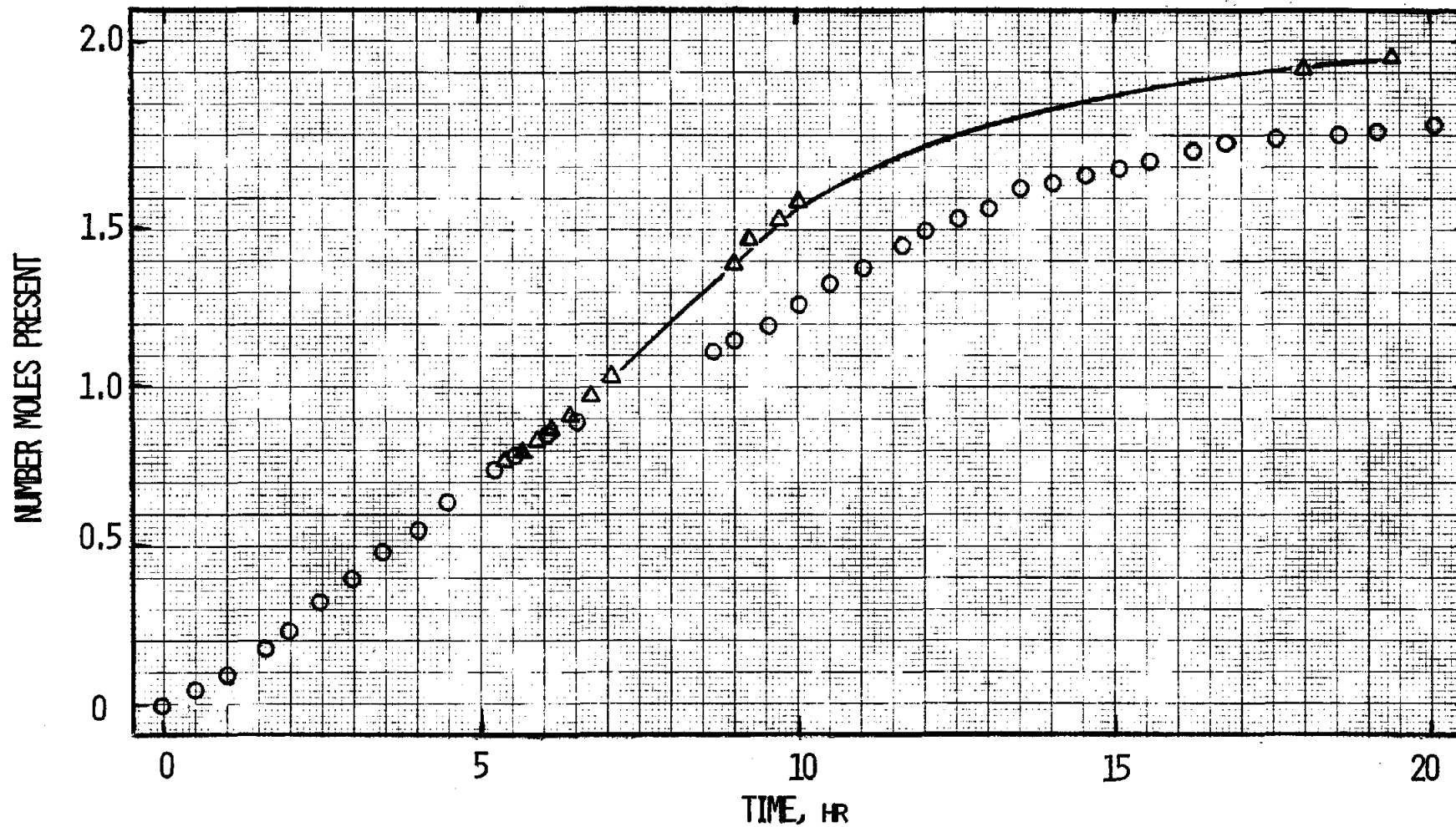
Fig. 27: Methanolation of 20 mesh $CaCl_2$ from an initial bed depth of 1.25 cm. Plate temperature = 40°C; CH_3OH pool at 5°C.
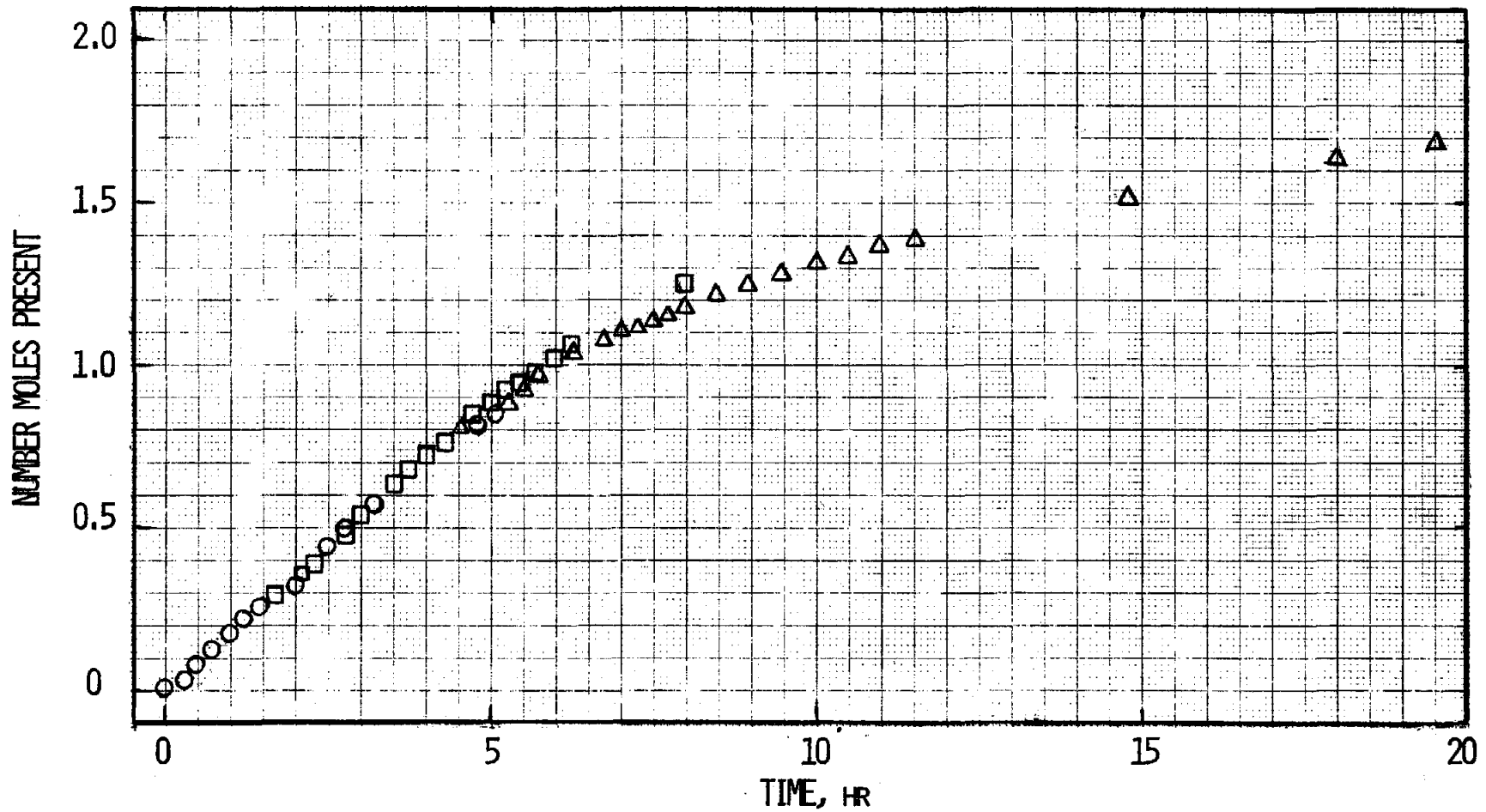
Fig. 28: Methanolation of 12 mesh CaCl$_2$ from an initial bed depth of 1.0 cm. Plate temperature = 40°C; CH$_3$OH pool at 5°C.

demethanolation (to 0.25 moles) and subsequent methanolation. The rates during the two methanolation cycles are comparable, although once again there is a slight acceleration (Figure 29).

3.3 Kinetics of Demethanolation of $CaCl_2$ Beds

Early attempts to obtain quantitative data for demethanolation met with a number of difficulties including unexpectedly slow kinetics. Later, we concentrated our efforts on an examination of reaction rate as a function of the stoichiometry of the methanolated salt, and on an examination of the effect of bed depth. Previously, we had always attempted to demethanolate from a fully methanolated bed, and it seemed likely that formation of a crust in the bed was related to the presence of excess CH_3OH. Later experiments seemed to confirm that crust formation does not occur if methanolation is not carried to completion.

Data for the demethanolation of a 20 mesh bed, initially 1.25 cm deep, are presented in Figure 30. Methanolation was stopped at $CaCl_2 \cdot 1.94$ CH_3OH to prevent crusting. The results are in good agreement with the simulation (see Section II.4) at an assumed 3.00 cm bed depth, which corresponds closely to the actual bed depth after methanolation. When the bed was remethanolated to a composition corresponding to $CaCl_2 \cdot 2.03 CH_3OH$, the rate of demethanolation decreased dramatically. Thus, in subsequent runs, the stoichiometry was maintained at $1.94 CH_3OH$ or less.

The results of demethanolation studies on a 1.0 cm initial bed depth system are shown in Figure 31. These results indicate a reduction in the reaction rate upon demethanolation from a partially methanolated bed. The rates of demethanolation observed in Figure 31 become prohibitively slow after the first few hours. For example, demethanolation of the salt corresponding to $CaCl_2 \cdot 1.76 CH_3OH$, shown in Figure 31, requires about 60 hours to go to 90% completion (see Figure 32). For this reason, additional experiments were carried out with a bed initially 0.5 cm deep. The results of these experiments, shown in Figure 33, are surprising: the rate of demethanolation remains slow. In addition, the rate of demethanolation from the partially methanolated bed (initially $CaCl_2 \cdot 1.1 CH_3OH$) is faster than from a more fully methanolated bed (initially $CaCl_2 \cdot 1.46 CH_3OH$).

The lack of correlation of reaction rate with bed depth is very puzzling: as seen in Figure 34, our simulation program predicts rapid reaction rates for reasonably thin beds. The puzzle is compounded by the apparently good agreement between theory and experiment seen in Figure 30 for a deeper bed.

Three possible explanations for the discrepancy seem worth considering. First, it is possible that a change from the reaction $CaCl_2 + CH_3OH \rightarrow CaCl_2 \cdot CH_3OH$ to the reaction $CaCl_2 \cdot CH_3OH \rightarrow CaCl_2 \cdot 2CH_3OH$ is involved: the abrupt change in reaction rate seen after 5 hours in Figure 30 suggests
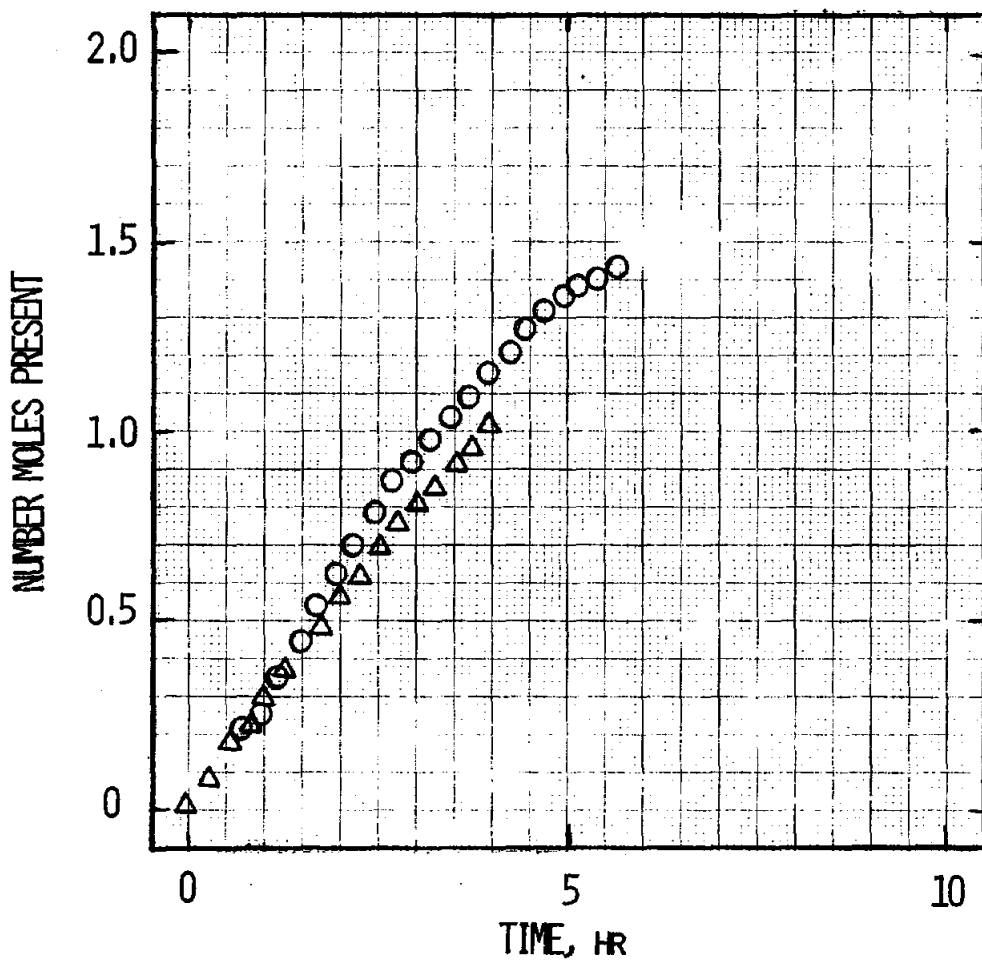
Fig. 29: Methanolation of 12 mesh $CaCl_2$ from an initial bed depth of 0.5 cm. Δ = 1st cycle; O = 2nd cycle.
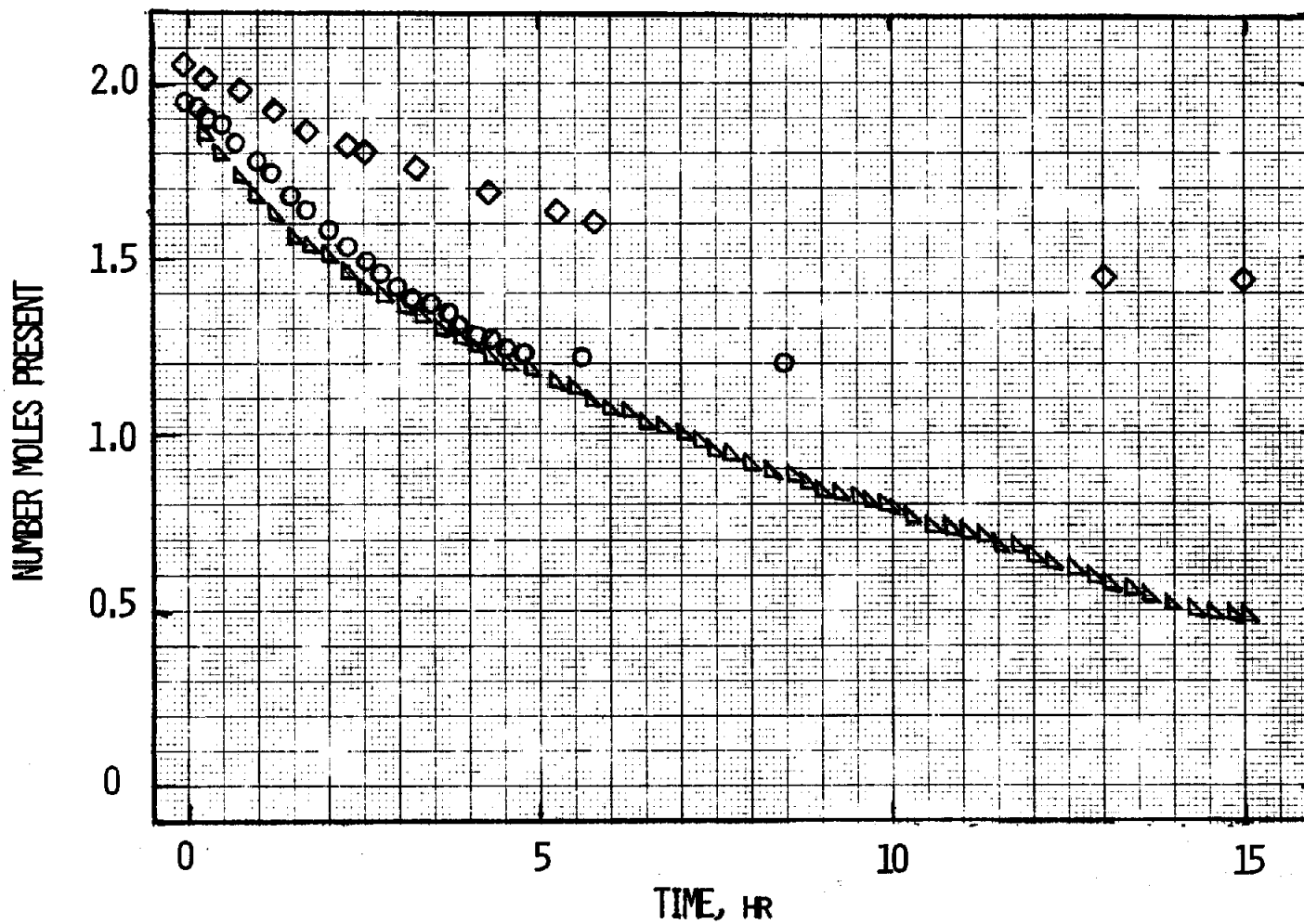
Fig. 30: Demethanolation at 150°C, 38 torr of 20 mesh CaCl$_2$, initially 1.25 cm deep. O = 1st cycle; ◇ = 2nd cycle; Δ = simulation (depth = 3.0 cm)
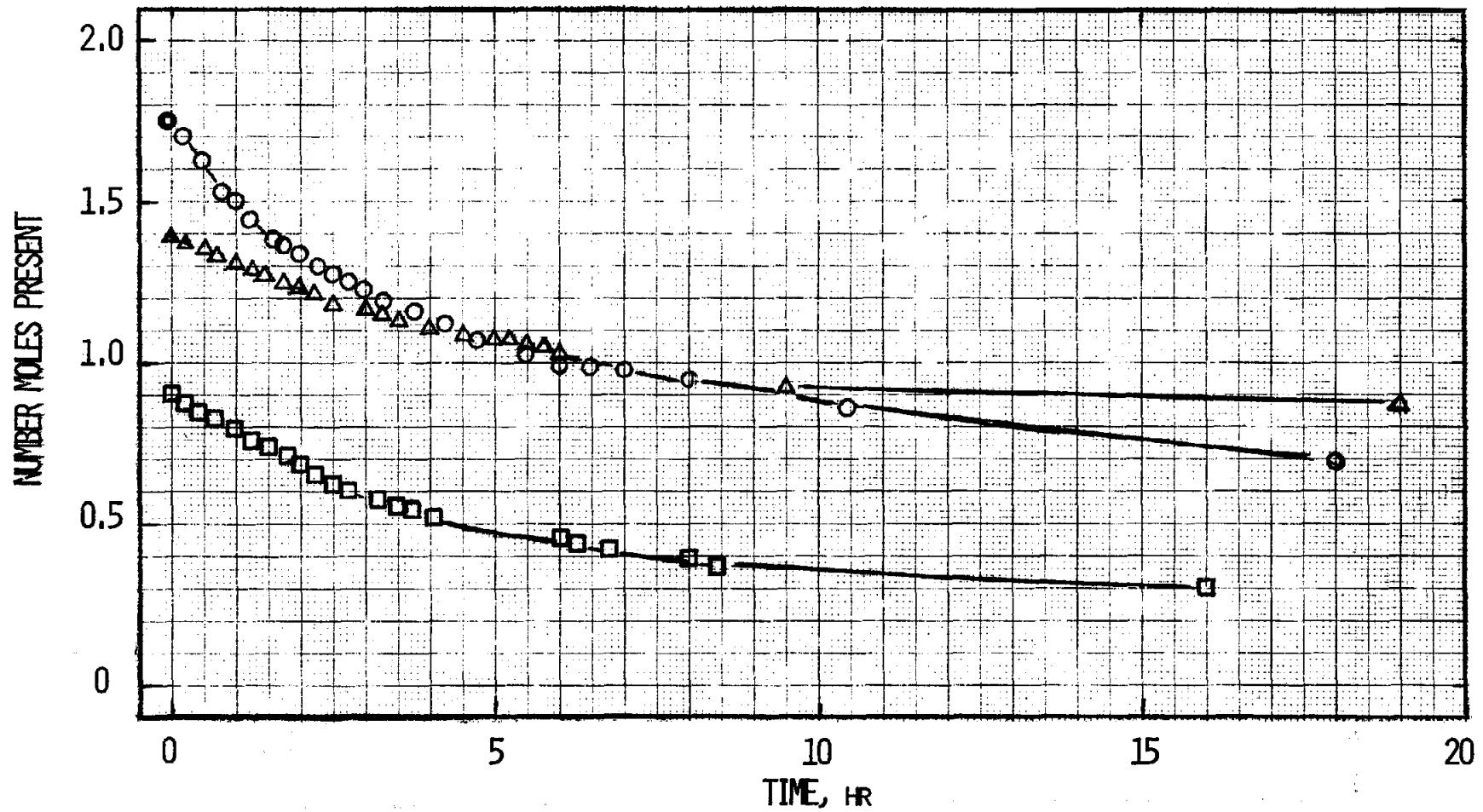
Fig. 31: Demethanolation at 150°C of 12 mesh CaCl$_2$ initially 1.0 cm deep (see text).
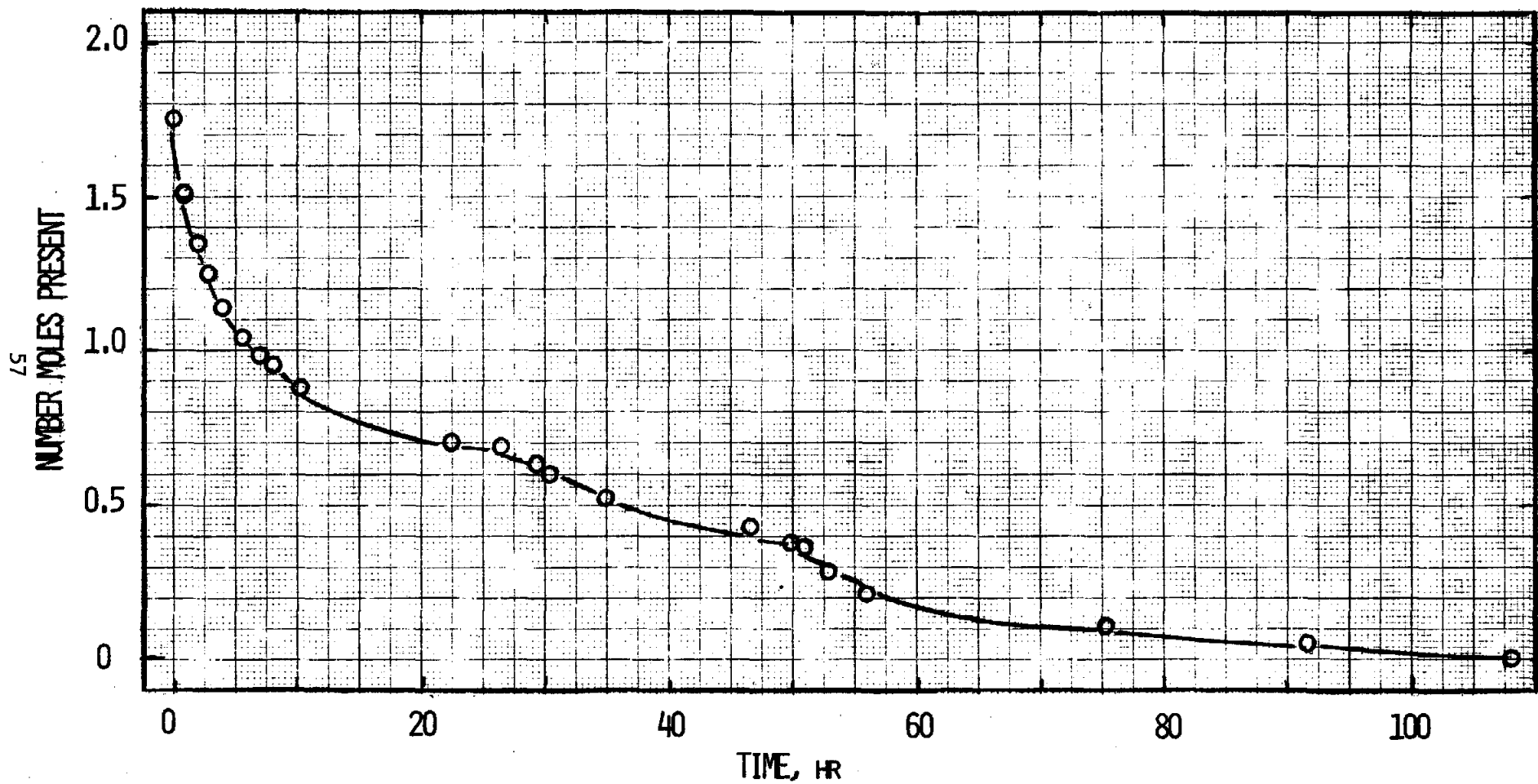
Fig. 32: Demethanolation at 150°C of 12 mesh $CaCl_2$, initially 1.0 cm deep (3rd demethanolation cycle).
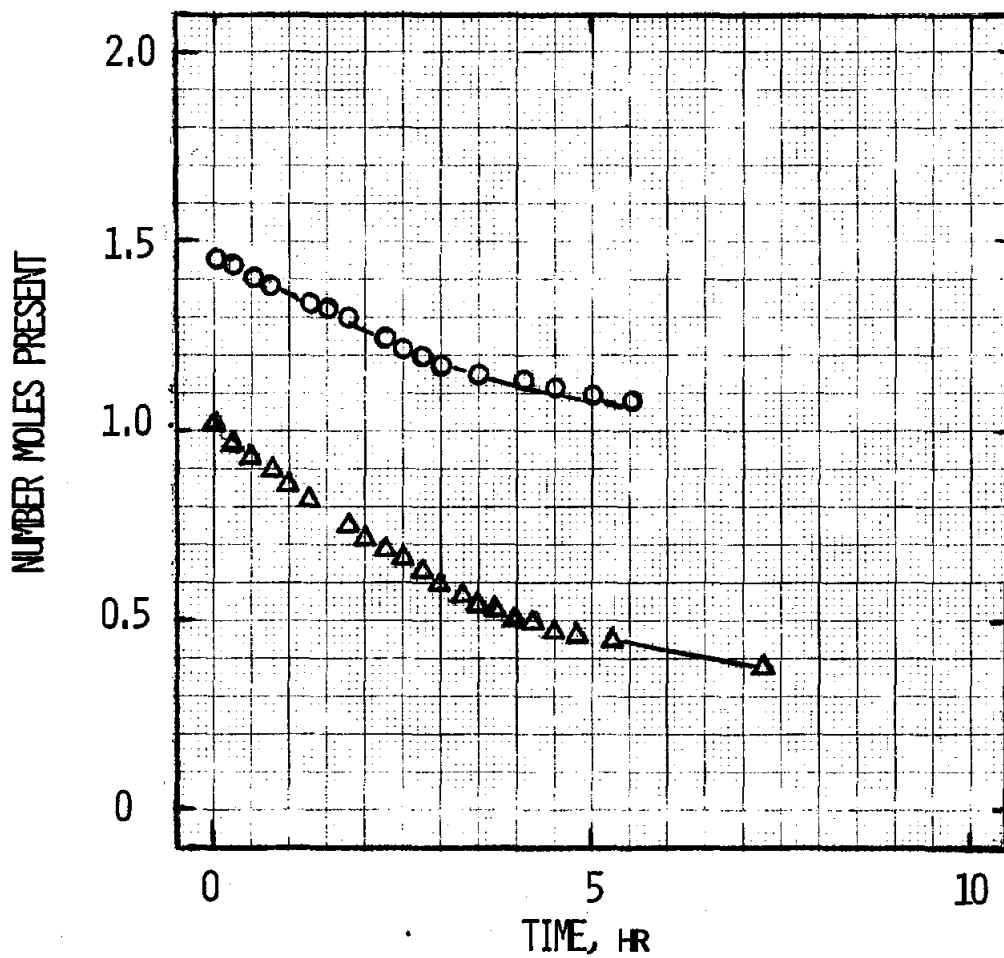
Fig. 33: Demethanolation of 12 mesh CaCl$_2$; initially 0.5 cm deep. Plate temperature = 150°C; pressure = 38 torr.
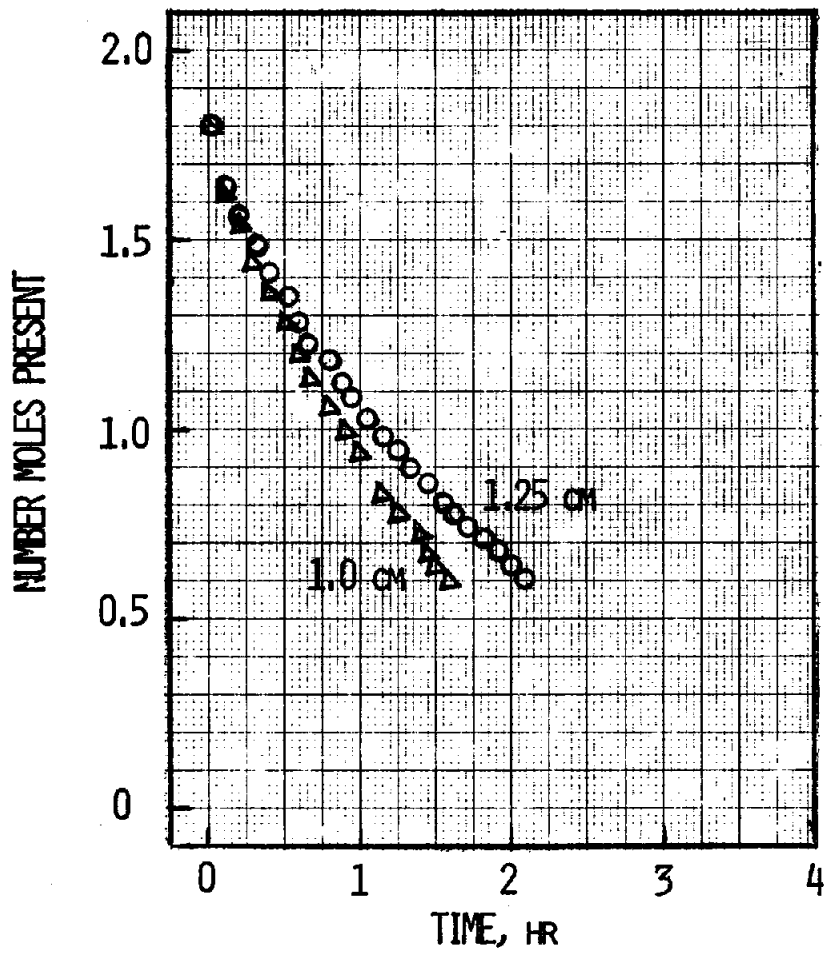
Fig. 34: Simulated demethanolation runs for plate
at 150°C and pool at 38 torr.

that this may be the case. However, even if such a transition occurs, it is difficult to connect this to the slow rates observed in the thin beds. Another possibility is that radiation cools the topmost layer of the bed, causing the reaction rate to slow down whenever the reactive zone is within ca. 0.5 of the top of the bed. This would explain both the decrease in rate observed in Figure 30 and the unexpectedly low rates in thin beds. This explanation implies that a more carefully insulated bed would react far more rapidly, and would show the expected correlation between bed depth and reaction rate.

We made a rough calculation of the rate of radiation from the bed, assuming it behaves as a black body. The calculated rate of radiation is

$$\dot{E} = a(T_2^4 - T_1^4) \tag{46}$$

where T_2 = 423 K is the temperature of the bed, T_1 = 313 K is the approximate temperature of the surroundings, and $\underline{a}$ is the black body radiation constant, 5.7×10^{-5} erg-cm^{-2}-sec^{-1}-deg^{-4}. The rate of radiation under these conditions works out to

$$\dot{E} = 110 \text{ cal/hour-cm}^2 \tag{47}$$

We next consider a bed of $CaCl_2$ 1 cm in depth, containing 80% voids. The total mass of $CaCl_2$ located below 1 cm^2 of surface area is 0.2 ρ = 0.43g, or 3.87×10^{-3} moles. Assuming the total heat of reaction (for 2 moles of CH_3OH) is 40 kcal, the heat that can be taken up in reaction below 1 cm^2 of surface is 155 cal. Thus, with reaction times of the order of one hour or more, the rate of radiation (per unit area) is comparable with -- and generally larger than -- the rate at which heat is taken up by the salt (per unit area) during reaction. This will of course reduce the actual bed temperature, thus reducing the rate of demethanolation. It is hence not surprising that the observed rate of demethanolation is smaller than predicted, particularly in thin beds where the thermal gradient is sharper and the rate at which heat is taken up by the reaction is small compared to the rate of radiation.

It is not possible to correct the observed rates of demethanolation for the effect of thermal radiation; among other difficulties, the actual rate of radiation from a $CaCl_2$ bed is not adequately described by the black body equation. Furthermore, it is difficult to redesign the current bell jar apparatus to reduce the rate of radiation sufficiently; it would be necessary to maintain the entire apparatus at approximately the same temperature as the heat transfer plate. We have therefore postponed further measurements of the rate of demethanolation until after the new plate configuration unit has been constructed in Phase II. This unit will be

designed to minimize radiative effects. Fortunately, the computer model should still prove useful for design work: agreement between the model and the methanolation experiments, and between the model and demethanolation experiments in the thicker beds, is satisfactory. It is of course possible that the model underestimates the rate of demethanolation, in which case the model provides a conservative estimate of the reaction rate.

In the design of a full scale system, radiation should not be a serious problem: much deeper salt beds will be used, the surface-to-volume ratio will be much smaller, and exterior surfaces of the heat transfer unit will be insulated.

A third possibility for the cause of low rates of demethanolation is blockage of the condenser by a small amount of air that has leaked into the system. Experiments carried out early in Phase II have shown that rigorous exclusion of air greatly improves the rate of demethanolation. Thus, it appears that the slow rates reported here were at least in part limited by the rate of condensation.

4. Analytical Modeling of Methanolation and Demethanolation

We have constructed a simple one-dimensional computer model to simulate the methanolation and demethanolation of a salt bed of arbitrary thickness and density. The FORTRAN code is given in Appendix A. The major assumptions used in the calculations are as follows:

$$\text{Rate of methanolation} = \exp(-22.922)\, \exp(8135/T)$$
$$\text{Rate of demethanolation} = \exp(30.095)\, \exp(-11950/T \tag{48}$$

where T is in Kelvins. The first expression is taken from measurements on $CaCl_2$ powder at 38 torr; the second expression was measured on 4 mesh $CaCl_2$ at 184 torr. These expressions are illustrative rather than definitive, but should be reasonably accurate in the range of interest. In any case, the rate of reaction depends far more on the thermal conductivity of the bed than on the intrinsic reaction rates.

$$\text{Thermal conductivity} = \text{(thermal conductivity of } CH_3OH \text{ vapor)} \times (1/(1 \text{ minus cube root of one minus the bed void fraction)}). \tag{49}$$

This expression should provide a good approximately to the bed conductivity (32). It is of interest to note that the thermal conductivity of the bed increases continually during methanolation due to the decrease in void fraction at constant salt volume.

61

The one dimensional model divides the volume between the heat transfer plate and the top of the salt bed into NDEEP elements. The program proceeds by calculating the quantity of CH_3OH that reacts within each of these elements during the time increment DELT. During the time increment, the temperature of the volume element is assumed to be constant, and the rate of reaction depends only on the temperature and the fraction of $CaCl_2$ that has not yet reacted, i.e., first-order kinetics are assumed (see program statements 11-131 in Appendix A). The program next calculates the void fraction in each volume element, which changes due to void occupancy by CH_3OH; the heat capacity of each element, which is also a function of the extent of reaction; and the thermal conductivity of each element (Statements 121-14). The heat generated by the reaction, and the heat flowing from adjoining volume elements, is calculated next (14-20 et seq.) This permits the calculation of the change in temperature for each volume element I, DELTEM(I).

Once the temperature change has been obtained, a new temperature is calculated for each volume element. At the same time, the average properties of the bed are calculated for possible print-out (DO loop 18). The time incrementing loop ends at Statement 80: having obtained new physical properties and temperatures for each volume element, the calculation is repeated for the next time increment, beginning with the quantity of CH_3OH reacted within each volume element.

The program represents a standard finite-difference solution to the differential equations governing heat and mass transfer within the bed. Vapor diffusion or flow within the bed is ignored, since it is expected to be essentially instantaneous for a bed of pellets. The program is equally applicable to methanolation or demethanolation. Since the rate equations employed do not take into account back reaction, which can be significant when the temperature of an element is very close to equilibrium, a sharp cut-off option is provided to insure that no element can have a temperature on the "wrong side" of the equilibrium value.

The program has been tested for a number of different values of the parameters NDEEP and NTIME. When NDEEP is 10 or greater, the results appear essentially independent of NDEEP. Likewise, the results are independent of NTIME if it is sufficiently large; if it is not, the results "blow up" in standard fashion, and the calculations must be repeated with a larger value. In this type of calculation, the results either diverge or converge absolutely: if NDEEP is sufficiently large to prevent divergence, the accuracy of the calculation will not be improved by using a larger value.

Simulation results for beds of various thickness are shown in Figure 35. In each case, it was assumed that the dehydrated bed contained 80% voids, and that the plate temperature was 40°C. For comparison purposes, the experimental data carried out on the first cycle of a 1.25 cm thick bed are shown. This bed puffed up to a thickness of about 3 cm during methanolation. Since
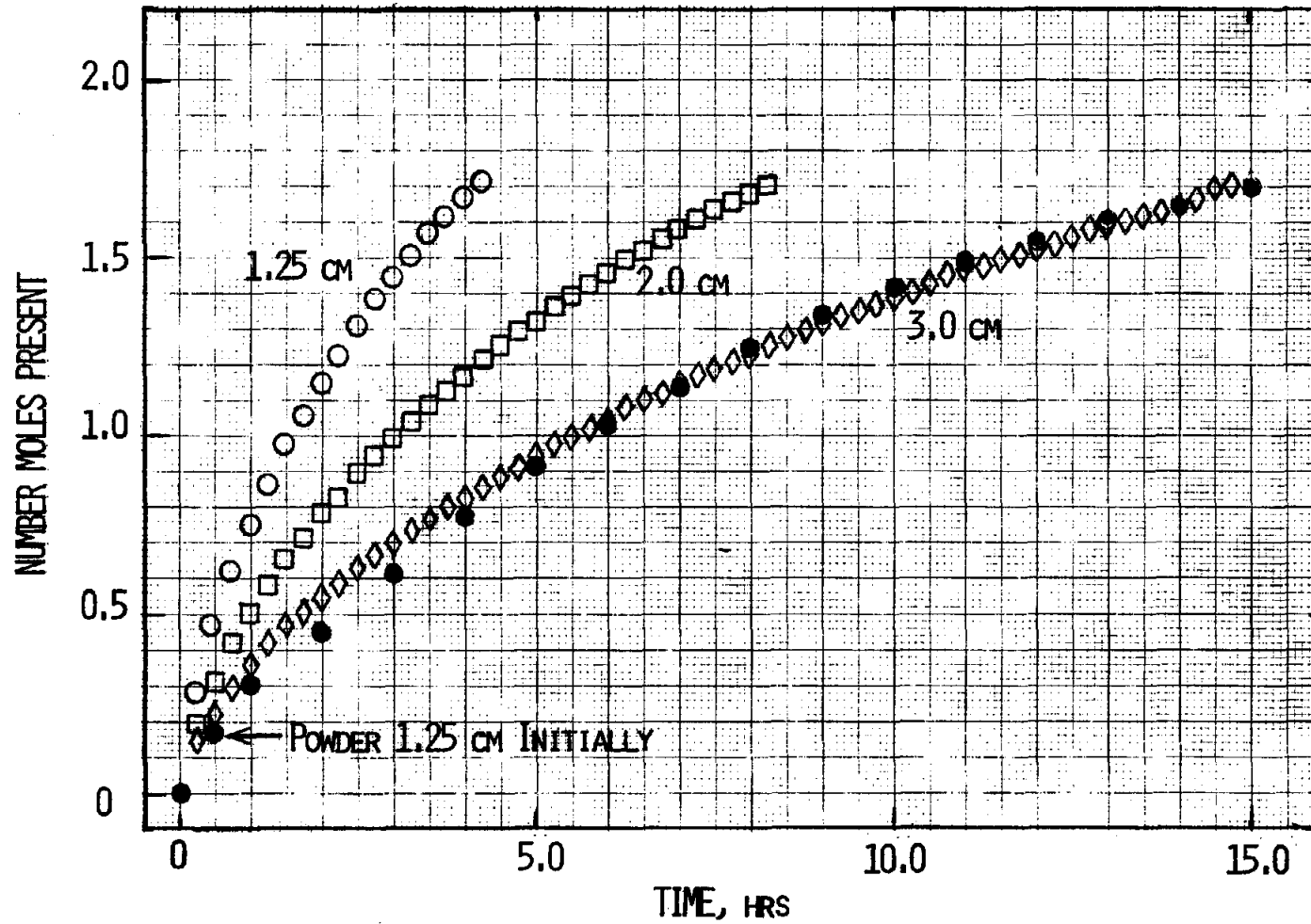
Fig. 35: Comparison of simulation calculations for various bed depths with experimental methanolation of a bed initially 1.25 cm deep.

the experimental results indicate that the rate after cycling (and swelling of the bed) are about the same as during the first cycle, the experimental results should actually be compared to the simulation run for a bed thickness around 3 cm. As can be ssen in Figure 35, the comparison indicates excellent agreement - better agreement than is in fact warranted by the accuracy of the model.

The same model has been used to calculate the rate of demethanolation of a 3 cm bed at a plate temperature of 150°C. As can be seen in Figure 36, the predicted rate under these conditions is rather slow. However, it is expected that the rate will be adequate for a thinner bed, or a finned bed, even at lower plate temperatures, as was seen, for example, in Figure 34.

It is also of interest to compare the predicted rates of reaction as a function of bed depth. As seen in Figure 35, the predicted time for 50% reaction in a 1.25 cm bed is 1.5 hours, compared to 2.9 hours in a 2.0 cm bed and 5.3 hours in a 3.0 cm bed. Thus, reaction time is predicted to increase somewhat faster than linearly with bed depth.

We have noted that the thermal conductivity of the salt bed is a strong function of the bed porosity: the lower the porosity, the higher the conductivity. Use of lower-porosity beds is also desirable in order to increase the energy density and decrease the cost of the container/heat-exchanger. We therefore carried out a brief study of the predicted rates of methanolation and demethanolation as functions of bed porosity. The results of the simulation are shown in Figure 37.

It may seem surprising at first glance that the predicted rates of reaction are somewhat slower when the bed porosity is reduced. However, this is misleading. A bed of given depth with 70% voids contains three times as much material as a bed with 90% voids. Thus, while the rate of reaction per mole of $CaCl_2$ is reduced when the porosity is reduced, the rate at which CH_3OH is given off or taken up is sharply increased. Thus, reduction in bed porosity has a favorable effect on rates, and is desirable as long as the bed is not so dense as to interfere with vapor passage, or cause problems in packing the material.

The one-dimensional computer model has been extensively modified to incorporate fins of arbitrary spacing and thickness. A copy of the program listing is given in Appendix B. While the program has not yet been extensively tested, it is believed to be correct, and the preliminary results are reasonable. For example, the model predicts that reasonable rates of reaction can be maintained in a "deep" bed (e.g., 10 cm) if the fin spacing is 2-3 cm. However, if the fin spacing is increased, reasonable rates cannot be maintained regardless of fin thickness. For a fin spacing in the range 2-3 cm, it appears that fin thicknesses of the order of 50 mils will be adequate to maintain adequate heat transfer. These results suggest that the heat exchanger for the salt bed can be relatively compact.
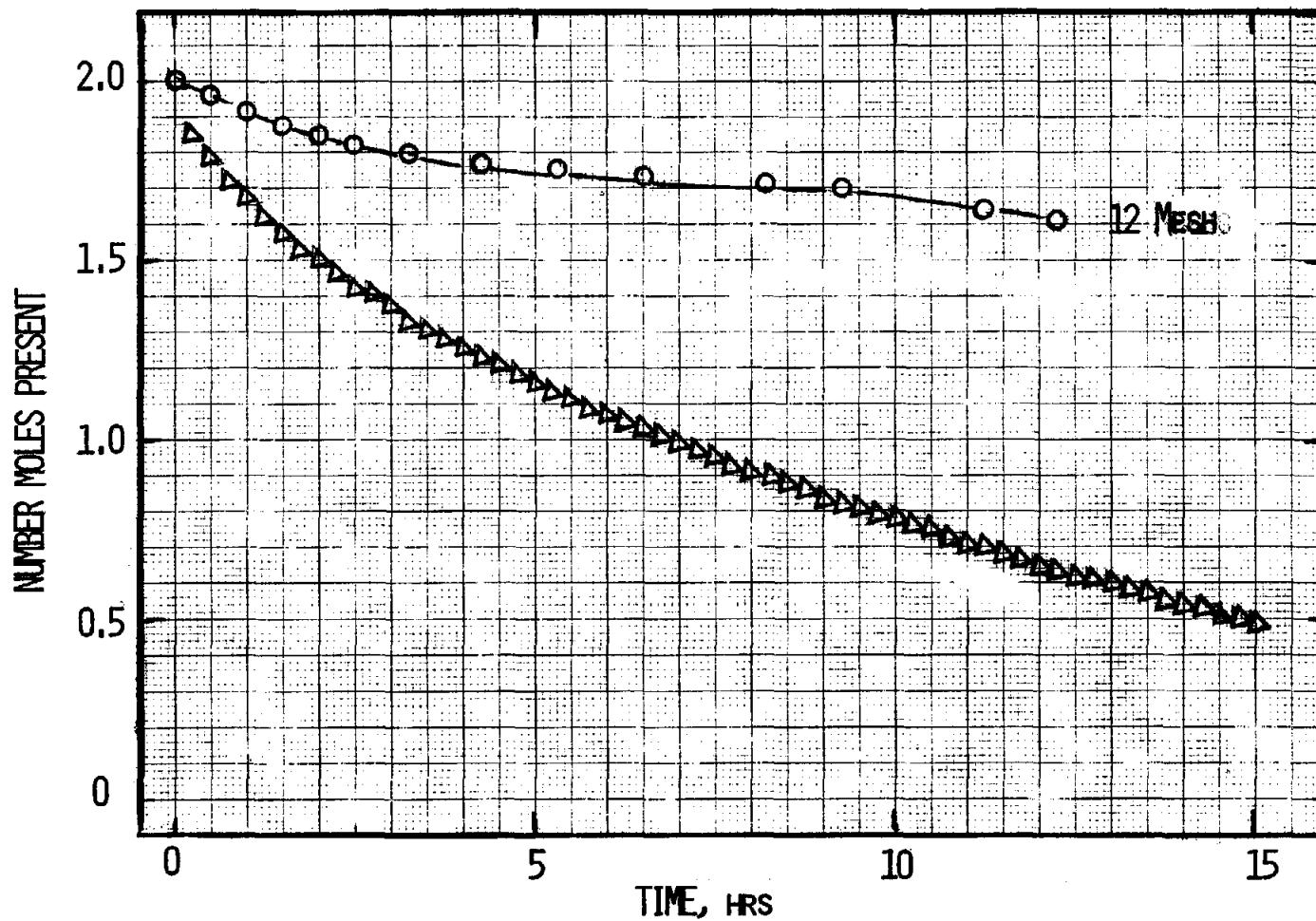
Fig. 36: Comparison of simulation calculation (bed depth = 3 cm, plate temperature = 150°C) with experimental demethanolation (bed depth = 6 cm, plate temperature = 130°C).
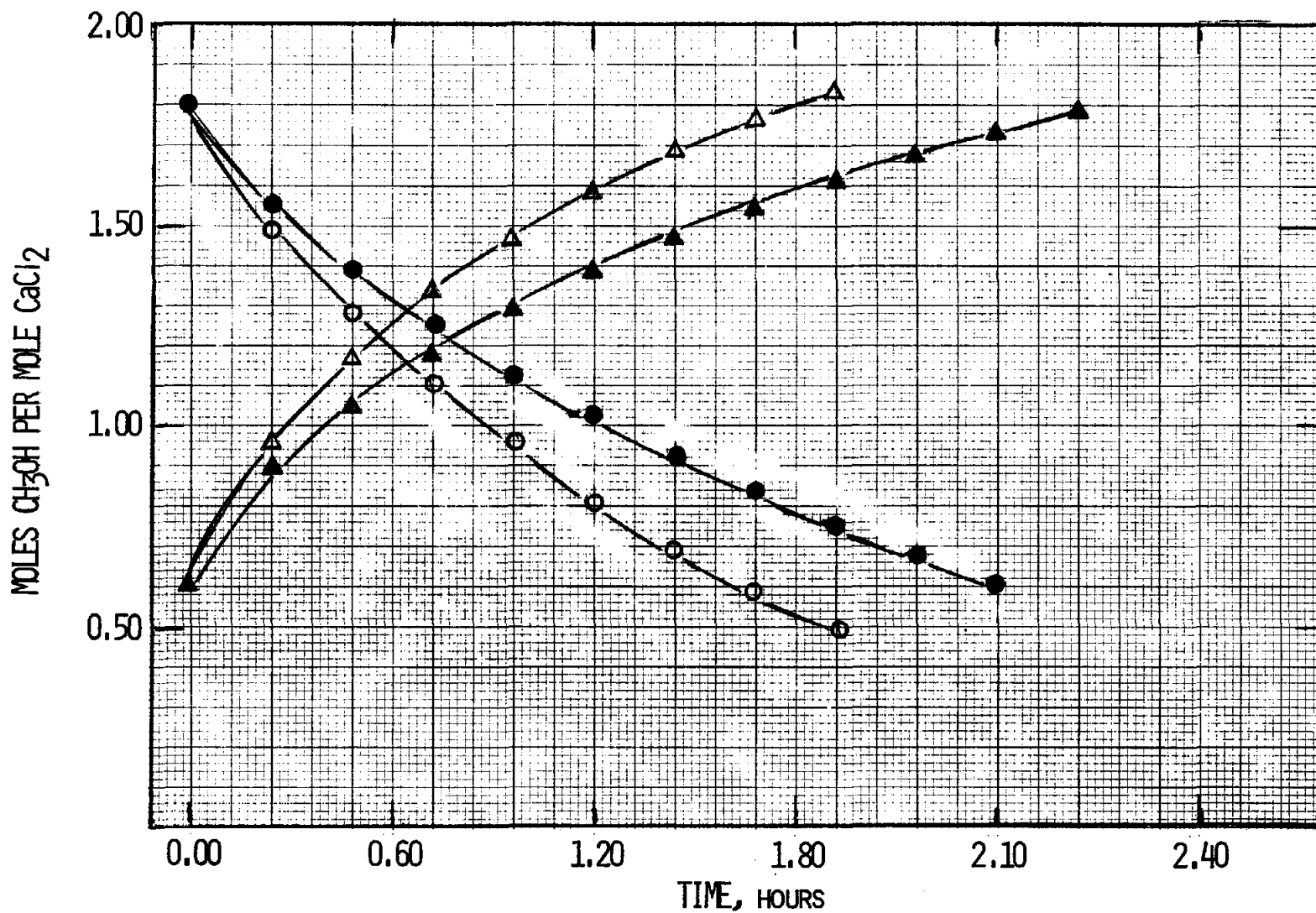
Fig. 37: Simulated rates of methanolation ($\triangle$,$\blacktriangle$) with plate = 40°C and demethanolation (O,●) with plate = 150°C and bed depth = 1.25 cm for $CaCl_2$ void fractions = 0.7 ($\blacktriangle$,●) and 0.9 ($\triangle$,O).

5. Density Measurements

We filled containers of known volume with the test salt and weighed the contents. Excess material was predried in an open dish in a 130°C oven and cooled in a desiccator. The containers were refilled and reweighed. The results are tabulated in Table 2.

There are some differences in density of the starting material; in particular, the 12 mesh material appears less dense. In our bed depth experiments, 2 cm of 12 mesh material weighed 137 grams, whereas 2 cm of 20 mesh material weighed 155 grams. The most significant change is observed in the methanolated salts. Once the salt has been methanolated it remains in its "puffed" condition, and does not appear to change volume upon further cycling. Drying and handling does not alter its apparent density and it does not repack.

According to the literature, the density of crystalline $CaCl_2$ is 2.15. Since its molecular weight is 111.0, the molar volume of $CaCl_2$ is 51.6 cm^3. The molar volume of liquid CH_3OH is 40.5 cm^3, so we may expect that the molar volume of $CaCl_2 \cdot 2CH_3OH$ will be roughly 133 cm^3 (density ca. 1.32). If crystalline $CaCl_2 \cdot 2CH_3OH$ is demethanolated without a volume change, its density would be about 0.83. Thus, measured densities around 0.4 imply a void fraction around 80% for the demethanolated material and around 50% for the methanolated salt.

6. Corrosion Testing and Long-Term Cycling

Corrosion test cells were prepared by sealing two of the arms of a Y-tube and placing $CaCl_2$ (plus a metal coupon) in one arm and CH_3OH in the other. The salt side was heated to remove H_2O vapor and, subsequently, the CH_3OH side was chilled to approximately -50°C while a vacuum line was connected to the third arm and the arm was sealed off. We have cycled the temperature of the salt up and down while maintaining the CH_3OH at a constant temperature. In this way, we have been able to cycle the salt bed in a way that approximates the intended use. As of this writing, cycling has just begun. A summary of the materials used for corrosion testing is shown in Table 3; Al and Cu are the most likely candidates because of their high thermal conductivity.

The glass Y tubes have an ID of 1.0 cm and arms are each 7 cm long, sealed at two ends. In one arm is placed the preweighed, degreased coupon. Then 3.0 grams (0.027 moles) of anhydrous $CaCl_2$ is put in the same arm. In another arm we need 0.054 moles or 2.19 cc of CH_3OH for a completely methanolated salt (ca. $CaCl_2 \cdot 2CH_3OH$). We did not want to have excess CH_3OH present, so we used 2.0 cc. A row of these tubes is set in a stand with one arm protruding. Heating tapes are wrapped around the salt and coupon arm and the Variac put on a timer so that the heating and cooling cycle can be continuously controlled. Thermocouples placed under the tape provide temperature profiles as a function of time.

TABLE 2

DENSITY MEASUREMENTS ON $CaCl_2$

	Out of Bottle	24 Hrs (130°C)	48 Hrs	72 Hrs
Mallinckrodt 4 mesh	0.970	0.964	0.915	0.960
Aldon Chemical 8 mesh	0.965	0.937	0.934	0.947
Baker Analyzed 12 mesh	0.910	0.952	0.863	0.815
Baker Analyzed 20 mesh	0.941	0.900		0.869
$CaCl_2 \cdot 2H_2O$	0.753 (assay 75-78%)			
	Initially			
Methanolated 4 mesh after 14% reaction	0.909	0.871	0.876	0.878
Methanolated 4 mesh (33% reaction)	0.676			0.657
Methanolated powder (after cycling)	0.498			0.392
Methanolated 12 mesh (after cycling)	0.454			0.437
Methanolated		0.495		

TABLE 3

MATERIALS SELECTED FOR CORROSION TESTING

	Designation	Thickness	Source
Al, sheet	3003-H14	0.305 cm	Admiral Brass, Woburn, Ma.
Al, extruded	6063-T52E	0.305 cm	Edgcomb Steel of New England, Inc., Architectural Sign, Waltham, Ma.
Cu, sheet	OFHC	0.305 cm	Admiral Brass
Cu, alloy	704 Cu-5% Ni	0.081 cm	Olin Metals Research Lab, New Haven, Conn.
Cu, alloy	715 Cu-30% Ni	0.081 cm	" "
Brass	HH	0.305 cm	Admiral Brass
Mild steel	WB1 AVC	0.158 cm	C.F.A.

For the actual corrosion and cycling test itself, the arm with CH_3OH was kept in a constant temperature bath at +5°C and the $CaCl_2$ arm was kept at room temperature. However, complete methanolation did not take place even after 24 hours. The salt appeared to have a thick crust. The salt side was then heated to 150°C to try to demethanolate. Methanol was driven off but the salt appeared to retain some of its crust. After 25 full cycles, 3 hours at each temperature, the ampule was opened and the aluminum sheet sample was weighed. The weight before rinsing was 1.6488 grams, identical to the initial starting weight. After rinsing, the sample weighed 1.6477 grams. The salt indeed had formed a crust and was extremely hard and caked. The sample was even difficult to remove.

A second system was set up with the 20 mesh $CaCl_2$, but the sample size was decreased to 1.0 gram and correspondingly the CH_3OH was reduced to 0.70 cc. The commercial grade mild steel had an initial weight of 2.9270 grams. Again after 25 cycles of attempting to methanolate and demethanolate (some exposures were 15 hours) the system was opened due to extremely slow kinetics of methanolation. The first weight prior to rinsing was 2.9323 grams. After rinsing, the weight within experimental error was essentially the initial weight, 2.9268 grams.

A third Y system was set up with 1.0 gram precycled 20 mesh $CaCl_2$ and 0.80 cc of CH_3OH and a coupon of Cu alloy 30% Ni. Even with the pre-cycled material we observed some crusting and we only attempted cycling 25 times. The initial weight was 2.9528 grams, the weight prior to rinsing was 2.9556 grams, and the weight after rinsing with distilled water and drying was 2.9268 grams. There was no visible change in appearance.

The next system we tried was 1.0 gram of 8 mesh precycled $CaCl_2$ and 0.65 cc of CH_3OH with a coupon of extruded aluminum. Again we cycled for 25 times, although as observed previously there was still some surface crusting which made each cycle very long. The weights observed were: initially – 1.7588 grams, prior to distilled water washing – 1.7596 grams, after rinsing – 1.7588 grams.

Our final test cycle was extruded aluminum half buried in 1.0 gram of precycled 8 mesh $CaCl_2$ and 0.59 cc of CH_3OH in the other arm. With these conditions, we observed methanolation to take place in ∿100 minutes and demethanolation in ∿20 minutes. The tube was then cycled continuously with the CH_3OH pool side immersed in a constant temperature bath held at +5°C. The salt side was held at room temperature for 2 hours to methanolate followed by 1 hour at 150°C to demethanolate. At the completion of 300 full cycles, the system was opened and no visible deterioration of the aluminum was observed. There was no differentiation due to the sample being imbedded in the salt. The initial weight was 2.5322 grams, after cycling 2.5338 grams but after rinsing with distilled water the weight was 2.5326 grams. The top of the salt was not crusted; however, the salt in the bottom of the tube was indeed difficult to remove. Measured

times of methanolation and demethanolation just prior to removal from the test cycle showed no deterioration or change from the initial rates observed. While these measurements are necessarily crude, due to limitations in reading the CH_3OH level, they do indicate that any deterioration of rates with cycling will be too small to measure over the course of tens of cycles, and may be too small to measure over the course of hundreds of cycles.

We now have 20 more coupons set up in Y tubes, 3 each of the following: copper alloy with 5% Ni; 715 Cu - 30% Ni, HH Brass, and Al sheet. Of the 3 samples of mild steel, two are the same configuration as above and one has an additional side arm which accommodates a break seal which when opened will allow evaluation of the trapped gases. Similarly, the 3 samples of OFHC copper sheet were set up the same way. Since one sample of extruded aluminum has been cycled, only one more was set up with the standard Y configuration and one with a break seal. It is hoped that we shall be able to run one set of samples for 100 cycles and leave the rest cycling for several hundred additional cycles.

III. ENGINEERING DESIGN AND ANALYSIS

1. Design of the Salt-Bed Heat Exchanger

The salt-bed container and heat exchanger must be designed with several purposes in mind. These include:

- Energy storage capacity

- Rate of energy transfer

- Temperature drops on the salt-side and air-side of the heat exchanger

- Fan power required for the air-side

- Ease of manufacture of the design

- Adequate strength of the container

- Minimization of container cost

- Minimization of container heat capacity

In order to obtain preliminary design data, we have begun design calculations on a simple flat plate model shown in Figure 38. A single plate thickness TP was assumed for all six walls of the salt container. No provision was made for wall supports, or for the space required for vapor leaving or entering the bed. As a first attempt to minimize the container cost, we have instead minimized container weight, varying fin spacings, fin heights, fin thicknesses, and the container geometry (L and W) subject to constraints on temperature drops, fan power, energy storage capacity, and rate of energy transfer. At this stage, ease of manufacture has not been taken explicitly into account.

For purposes of calculation, we use the nomenclature shown in Table 4. Where appropriate, we have indicated the numerical values of the parameters used. The assumed storage capacity, 10^6 BTU, is quite large, and the charge time, 6 hours, is sufficiently short to allow complete charge by solar collection in winter. These values are illustrative only; actual values can only be selected through a complete system analysis.

Calculations are carried out as follows. First, we select preliminary values for all geometrical parameters shown in Figure 38. In addition, values for Δ_A (air temperature rise or fall) and Δp (air-side pressure drop) are chosen. Next, we calculate the air-side convection heat transfer coefficient h_A (BTU/hr-ft^2-°F) from the equation (ref. 33).

$$h_A = 8.7 \times 10^{-3} \, k_A \left(\frac{HAS + SAS}{HAS \cdot SAS} \right)^{0.2} \left(\frac{E_d \cdot HSS \cdot L}{\mu_A \theta \cdot HAS \cdot C_A \Delta_A} \right)^{0.8} \tag{50}$$
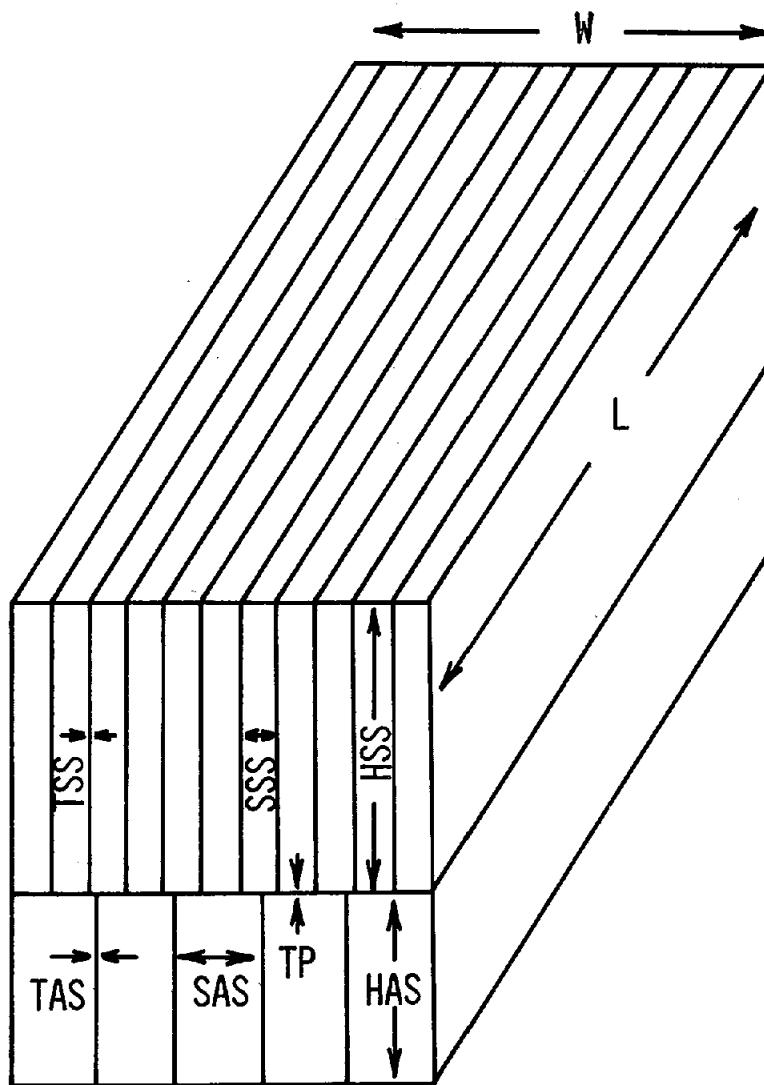
TAS - THICKNESS OF AIR-SIDE FINS
TSS - THICKNESS OF SALT-SIDE FINS
TP - THICKNESS OF PLATE
SSS - FIN SEPARATION, SALT-SIDE
SAS - FIN SEPARATION, AIR-SIDE
HSS - FIN & SALT-BED HEIGHT
HAS - FIN HEIGHT, AIR SIDE

Fig. 38:   Schematic design of the salt-bed heat exchanger.

TABLE 4

PARAMETERS USED IN SALT-BED HEAT EXCHANGER DESIGN

Value	Name	Description
13,000[1]	E_d	Salt-bed volumetric energy density, BTU/ft^3
0.04[+]	k_S	Salt-bed thermal conductivity, BTU/hr-ft-$°F$
0.052[†]	ρ_A	Air density, lb/ft^3
0.25[†]	C_A	Air heat capacity, BTU/lb-$°F$
0.023[†]	μ_A	Air viscosity, cp
0.016[†]	k_A	Air thermal conductivity, BTU/hr-ft-$°F$
170[†]	ρ_M	Plate and fin density, lb/ft^3 (Al)
120[†]	k_M	Plate and fin thermal conductivity, BTU/hr-ft-$°F$
10^6[θ]	E	Energy storage capacity, BTU
6[θ]	θ	Cycle time, hours
*	Δ_A	Rise or fall in air temperature, $°F$
*	Δp	Air-side pressure drop, inches H_2O
*	Δ_S	Salt-side rise or fall in temperature, $°F$
*	Δ_p	Rise or fall in temperature through the plate, $°F$

[*] Variation of these design parameters has been examined.

[1] Estimated from measured salt density, extent of reaction, and heat of reaction.

[+] Calculated from known salt and vapor phase thermal conductivity and estimated bed void fraction (ref. 32).

[†] Handbook values for air and aluminum.

[θ] Design parameters.

The salt- and air-side fin effectiveness parameters, η_{SS} and η_{AS}, are calculated next (ref. 34):

$$\zeta_{SS} = 2HSS \cdot \left(\frac{2k_S}{k_M SSS \cdot TSS}\right)^{1/2}$$

$$\zeta_{AS} = 2HAS \cdot \left(\frac{h_A}{2k_M TAS}\right)^{1/2} \qquad (51)$$

$$\eta_{SS} = \tanh\left(\zeta_{SS}\right)/\zeta_{SS}$$

$$\eta_{AS} = \tanh\left(\zeta_{AS}\right)/\zeta_{AS}$$

In addition, the air-side pressure drop is calculated from the equation (ref. 35)

$$\Delta p = 3.9 \times 10^{-11} \; L \; \frac{\mu_A{}^{0.25}}{\rho_A} \left(\frac{HAS + SAS}{HAS \cdot SAS}\right)^{1.25} \left(\frac{E_d HSS \cdot L}{\theta HAS \cdot C_A \Delta_A}\right)^{1.75} \qquad (52)$$

Finally, the temperature drops on the air side, through the plate, and on the salt side are calculated:

$$\Delta_A = \frac{E_d HSS \cdot SAS}{2\theta h_A (HAS \cdot \eta_{AS} + SAS/2)}$$

$$\Delta_P = \frac{E_d TP \cdot HSS}{\theta k_M} \qquad (53)$$

$$\Delta_S = \frac{E_d HSS \cdot SSS^2}{8\theta k_S (HSS \cdot \eta_{SS} + SSS/2)}$$

In addition, the total weight of the container and the fins is calculated.

The values of Δp, Δ_A, and Δ_S will not generally agree with those selected for the design. To reduce Δ_S, it is necessary to increase TSS, the salt-side fin thickness, or reduce SSS, the salt-side fin separation. Likewise, altering TAS, the air-side fin thickness, SAS, the air-side fin separation, and HAS, the air-side fin height, will affect both Δ_A and Δp. We have generally found it best to decrease Δp by increasing the air-side fin depth HAS, and to decrease Δ_A by decreasing the air-side fin spacing, while keeping constant fin thickness TAS. The changes must be made iteratively to obtain the desired Δp and Δ_A.

Preliminary calculations indicated no optimum fin thickness: it appears that the weight of metal is minimized by using extremely thin fins

spaced closely together. For this reason, we set the fin thickness at 0.002' (24 mils) in all further calculations; it will be necessary to set fin thickness by criteria related to the ease and cost of manufacture. In the absence of further information, the plate thickness was set equal to 0.1" (100 mils); the same thickness was used for all six walls of the salt container.

The fan power requirement was set equal to 0.53 hp, which corresponds to a pressure drop of 0.4" H_2O when the air-side Δ_A is 18°F (10°C). A higher fan power is perhaps appropriate for a system operating at $10^6/6 = 166,667$ BTU/hr. Nevertheless, the calculations indicate that the heat exchange design need not be excessively elaborate to achieve high-rate operation at low parasitic power consumption.

After selection of salt-side and air-side temperature drops, the remaining two independent geometrical parameters in Figure 38 -- the length L and salt-side depth HSS -- were systematically varied to obtain the minimum weight of the container. It was found that the weight was a rather weak function of L. Furthermore, near the optimum depth, HSS could be varied substantially with little effect on the weight -- the optimum is quite broad. These results are summarized in Table 5.

We also briefly investigated the effect of using unequal temperature drops on the air and salt sides. These calculations indicate that the optimum occurs at very nearly equal values of Δ_A and Δ_S. This is not surprising since the thermal properties of the two sides are similar.

The effect on total weight of varying the assumed temperature drop $\Delta_A + \Delta_S$ is shown in Figure 39. Doubling the allowed temperature drop from 36°F (20°C) to 72°F (40°C) reduces the total weight by about 30%, from 1581 lbs to 1110 lbs. Since the total weight of salt plus vapor for 10^6 BTU storage is likely to be greater than 2000 lbs, these weights are reasonable from the point of view of container heat capacity, and it appears possible to design a system for rather small ΔT and low parasitic power consumption without an excessive penalty in total container cost.

It is also of interest to note that the optimum salt depth is of the order of 6". It should not be difficult to achieve bed depths in this range with pelletized desiccant material such as $CaCl_2$. No appreciable pressure drop should occur through a pelletized bed of this depth, so that vapor flow should not be hindered by diffusion.

It is important to stress once again the preliminary nature of these results. We have not established the optimum storage capacity or rate, nor have we considered the ease and cost of manufacture of the design, nor the adequacy of the container strength. (All of these factors are of course under study.) Nevertheless, we have established a design procedure, and have shown that large storage capacity, high rate, and

TABLE 2

SALT-BED HEAT EXCHANGER DESIGNS
FOR VARIOUS TEMPERATURE DROPS

Weight (lbs)	Fan Power (hp)	Δ_A (°F)	Δ_S (°F)	L (ft)	W* (ft)	HSS (ft)	SSS (ft)	HAS (ft)	SAS (ft)
1858	0.56	18.2	18.1	2	192.3	0.20	0.048	0.029	0.028
1591	0.52	18.1	18.0	2	109.9	0.35	0.037	0.050	0.022
1581	0.54	18.0	17.9	2	96.2	0.40	0.034	0.056	0.021
1600	0.56	18.0	18.1	2	76.9	0.50	0.0295	0.069	0.0195
1668	0.55	18.0	18.0	2	64.1	0.60	0.026	0.085	0.018
1581	0.54	18.0	17.9	2	96.2	0.40	0.034	0.056	0.021
1582	0.53	17.9	17.9	3	64.1	0.40	0.034	0.087	0.027
1285	0.52	27.1	27.0	3	64.1	0.40	0.0448	0.048	0.033
1140	0.53	36.1	36.1	3	64.1	0.40	0.0543	0.032	0.041
1110	0.55	36.2	35.9	3	51.3	0.50	0.0472	0.0385	0.036
1112	0.53	36.2	36.2	3	42.7	0.60	0.0420	0.0462	0.0326

*In actual manufacture, the width would be reduced to a reasonable value (e.g., 3 ft) by using stacked multiple units.
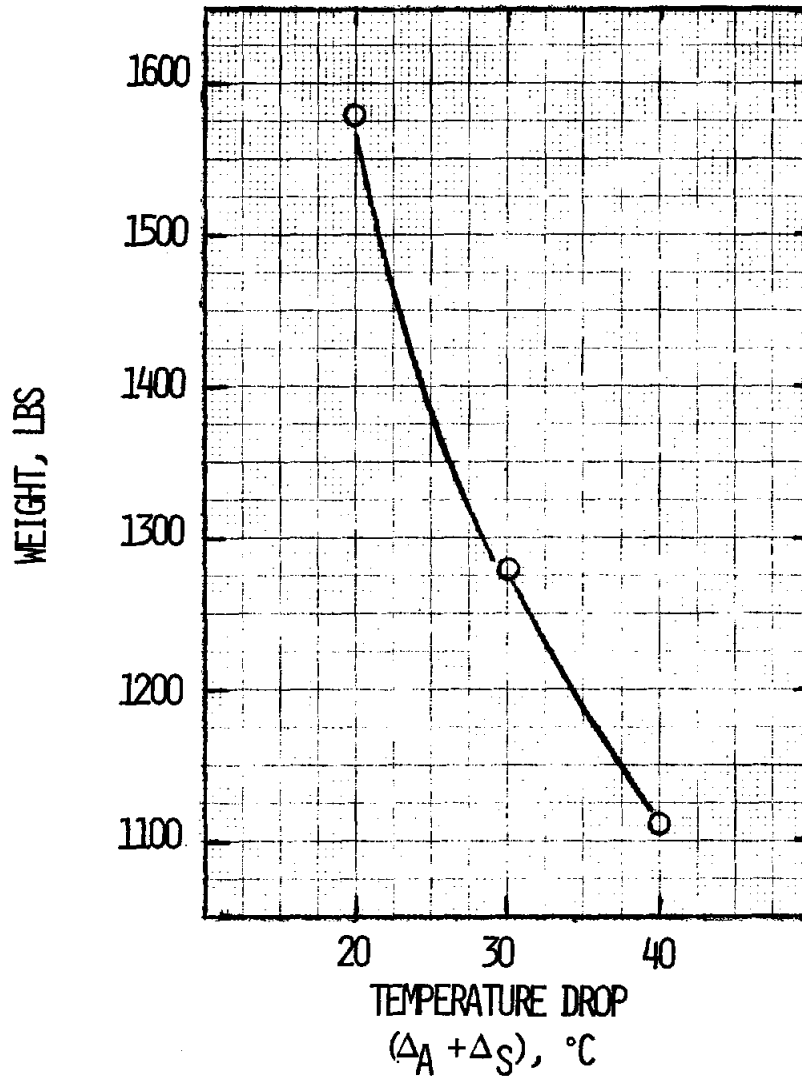
Fig. 39: Variation of calculated heat exchanger
and container weight with total allowed
temperature drop.

low parasitic power consumption can be achieved without an excessive container heat capacity and without excessive temperature drops. Calculations of this type will be continued when we have considered the manufacturing costs of these preliminary designs.

2. Alternative Designs

The evaluation of the preceding section was based on a salt containment configuration involving the use of a series of horizontal flat plates to provide support for the salt, an area for vapor passage to and from the bed, and for passage of the heating/cooling medium through the unit. Such a design meets the essential requirements of supporting the salt, providing a simple means of configuring the required surface extension to obtain reasonable conductive heat transfer rates in the bed, and providing for adequate vapor passage through the salt bed. The latter requirement might be critical if, for design reasons, it proved necessary to use a very deep salt bed and/or small salt particles.

It might prove difficult, however, to construct a low cost storage unit with this type of design. A large number of joints would have to be properly sealed, some additional stiffening – or heavier plate thicknesses might have to be provided for larger units, and some means of retaining salt in place might have to be devised. These problems would be more severe if shallow bed depths were used. Alternative styles of containment vessels can be conceived, which would be equally effective in providing the required surface extension for heat transfer within the bed. However, the problem of vapor access to the depths of the bed, vapor phase pressure drops if small salt particles are used, and salt containment must be addressed for any alternative considered.

We have recently begun design calculations on the heat exchange configuration shown in Figure 40. In this configuration, heat transfer fluid passes through tubes with internal fins. The tubes are connected to fins on the salt bed side, and the salt is supported on plates which are not, however, used for heat transfer. The salt bed support plates could be contained within a drum, as shown in Figure 41. In this arrangement, containment of the low pressure vapor is provided by the drum rather than by individual salt-bed containers. Since a cylindrical shape can withstand a given pressure force with a thinner wall than can a flat shape, this design will not only reduce the amount of metal, but should also greatly simplify vacuum sealing, which will only be required at the two ends of the drum.

We have also begun to consider the use of pressurized water on other liquid heat transfer fluid as an alternative to air. This is particularly advantageous in the design shown in Figures 40 and 41, since water or other heat transfer fluids under pressure can be more effectively contained in relatively small diameter tubes than in a large, flat area

PELLETIZED
SALT

SALT BED
FINS

INTERNALLY
FINNED TUBES
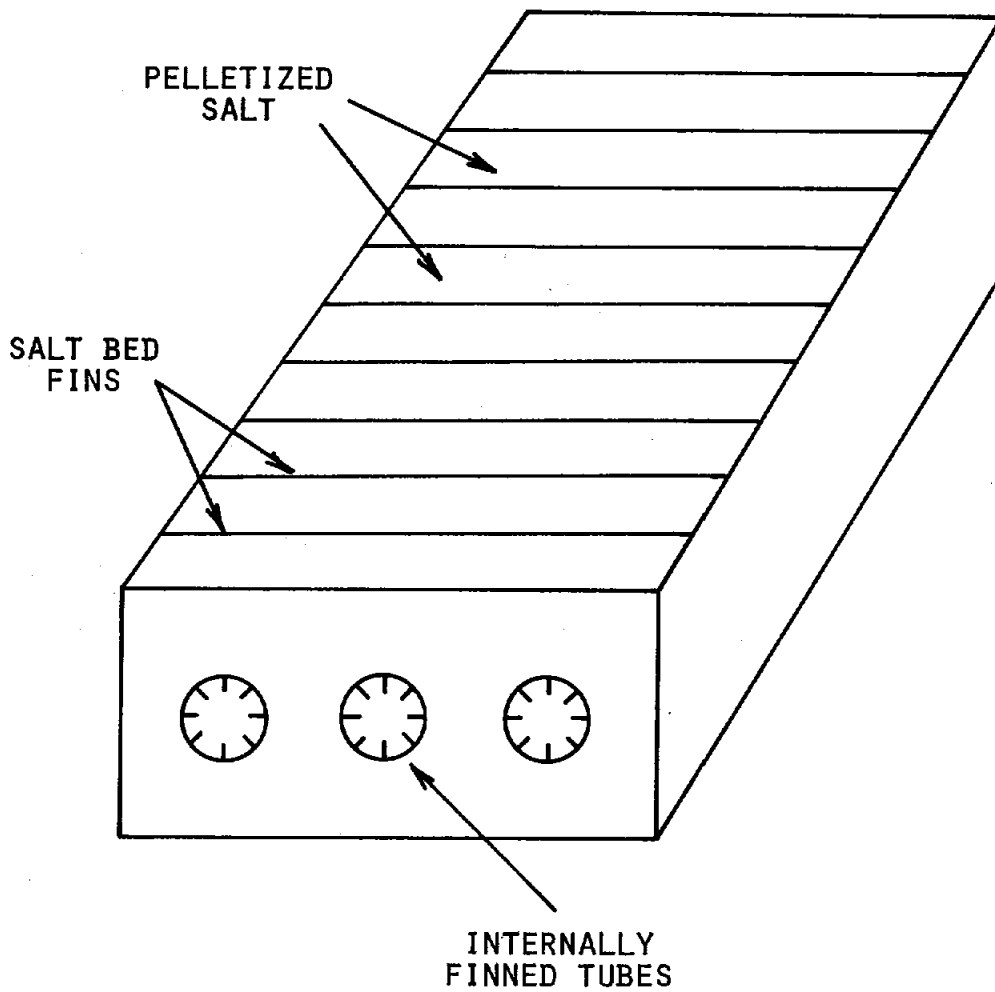
Fig. 40:   Alternative salt-bed heat exchanger design
using finned tubes.
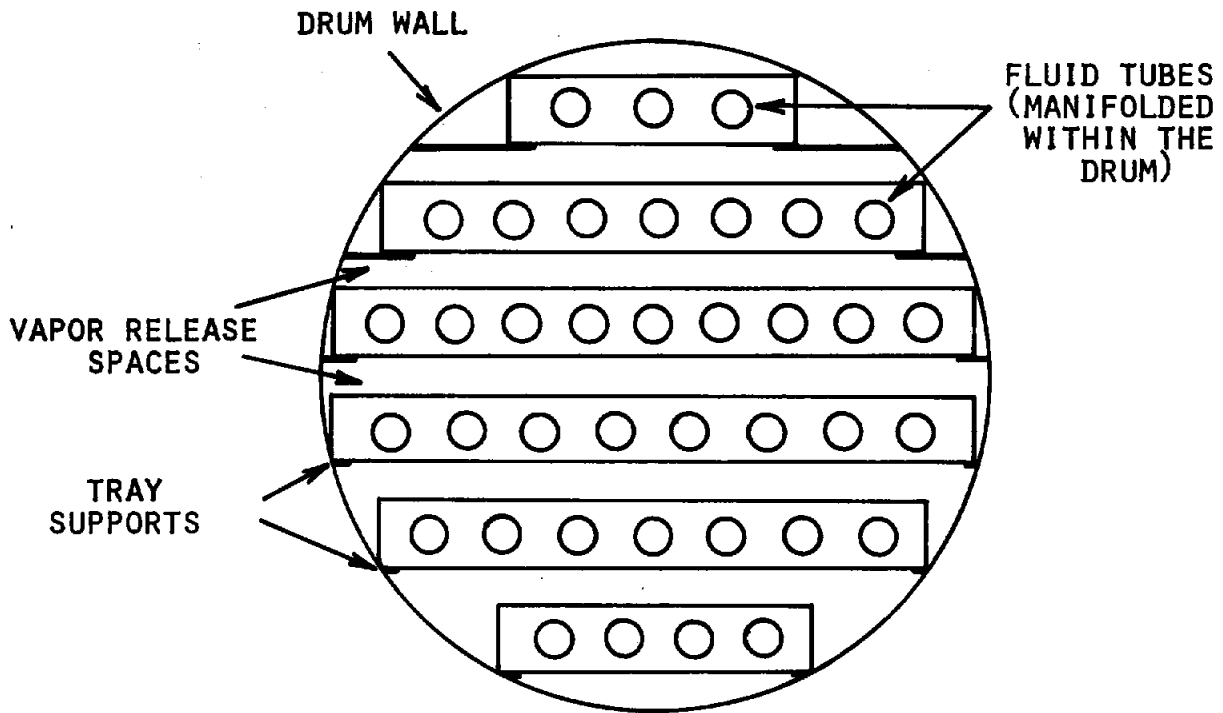
Fig. 41: Schematic arrangement of finned-tube salt-bed heat exchangers within a vapor containment drum.

unless significant additional stiffening is provided. However, this design requires a second (water-to-air) heat exchanger for forced-air heat rejection, which implies additional costs and temperature drops. We will evaluate this design more fully in Phase II, prior to construction of the test unit and the prototype.

3. Overall Systems Analysis

The salt bed heat exchanger must be designed with two primary functions in mind. First, it must act as a "generator," taking up energy from the solar collector and releasing CH_3OH vapor. Second, it must act as an "absorber," accepting vapor and releasing heat. The rate at which the system can be "charged" -- i.e., the rate at which it can accept energy from the collector -- depends on many factors, including the solar collector fluid temperature, the heating rate, the superheating required for vapor desorption kinetics, the approach temperature in the salt bed, the effective UA of the salt-bed heat exchanger, the thermodynamics of the vapor-salt reaction, the CH_3OH condensation temperature, and so on. In a similar way, the rate at which the salt bed can take up vapor and provide heat pumping or air conditioning depends on the vapor pressure in the evaporator, the subcooling required for sorption kinetics, the thermodynamics of the vapor-salt reaction, the outdoor ambient temperature, and so on. It is obvious that a design optimal for sorption ("discharging") may be poor for desorption, and vice versa. One of the most important aspects of system design is the required relationship between the two modes of operation. In addition, it is necessary to consider both summer and winter operation, and to design the system with adequate storage capacity.

We have tentatively decided to design the system to accept solar energy at a rate of 50,000 BTU/hr. In order to maintain a high coefficient of performance, it is desirable that the system not be switched from the charge to the discharge mode during solar collection; for this reason, the minimum storage capacity (for winter operation) should be about 400,000 BTU. However, during summer operation, the maximum total energy collected daily will increase to about 800,000 BTU, which should provide about 400,000 BTU of cooling. In principle, it would be desirable to use two units, each with 800,000 BTU storage capacity, to avoid switching between modes during solar collection. One unit would act as the absorber while the other would act as the generator. Nevertheless, it is not clear that a storage capacity of this magnitude is justified: the total energy available for cooling may be sufficiently large that some operating inefficiency can be tolerated, and a smaller storage capacity may be adequate.

Questions of this type are critical to system design, but are difficult to answer in the absence of a complete systems simulation. Fortunately, work we are carrying out on another contract -- EG-77-C-03-4483 - Analysis of Advanced Thermal Storage Subsystems for Solar Heating and Cooling -- should provide most of the information needed. As part of

that contract, we have written simulation routines for methanol-based heat pumps, including all controls. We have tested these routines using realistic building loads and hourly solar and weather data, and they appear to represent our proposed systems adequately. We will use the data from this program to study the trade-off between storage size and system performance and, ultimately, in the design of the salt-bed heat exchanger.

In the interim, we have been considering the design trade-offs between sorption and desorption. Our preliminary results indicate that, given the high performance solar collectors that are rapidly becoming available, the system should be designed for efficient sorption, i.e., pumping and delivery of heat from ambient to the indoors. Optimization of the system for this application will insure that the minimum temperature from which heat can be pumped will be sufficiently low that the system can be used in a fairly wide variety of climates.

IV. CONCLUSIONS

No major technical obstacles to the development of a CH_3OH-based solar heat pump/thermal storage system have been encountered. The reaction of $CaCl_2$ with CH_3OH vapor to produce $CaCl_2 \cdot 2CH_3OH$ appears both thermodynamically and kinetically suitable. Excessive vapor pressure drops through the bed can be prevented by use of $CaCl_2$ pellets, which do not appear to expand/contract or decrepitate during repeated methanolation and demethanolation. Corrosion does not appear to be a problem at this time, although experiments to date have been limited to 300 complete cycles over a period of a month. Formation of a bed "crust", or pellet agglomeration, observed over this period, did not markedly affect the cycling rates, although it would be expected to cause problems in the long run. Analytical and experimental work indicate that the salt-bed heat exchanger can be of relatively compact construction, and the energy density for storage is about 13,000 BTU/ft^3.

In Phase II of the development program we will design and construct a prototype system. At the same time, a search for salts alternative to $CaCl_2$ will be made in order to allow the design of CH_3OH-based systems for the widest variety of climates. Cycling and corrosion testing of $CaCl_2$ will continue. Methods of preventing pellet agglomeration through the use of coatings and binders will be investigated. Systems analysis through computer simulation and economic evaluations will be carried out to study the trade-offs among storage size, heat exchanger design, and system performance. Prior to the design of the prototype, additional performance data will be obtained from a small scale unit with a storage capacity around 1000 BTU.

V. REFERENCES

1. G. F. Hüttig, Z. Anorg. Chem., 123, 31 (1922).

2. W. Blitz, Z. Anorg. Chem., 130, 93 (1923).

3. Private communications from Doug Huxtable, Rocket Research Corp., Redmond, Washington.

4. Carrier Corporation, Form 38 BQ-8P: Carrier Heat Pump Systems (1974).

5. H. Brusset and I. Bkouche-Waksman, Bull. Soc. Chim. Fr., 1969 (1), 54-6.

6. F. Hájek and F. Jost, Croat. Chem. Acta, 29, 457-60 (1957).

7. G. B. Seifer, Zhur. Neorg. Khim, 2 (1957).

8. A. Z. Chkhenkili, Zhur. Neorg. Khim, 2, 787-9 (1957).

9. L. M. Dzhanpoladyan, Izrest. Ahad. Nauk Armyan SSR, Fitz.-Mat., Estestren. i Tech. Nanki, 5(5), 39-47 (1952).

10. F. Kloges, H. Meuresch and W. Stepfich. Ann., 592, 81-119 (1955).

11. M. Gerhold and L. Kahovec, Acta Phys. Austriaca, 1, 366-9 (1948).

12. D. R. Chesterman, J. Chem. Soc., 1935, 906-10.

13. O. E. Zvyagintser and Sh.N. Matatashvili, Bull. Acad. Sci. Georgian SSSR, 3, 1035-41 (1942).

14. M. L. Quinet, Bull. Soc. Chim., 3, 1823-9 (1936).

15. G. C. Gibson, J. O'L. Driscoll and W. J. Jones, J. Chem. Soc., 1929, 1440-3.

16. J. K. Betse, Praktika (Akad. Athenon), 6, 148-53 (1931).

17. I. Bkouche-Waksman, C. R. Acad. Sci., Ser. C, 271, 581-4 (1970).

18. V. N. Marchenko and O. A. Osipov, Zh. Obshch. Khim, 36, 599-605 (1966).

19. J. J. P. Martin, Compt. Rend., 261, 3622-4 (1965).

20. J. Galvez-Flores, An. Univ. Murcia, Lienc 1970-1971, 29, 117-62.

21. P. L'Haridon and J. Lang, Rev. Chim. Miner., <u>8</u>, 813-18 (1971).

22. H. H. Emons, H. H. Seyforth and F. Winkler, Krist. Tech., <u>6</u>, 521-31 (1971).

23. H. Gillier-Pandrand and M. Pheloche-Levisalles, C. R. Acad. Sci., Ser. C, <u>273</u>, 949-51 (1971).

24. F. Winkler and H. H. Emons, Wiss. Z. Tech. Hochsch. Chem-Leuna-Merseburg, <u>11</u>, 236-42 (1969).

25. E. R. Grosman and V. Ya. Zhuravlenko, Kholvd. Tekh, <u>46</u>, 40-2 (1969).

26. S. J. Frakin, M. Kh. Karapat'yants and R. Kh. Kurmelieva, Zh. Neorg. Khim, <u>14</u>, 2697-2700 (1969).

27. N. Ya. Turova, E. P. Turevskaya and A. V. Noroselova, Zh. Neorg. Khim, <u>12</u>, 1712-14 (1967).

28. P. Silker, D. Zins, M. Robineau and M. Brianso-Perevcand, Rev. Chim. Miner, <u>12</u>, 347-56 (1975).

29. I. Bkouche-Waksman, Bull. Soc. Chim. Fr. 1972, 1776-81.

30. M. Abrouk, C. R. Acad. Sci., Ser. C, <u>278</u>, 875-7 (1974).

31. A. LeClaire, Acta Crystallver., Sec. B, <u>B30</u>, Pt. 9, 2259-60 (1974).

32. Chemical Engineers' Handbook, Fifth Edition, R. H. Perry and C. H. Chilton, eds. (New York: McGraw Hill, 1973), Section 3, pp. 241-242. See also Russel, J. Am. Ceram. Soc., <u>18</u>, 1 (1935).

33. Reference 32, Equ. 10-50.

34. Wm. H. McAdams, Heat Transmission, McGraw Hill, New York, 1954. Equ. 10-8.

35. Reference 32, Equ. 5-52.

APPENDIX A

FORTRAN LISTING OF XCHANG

```
C* HEAT TRANSFER MODEL - ONE DIMENSIONAL - SALT/METHANOL EXCHANGER
C*---STREAMLINED VERSION---
      DIMENSION REAFRN(100),CAPPA(100),TEMP(100),DELTEM(100),HETCAP(100)
     1,DELMET(100)
      IN=103
      IOUT=108
    1 READ(IN,100) NDEEP,MODE,MODEL,NTIME,MOLES,NREPRT
C NDEEP -- # SEGMENTS FOR BED DEPTH - CA. 10
C MODE    -- 0 FOR DEMETH, 1 FOR METHANOLATION
C MODEL -- 0 FOR SHARP CUT-OFF RATE MODEL
C NTIME -- # OF TIME STEPS IN 24 HOURS
C MOLES -- # OF MOLES OF CH3OH PER MOLE OF SALT
C NREPRT #OF TIME STOPS BEFORE A RESULT IS PRINTED OUT
      N=NDEEP
      IF(N.LE.0) CALL EXIT
C
      READ(IN,101) DEPTH,DRYDEN,FRCTN1,FRCTN2,TEMPIN,WT,VOID
C DEPTH -- BED DEPTH, CM.
C DRYDEN -- ACTUAL DENSITY OF FULLY DEMETHANOLATED SALT,
C             NOT CORRECTED FOR VOIDS
C FRCTN1 -- FRACTION OF MAX. POSSIBLE CH3OH IN BED WHEN
C             DEMETHANOLATED (CA. 0.1)
C FRCTN2 -- FRACTION OF MAX. POSSIBLE CH3OH IN BED WHEN
C             FULLY METHANOLATED (CA. 0.9)
C TEMPIN -- INITIAL BED TEMPERATURE, DEG. C.
C WT      -- MOLECULAR WEIGHT OF SALT
C VOID    -- VOID FRACTION IN FULLY DEMETHANOLATED BED
C
      READ(IN,101) PRE,PREP,ACTIVE,ESUBA,TCRIT1,TCRIT2,PLATEM
C PRE,PREP,ACTIVE,ESUBA --
C -- RATE OF METHANOLATION = EXP(PRE)*EXP(ACTIVE/(273.+TEMP))
C -- RATE OF DEMETH = EXP(PREP)*EXP(-ESUBA/(273.+TEMP))
C --  RATES ARE MOLES OF CH3OH PER HOUR PER MOLE OF SALT
C --  WHEN MODEL=0, RATES MAY BE SET EQUAL TO ZERO PER
C      THE ALGORITHM BELOW
C TCRIT1 -- TEMPERATURE ABOVE WHICH RATE = 0 FOR METHANOLATION
C TCRIT2 -- TEMPERATURE BELOW WHICH RATE = 0 FOR DEMETHANOLATION
C
C PLATEM -- PLATE TEMPERATURE (CA. 50 DEG. C FOR METHANOLATION)
C                  (CA. 130 DEG. C FOR DEMETHANOLATION)
      READ(IN,101) THRCN1,THRCN2,CP1,CP2,HEAT
C THRCN1 AND THRCN2 ARE THERMAL CONDUCTIVITIES OF CH3OH AT 50
C    AND 120 DEG C. IN BTU/HR-FT-DEG F
C CP1 AND CP2 ARE SPECIFIC HEATS OF SALT AND FULLY METH. SALT
C HEAT -- HEAT OF REACTION PER MOLE OF CH3OH (POSITIVE)
      THRCN1=THRCN1/242.
      THRCN2=THRCN2/242.
      PRE=EXP(PRE)
      PREP=EXP(PREP)
      AREA=100.
      DX=DEPTH/N
      DXAREA=DX*AREA
      FR=FRCTN1
      IF(MODE.EQ.0) FR=FRCTN2
```

88

```
      XMOLES=(1.-VOID)*DXAREA*DRYDEN/WT
      DELT=24./NTIME
      TIME=0.
      YMOLES=MOLES
      XYMOLE=XMOLES*YMOLES
      WEIGHT=XMOLES*WT+ 32.*XYMOLE*FR
      COE1=PRE*DELT*XMOLES
      COE1P=PREP*DELT*XMOLES
      COE2=XMOLES*WT/DRYDEN
      COE3=XYMOLE/0.8
      COE4=3600.*AREA*DELT/DX
      COE5=WT*XMOLES
      COE6=32.*XYMOLE
      VOLUME=COE2+COE3*FR
      VOIDFR=VOLUME/DXAREA
      ONETH=1./3.
      COND=1.0/(1.-VOIDFR**ONETH)
      SLOPE=(THRCN2-THRCN1)/70.
      CEPT=THRCN1-50.*SLOPE
      COND=COND*(CEPT+TEMPIN*SLOPE)
      DELCP=CP2-CP1
      CP=CP1+FR*DELCP
C
      DO 10  I=1,N
      REAFRN(I)=FR
      TEMP(I)=TEMPIN
      CAPPA(I)=COND
      HETCAP(I)=CP
   10 CONTINUE
C
      ICOUNT=0
C
      DO 80  J=1,NTIME
   11 TIME=TIME+DELT
C BEGIN RATE LOOP
      IF(MODE.EQ.0) GO TO 13
      DO 12 I=1,N
      DELMET(I)=COE1*EXP(ACTIVE/(273.+TEMP(I)))*(1.-REAFRN(I))
      IF(MODEL.EQ.0.AND.TEMP(I).GT.TCRIT1) DELMET(I)=0.0
   12 CONTINUE
      GO TO 121
   13 DO 131 I=1,N
      DELMET(I)=-COE1P*EXP(-ESUBA/(273.+TEMP(I)))*REAFRN(I)
      IF(MODEL.EQ.0.AND.TEMP(I).LT.TCRIT2) DELMET(I)=0.0
  131 CONTINUE
C
C  HAVING CALCULATED THE METHANOL RATE, WE NOW CALCULATE THE
C  PROPERTIES OF EACH SEGMENT.
C
  121 DO 14 I=1,N
      REAFRN(I)=(XYMOLE*REAFRN(I)+DELMET(I))/XYMOLE
      HETCAP(I)=CP1+REAFRN(I)*DELCP
      CAPPA(1)=(CEPT+TEMP(I)*SLOPE)/(1.-( (COE2+COE3*REAFRN(I))/
     1 DXAREA)**ONETH)
   14 CONTINUE
C
C  HAVING CALCULATED THE NEW PROPERTIES, WE NOW CALCULATE THE
```

```
C     HEAT FLOW AND THE CHANGES IN TEMPERATURE.
C
      IF(N.EQ.1) GO TO 17
C TOP SEGMENT
      FLUX=COE4*CAPPA(1)*(TEMP(2)-TEMP(1))
      DELTEM(1)=(FLUX+HEAT*DELMET(1))/
     1 ((COE5+COE6*REAFRN(1))*HETCAP(1))
      IF(N.EQ.2) GO TO 20
C MIDDLE SEGMENTS
      DO 16 I=2,N-1
      FLUX=COE4*CAPPA(I)*(TEMP(I-1)+TEMP(I+1)-2.*TEMP(I))
      DELTEM(I)=(FLUX+HEAT*DELMET(I))/
     1 ((COE5+COE6*REAFRN(I))*HETCAP(I))
   16 CONTINUE
C BOTTOM SEGMENT
   17 TOPTEM=TEMP(1)
   20 IF(N.NE.1) TOPTEM=TEMP(N-1)
      FLUX=COE4*CAPPA(N)*((PLATEM-TEMP(N))*2.+TOPTEM-TEMP(N))
      DELTEM(N)=(FLUX+HEAT*DELMET(N))/
     1 ((COE5+COE6*REAFRN(N))*HETCAP(N))
C
C     CALCULATE CHANGES IN TEMPERATURE AND AVERAGE PROPERTIES
C
      FRA=0.
      CPA=0.
      TA=0.
      CAPAV=0.
      DO 18  I=1,N
      TEMP(I)=TEMP(I)+DELTEM(I)
       TA=TA+TEMP(I)
      FRA=FRA+REAFRN(I)
      CPA=CPA+HETCAP(I)
      CAPAV=CAPAV+CAPPA(I)
   18 CONTINUE
      XDEEP=NDEEP
      TA=TA/XDEEP
      FRA=FRA/XDEEP
      CPA=CPA/XDEEP
      CAPAV=CAPAV/XDEEP
      ICOUNT=ICOUNT+1
      IF(ICOUNT.LT.NREPRT) GO TO 80
      ICOUNT=0
C
C     PRINT RESULTS OF MAJOR IMPORTANCE
C
      WRITE(IOUT,110) J,TEMP(1),TA,TEMP(N),REAFRN(1),FRA,
     1 REAFRN(N),CPA,CAPAV,FLUX
      WRITE(IOUT,115) (TEMP(I),I=1,NDEEP)
      IF(MODE.EQ.0.AND.FRA.LE.FRCTN1+.01)GOTO 1
      IF(MODE.EQ.1.AND.FRA.GE.FRCTN2-.01)GOTO 1
   80 CONTINUE
      GO TO 1
  110 FORMAT(1X,I5,3F10.2,5X,3F10.3,5X,F10.4,2F10.5)
  115 FORMAT(10E12.4)
  100 FORMAT(10I5)
  101 FORMAT(8F10.5)
      END
```

90

APPENDIX B

FORTRAN LISTING OF TWODIM

```
      NAME = TWODIM


C* HEAT TRANSFER MODEL - TWO DIMENSIONAL - SALT/METHANOL EXCHANGER
C*---STREAMLINED VERSION---
      DIMENSION REAFRN(20,20),CAPPA(20,20),TEMP(20,20),
     1 DELTEM(20,20),HETCAP(20,20),DELMET(20,20),TOPTEM(20)
     2 ,FINFLX(20),PLTFLX(20),FINCAP(20),FINTEM(20)
     3 ,FINTHK(20),DELFIN(20)
      IN=103
      IOUT=108
    1 READ(IN,100) NDEEP,MWIDE,MODE,MODEL,NTIME,MOLES,NREPRT,ISHAPE
C NDEEP -- # DIVISIONS FOR BED DEPTH - CA. 10
C MWIDE -- # DIVISIONS FOR BED WIDTH - CA. 10
C MODE  -- 0 FOR DEMETHANOLATION, 1 FOR METHANOLATION
C MODEL -- 0 FOR SHARP CUT-OFF RATE MODEL
C NTIME -- # IN INPUT IS # OF TIMESTEPS IN 24 HRS. DIVIDED BY 100
C MOLES -- # OF MOLES OF CH3OH PER MOLE OF SALT
C NREPRT #OF TIME STOPS BEFORE A RESULT IS PRINTED OUT
C ISHAPE -- =0 FOR RECTANGULAR FIN PROFILE, OTHERWISE TRIANGULAR
      NTIME=NTIME*100
      WRITE(IOUT,102) NDEEP,MWIDE,MODE,MODEL,NTIME,MOLES,NREPRT,ISHAPE
      N=NDEEP
      IF(N.LE.0) CALL EXIT
      M=MWIDE
      DO 2 I=1,20
      FINFLX(I)=0.
    2 PLTFLX(I)=0.
C
      READ(IN,101) DEPTH,WIDTH,DRYDEN,FRCTN1,FRCTN2,TEMPIN,WT,VOID
      WRITE(IOUT,103) DEPTH,WIDTH,DRYDEN,FRCTN1,FRCTN2,TEMPIN,WT,VOID
C DEPTH  -- BED DEPTH, CM.
C WIDTH  -- BED WIDTH, CM.- EQUAL TO ONE HALF THE DIMENSION
C              BETWEEN FINS OF HEIGHT EQUAL TO BED DEPTH
C DRYDEN -- ACTUAL DENSITY OF FULLY DEMETHANOLATED SALT,
C              NOT CORRECTED FOR VOIDS
C FRCTN1 -- FRACTION OF MAX. POSSIBLE CH3OH IN BED WHEN
C              DEMETHANOLATED (CA. 0.1)
C FRCTN2 -- FRACTION OF MAX. POSSIBLE CH3OH IN BED WHEN
C              FULLY METHANOLATED (CA. 0.9)
C TEMPIN -- INITIAL BED TEMPERATURE, DEG. C.
C WT       -- MOLECULAR WEIGHT OF SALT
C VOID    -- VOID FRACTION IN FULLY DEMETHANOLATED BED
C
      READ(IN,101) PRE,PREP,ACTIVE,ESUBA,TCRIT1,TCRIT2,PLATEM
      WRITE(IOUT,103) PRE,PREP,ACTIVE,ESUBA,TCRIT1,TCRIT2,PLATEM
C PRE,PREP,ACTIVE,ESUBA --
C  -- RATE OF METHANOLATION = EXP(PRE)*EXP(ACTIVE/(273.+TEMP))
C  -- RATE OF DEMETH = EXP(PREP)*EXP(-ESUBA/(273.+TEMP))
C  --   RATES ARE MOLES OF CH3OH PER HOUR PER MOLE OF SALT
C  --   WHEN MODEL=0, RATES MAY BE SET EQUAL TO ZERO PER
C          THE ALGORITHM BELOW
C TCRIT1 -- TEMPERATURE ABOVE WHICH RATE = 0 FOR METHANOLATION
C TCRIT2 -- TEMPERATURE BELOW WHICH RATE = 0 FOR DEMETHANOLATION
C
C PLATEM -- PLATE TEMPERATURE (CA. 50 DEG. C FOR METHANOLATION)
C                (CA. 130 DEG. C FOR DEMETHANOLATION)
```

```
      READ(IN,101) THRCN1,THRCN2,CP1,CP2,HEAT,THKFIN,THRCNF,CPFIN
      WRITE(IOUT,103) THRCN1,THRCN2,CP1,CP2,HEAT,THKFIN,THRCNF,CPFIN
C THRCN1 AND THRCN2 ARE THERMAL CONDUCTIVITIES OF CH3OH AT 50
C      AND 120 DEG C. IN BTU/HR-FT-DEG F
C CP1 AND CP2 ARE SPECIFIC HEATS OF SALT AND FULLY METH. SALT
C HEAT -- HEAT OF REACTION PER MOLE OF CH3OH (POSITIVE)
C THKFIN -- HALF THE TOTAL FIN THICKNESS (CM.)
C THRCNF -- FIN THERMAL CONDUCITIVITY (BTU/HR-FT-DEG F)
C CPFIN -- SPECIFIC HEAT OF FIN MATERIAL
      THRCN1=THRCN1/242.
      THRCN2=THRCN2/242.
      THRCNF=THRCNF/242.
      PRE=EXP(PRE)
      PREP=EXP(PREP)
      LENGTH=10.
      DX=DEPTH/N
      DY=WIDTH/M
      SEGMNT=N*M
      DXLONG=DX*LENGTH
      DELVOL=DXLONG*DY
      DIM1=DXLONG/DY
      DIM2=DY*LENGTH/DX
      FR=FRCTN1
      IF(MODE.EQ.0) FR=FRCTN2
      XMOLES=(1.-VOID)*DELVOL*DRYDEN/WT
      DELT=24./NTIME
      TIME=0.
      YMOLES=MOLES
      XYMOLE=XMOLES*YMOLES
      COE1=PRE*DELT*XMOLES
      COE1P=PREP*DELT*XMOLES
      COE2=XMOLES*WT/DRYDEN
      COE3=XYMOLE/0.8
      COE4=3600.*DELT
      COE5=WT*XMOLES
      COE6=32.*XYMOLE
      VOLUME=COE2+COE3*FR
      VOIDFR=VOLUME/DELVOL
      ONETH=1./3.
      COND=1./(1.-(VOIDFR**ONETH))
      SLOPE=(THRCN2-THRCN1)/70.
      CEPT=THRCN1-50.*SLOPE
      COND=COND*(CEPT+TEMPIN*SLOPE)
      DELCP=CP2-CP1
      CP=CP1+FR*DELCP
C DENSITY OF ALUMINUM (GRAMS PEBR CU. CM.)
      ALDEN=2.700
C
C NOTE FOLLOWING CHOICE OF SUBSCRIPTS:
C I FOR DEPTH SUBDIVISIONS WITH I=1 AT TOP, I=N AT BOTTOM
C J FOR WIDTH SUBDIVISIONS WITH J=1 NEXT TO MIDDLE OF FIN SPACE,
C                                   J=M NEXT TO FIN
      IF(ISHAPE.EQ.0) GO TO 5
      DO 4 I=1,N
    4 FINTHK(I)=THKFIN*(I-.5)/N
      GO TO 7
    5 DO 6 I=1,N
```

```
      6 FINTHK(I)=THKFIN
      7 DO 10 I=1,N
        FINTEM(I)=PLATEM
        FINCAP(I)=CPFIN*DXLONG*FINTHK(I)*ALDEN
        DO 10   J=1,M
        REAFRN(I,J)=FR
        TEMP(I,J)=TEMPIN
        CAPPA(I,J)=COND
        HETCAP(I,J)=CP
     10 CONTINUE
C
        ICOUNT=0
C
        DO 80   K=1,NTIME
     11 TIME=TIME+DELT
C BEGIN RATE LOOP
        IF(MODE.EQ.0) GO TO 13
        DO 12 I=1,N
        DO 12 J=1,M
        DELMET(I,J)=COE1*EXP(ACTIVE/(273.+TEMP(I,J)))*(1.-REAFRN(I,J))
        IF(MODEL.EQ.0.AND.TEMP(I,J).GT.TCRIT1) DELMET(I,J)=0.0
     12 CONTINUE
        GO TO 121
     13 DO 131 I=1,N
        DO 131 J=1,M
        DELMET(I,J)=-COE1P*EXP(-ESUBA/(273.+TEMP(I,J)))*REAFRN(I,J)
        IF(MODEL.EQ.0.AND.TEMP(I,J).LT.TCRIT2) DELMET(I,J)=0.0
    131 CONTINUE
C
C  HAVING CALCULATED THE METHANOL RATE, WE NOW CALCULATE THE
C   PROPERTIES OF EACH SEGMENT.
C
    121 DO 14 I=1,N
        DO 14 J=1,M
        REAFRN(I,J)=(XYMOLE*REAFRN(I,J)+DELMET(I,J))/XYMOLE
        HETCAP(I,J)=CP1+REAFRN(I,J)*DELCP
        CAPPA(I,J)=(CEPT+TEMP(I,J)*SLOPE)/
       1 (1.-(((COE2+COE3*REAFRN(I,J))/DELVOL)**ONETH))
     14 CONTINUE
C
C  HAVING CALCULATED THE NEW PROPERTIES, WE NOW CALCULATE THE
C   HEAT FLOW AND THE CHANGES IN TEMPERATURE.
C
        IF(N.EQ.1) GOTO 206
C***********************************************************************
C TOP HEIGHT SUBDIVISION
        IF(M.EQ.1) GOTO 200
C WIDTH SUBDIVISION AT INSULATED BOUNDARY
        FLUX=COE4*CAPPA(1,1)*(DIM2*(TEMP(2,1)-TEMP(1,1))
       1 +DIM1*(TEMP(1,2)-TEMP(1,1)))
        DELTEM(1,1)=(FLUX+HEAT*DELMET(1,1))/
       1 ((COE5+COE6*REAFRN(1,1))*HETCAP(1,1))
        IF(M.EQ.2) GOTO 201
C INTERIOR WIDTH SUBDIVISIONS
        DO 199 J=2,M-1
        FLUX=COE4*CAPPA(1,J)*(DIM2*(TEMP(2,J)-TEMP(1,J))
       1 +DIM1*(TEMP(1,J-1)+TEMP(1,J+1)-2.*TEMP(1,J)))
```

```
         DELTEM(1,J)=(FLUX+HEAT*DELMET(1,J))/
       1 ((COE5+COE6*REAFRN(1,J))*HETCAP(1,J))
     199 CONTINUE
   C WIDTH SUBDIVISION NEXT TO FIN
     200 SIDTEM=TEMP(1,1)
     201 IF(M.NE.1) SIDTEM=TEMP(1,M-1)
         FINTRN=COE4*((DY+FINTHK(1))/(DY/CAPPA(1,M)+FINTHK(1)/THRCNF))
       1 *DXLONG*(FINTEM(1)-TEMP(1,M))/(.5*(DY+FINTHK(1)))
         FLUX=COE4*CAPPA(1,M)*(DIM2*(TEMP(2,M)-TEMP(1,M))
       1 +DIM1*(SIDTEM-TEMP(1,M)))
         DELTEM(1,M)=(FLUX+FINTRN+HEAT*DELMET(1,M))/
       1 ((COE5+COE6*REAFRN(1,M))*HETCAP(1,M))
   C TOP FIN SUBDIVISION
         FLUX=COE4*THRCNF*(FINTHK(1)+FINTHK(2))/2.
       1 *LENGTH*(FINTEM(2)-FINTEM(1))/DX
         DELFIN(1)=(FLUX-FINTRN)/FINCAP(1)
         FINFLX(1)=FINFLX(1)+FINTRN
         IF(N.EQ.2) GOTO 208
   C***********************************************************************
   C INTERIOR HEIGHT SUBDIVISIONS
         DO 205 I=2,N-1
         IF(M.EQ.1) GOTO 203
   C WIDTH SUBDIVISION AT INSULATED BOUNDARY
         FLUX=COE4*CAPPA(I,1)*(DIM2*(TEMP(I-1,1)+TEMP(I+1,1)-2.*TEMP(I,1))
       1 +DIM1*(TEMP(I,2)-TEMP(I,1)))
         DELTEM(I,1)=(FLUX+HEAT*DELMET(I,1))/
       1 ((COE5+COE6*REAFRN(I,1))*HETCAP(I,1))
         IF(M.EQ.2) GOTO 204
   C INTERIOR WIDTH SUBDIVISIONS
         DO 202 J=2,M-1
         FLUX=COE4*CAPPA(I,J)*(DIM2*(TEMP(I-1,J)+TEMP(I+1,J)-2.*TEMP(I,J))
       1 +DIM1*(TEMP(I,J-1)+TEMP(I,J+1)-2.*TEMP(I,J)))
         DELTEM(I,J)=(FLUX+HEAT*DELMET(I,J))/
       1 ((COE5+COE6*REAFRN(I,J))*HETCAP(I,J))
     202 CONTINUE
   C WIDTH SUBDIVISION NEXT TO FIN
     203 SIDTEM=TEMP(I,M)
     204 IF(M.NE.1) SIDTEM=TEMP(I,M-1)
         FINTRN=COE4*((DY+FINTHK(I))/(DY/CAPPA(I,M)+FINTHK(I)/THRCNF))
       1 *DXLONG*(FINTEM(I)-TEMP(I,M))/(.5*(DY+FINTHK(I)))
         FLUX=COE4*CAPPA(I,M)*(DIM2*(TEMP(I-1,M)+TEMP(I+1,M)
       1 -2.*TEMP(I,M))+DIM1*(SIDTEM-TEMP(I,M)))
         DELTEM(I,M)=(FLUX+FINTRN+HEAT*DELMET(I,M))/
       1 ((COE5+COE6*REAFRN(I,M))*HETCAP(I,M))
   C INTERIOR FIN SUBDIVISIONS
         FLUX=COE4*THRCNF*((FINTHK(I-1)+FINTHK(I))/2.
       1 *(FINTEM(I-1)-FINTEM(I))+(FINTHK(I+1)+FINTHK(I))/2.
       2 *(FINTEM(I+1)-FINTEM(I)))*LENGTH/DX
         DELFIN(I)=(FLUX-FINTRN)/FINCAP(I)
         FINFLX(I)=FINFLX(I)+FINTRN
     205 CONTINUE
   C***********************************************************************
   C BOTTOM HEIGHT SUBDIVISION
         IF(N.GT.1) GOTO 208
     206 DO 207 L=1,M
         TOPTEM(L)=TEMP(1,L)
     207 CONTINUE
```

95

```
      FINTOP=FINTEM(1)
      TOPTHK=FINTHK(1)
      GOTO 210
  208 DO 209 L=1,M
      TOPTEM(L)=TEMP(N-1,L)
  209 CONTINUE
      FINTOP=FINTEM(N-1)
      TOPTHK=FINTHK(N-1)
  210 IF(M.EQ.1) GOTO 212
C WIDTH SUBDIVISION AT INSULATED BOUNDARY
      FLUX=COE4*CAPPA(N,1)*(DIM2*((PLATEM-TEMP(N,1))*2.
     1 +TOPTEM(1)-TEMP(N,1))+DIM1*(TEMP(N,2)-TEMP(N,1)))
      PLTFLX(1)=PLTFLX(1)+COE4*CAPPA(N,1)*DIM2*
     1 (PLATEM-TEMP(N,1))*2.
      DELTEM(N,1)=(FLUX+HEAT*DELMET(N,1))/
     1 ((COE5+COE6*REAFRN(N,1))*HETCAP(N,1))
      IF(M.EQ.2) GOTO 213
C INTERIOR WIDTH SUBDIVISIONS
      DO 211 J=2,M-1
      FLUX=COE4*CAPPA(N,J)*(DIM2*((PLATEM-TEMP(N,J))*2.+TOPTEM
     1 (J)-TEMP(N,J))+DIM1*(TEMP(N,J-1)+TEMP(N,J+1)
     2 -2.*TEMP(N,J)))
      PLTFLX(J)=PLTFLX(J)+COE4*CAPPA(N,J)*DIM2*
     1 (PLATEM-TEMP(N,J))*2.
      DELTEM(N,J)=(FLUX+HEAT*DELMET(N,J))/
     1 ((COE5+COE6*REAFRN(N,J))*HETCAP(N,J))
  211 CONTINUE
C WIDTH SUBDIVISION NEXT TO FIN
  212 SIDTEM=TEMP(N,M)
  213 IF(M.NE.1) SIDTEM=TEMP(N,M-1)
      FINTRN=COE4*((DY+FINTHK(N))/(DY/CAPPA(N,M)+FINTHK(N)/THRCNF))
     1 *DXLONG*(FINTEM(N)-TEMP(N,M))/(.5*(DY+FINTHK(N)))
      FLUX=COE4*CAPPA(N,M)*(DIM2*((PLATEM-TEMP(N,M))*2.
     1 +TOPTEM(M)-TEMP(N,M))+DIM1*(SIDTEM-TEMP(N,M)))
      PLTFLX(M)=PLTFLX(M)+COE4*CAPPA(N,M)*DIM2*
     1 (PLATEM-TEMP(N,M))*2.
      DELTEM(N,M)=(FLUX+FINTRN+HEAT*DELMET(N,M))/
     1 ((COE5+COE6*REAFRN(N,M))*HETCAP(N,M))
C BOTTOM FIN SUBDIVISION
      FLUX=COE4*THRCNF*((TOPTHK+FINTHK(N))/2.*
     1 (FINTOP-FINTEM(N))+(THKFIN+FINTHK(N))/2.
     2 *(PLATEM-FINTEM(N))*2.)*LENGTH/DX
      DELFIN(N)=(FLUX-FINTRN)/FINCAP(N)
      FINFLX(N)=FINFLX(N)+FINTRN
C*****************************************************************************
C
C   CALCULATE CHANGES IN TEMPERATURE AND AVERAGE PROPERTIES
C
      FRA=0.
      CPA=0.
      TA=0.
      CAPAV=0.
      DO 18  I=1,N
      FINTEM(I)=FINTEM(I)+DELFIN(I)
      DO 18 J=1,M
      TEMP(I,J)=TEMP(I,J)+DELTEM(I,J)
      TA=TA+TEMP(I,J)
```

96

```
      FRA=FRA+REAFRN(I,J)
      CPA=CPA+HETCAP(I,J)
      CAPAV=CAPAV+CAPPA(I,J)
   18 CONTINUE
      TA=TA/SEGMNT
      FRA=FRA/SEGMNT
      CPA=CPA/SEGMNT
      CAPAV=CAPAV/SEGMNT
      ICOUNT=ICOUNT+1
      IF(ICOUNT.LT.NREPRT) GO TO 80
      ICOUNT=0
C
C  PRINT RESULTS OF MAJOR IMPORTANCE
C
      WRITE(IOUT,110) K,TIME,TEMP(1,1),TEMP(1,M),TEMP(N,1),TEMP(N,M),TA
      WRITE(IOUT,111) REAFRN(1,1),REAFRN(1,M),REAFRN(N,1),
     1 REAFRN(N,M),FRA
      WRITE(IOUT,111) CPA,CAPAV
      WRITE(IOUT,112) (FINFLX(I), I=1,N)
      WRITE(IOUT,112) (PLTFLX(J), J=1,M)
      DO 888 I=1,N
      WRITE(IOUT,115) (TEMP(I,J), J=1,MWIDE),FINTEM(I)
  888 CONTINUE
      IF(MODE.EQ.0.AND.FRA.LE.FRCTN1+.01) GOTO 1
      IF(MODE.EQ.1.AND.FRA.GE.FRCTN2-.01) GOTO 1
   80 CONTINUE
      GO TO 1
  110 FORMAT(//,I5,F10.5,5F10.2)
  111 FORMAT(6X,5F10.5)
  112 FORMAT(10E10.4)
  115 FORMAT(/,10F10.2)
  100 FORMAT(10I5)
  101 FORMAT(8F10.3)
  102 FORMAT(10I8)
  103 FORMAT(8(F11.5,1H ))
      END
```

W. E. Wentworth
Department of Chemistry
Central Campus
University of Houston
Houston, Texas   77004

Lawrence Berkeley Laboratory
Building 90, Room 3100
University of California
Berkeley, California   94720
Attn: Michael Wahlig
        Ezzat Wali

F. A. Jaeger
Martin Marietta
P. O. Box 179
Denver, Colorado   80201

Melvin B. Singer
New York State Energy Research
    and Development Authority
Agency Building No. 2
Empire State Plaza
Albany, New York   12223

Oak Ridge National Laboratory
P. O. Box Y
Oak Ridge, Tennessee   37830
Attn: Herbert Hoffman
        Robert J. Kedl, Building 9204-1, MS - 3

David D. Perlmutter
Department of Chemical and
    Biochemical Engineering
University of Pennsylvania
311 Towne Building D3
Philadelphia, Pennsylvania   19174

Douglas D. Huxtable
Rocket Research Company
York Center
Redmond, Washington   98052

Tom Springer
Rockwell International
8900 DeSoto Avenue
Canoga Park, California   91304

Division of Physical Chemistry
Royal Institute of Technology
S-100 44
Stockholm 70, SWEDEN
Attn: Wiktor Raldow
      Prof. G. Wettermark

Solar Energy Research Institute
1536 Cole Boulevard
Golden, Colorado 80401
Attn: Frank Baylin
      Charles J. Bishop
      Ben Shelpuk
      Charles Wyman

Prof. M. Taube
Swiss Federal Institute
   for Reactor Research
CH-5303
Wuerenlingen, SWITZERLAND

Glenn T. Chinery
TVA
Bank Building
350 Commerce Union
Chattanooga, Tennessee 37401

S. A. Klein
College of Engineering
University of Wisconsin
1500 Johnson Drive
Madison, Wisconsin 53706

Dimiter Tchernev
Zeopower Company
75 Middlesex Avenue
Natick, Massachusetts 01760

J. H. Scott, 4700
G. E. Brandvold, 4710
V. L. Dugan, 4720
T. B. Cook, 8000, Attn: A. N. Blackwell, 8200
B. F. Murphey, 8300
D. M. Schuster, 8310
R. W. Carling, 8313
R. W. Mar, 8313
L. Gutierrez, 8400

R. C. Wayne, 8450
J. D. Fish, 8451
W. G. Wilson, 8451
A. C. Skinrood, 8452
T. T. Bramlette, 8453 (10)
J. D. Gilson, 8453
C. C. Hiller, 8453
Publications and Public Information Division, 8265, for TIC (27)
F. J. Cupps, 8265/Technical Library Processes Division, 3141
Technical Library Processes Division, 3141 (2)
Library and Security Classification Division, 8266-2 (3)

```
      XMOLES=(1.-VOID)*DXAREA*DRYDEN/WT
      DELT=24./NTIME
      TIME=0.
      YMOLES=MOLES
      XYMOLE=XMOLES*YMOLES
      WEIGHT=XMOLES*WT+ 32.*XYMOLE*FR
      COE1=PRE*DELT*XMOLES
      COE1P=PREP*DELT*XMOLES
      COE2=XMOLES*WT/DRYDEN
      COE3=XYMOLE/0.8
      COE4=3600.*AREA*DELT/DX
      COE5=WT*XMOLES
      COE6=32.*XYMOLE
      VOLUME=COE2+COE3*FR
      VOIDFR=VOLUME/DXAREA
      ONETH=1./3.
      COND=1.0/(1.-VOIDFR**ONETH)
      SLOPE=(THRCN2-THRCN1)/70.
      CEPT=THRCN1-50.*SLOPE
      COND=COND*(CEPT+TEMPIN*SLOPE)
      DELCP=CP2-CP1
      CP=CP1+FR*DELCP
C
      DO 10  I=1,N
      REAFRN(I)=FR
      TEMP(I)=TEMPIN
      CAPPA(I)=COND
      HETCAP(I)=CP
   10 CONTINUE
C
      ICOUNT=0
C
      DO 80  J=1,NTIME
   11 TIME=TIME+DELT
C BEGIN RATE LOOP
      IF(MODE.EQ.0) GO TO 13
      DO 12 I=1,N
      DELMET(I)=COE1*EXP(ACTIVE/(273.+TEMP(I)))*(1.-REAFRN(I))
      IF(MODEL.EQ.0.AND.TEMP(I).GT.TCRIT1) DELMET(I)=0.0
   12 CONTINUE
      GO TO 121
   13 DO 131 I=1,N
      DELMET(I)=-COE1P*EXP(-ESUBA/(273.+TEMP(I)))*REAFRN(I)
      IF(MODEL.EQ.0.AND.TEMP(I).LT.TCRIT2) DELMET(I)=0.0
  131 CONTINUE
C
C  HAVING CALCULATED THE METHANOL RATE, WE NOW CALCULATE THE
C   PROPERTIES OF EACH SEGMENT.
C
  121 DO 14 I=1,N
      REAFRN(I)=(XYMOLE*REAFRN(I)+DELMET(I))/XYMOLE
      HETCAP(I)=CP1+REAFRN(I)*DELCP
      CAPPA(I)=(CEPT+TEMP(I)*SLOPE)/(1.-( (COE2+COE3*REAFRN(I))/
     1 DXAREA)**ONETH)
   14 CONTINUE
C
C  HAVING CALCULATED THE NEW PROPERTIES, WE NOW CALCULATE THE
```